Fundamental Reactivity and Metal-Ligand Cooperation Behavior of Fe Complexes Bearing a Tetradentate PNNP Ligand

Monika Gautam

November 2021

Fundamental Reactivity and Metal-Ligand Cooperation Behavior of Fe Complexes Bearing a Tetradentate PNNP Ligand

Monika Gautam

Doctoral Program in Chemistry

Submitted to the Graduate School of
Pure and Applied Sciences
in Partial Fulfillment of the Requirements
for the Degree of Doctor of Philosophy in
Science

at the

University of Tsukuba

Table of Contents

Chapter 1

General Introduction

In the history of organometallic chemistry, precious metal complexes have been mainly applied to homogeneous catalysis due to their inherent 2e redox process, which is often favored for organic synthesis.[1] However, precious metal catalysts fail to fulfil the requirement for development of sustainable and green chemistry due to their high cost and potential toxicity.[2] Thus, to substitute precious metal catalysts with those using more abundant and cheaper first row transition metals have become a widespread research subject in the field of homogeneous catalysis.[3] Among 3d transition metal catalysts, iron is a preferable metal because it is most abundant (43200 ppm in the continental crust)[4], low cost, and non-toxic. Apart from homogeneous catalysis in industry, iron-based enzymes function as catalysts in nature. Another aspect of iron catalyst is that they adopt various oxidation states ranging from –2 to +5 (rarely to +8) and various spin states such as low spin, intermediate spin, and high spin.[5] Moreover, spin states easily change via spin crossover due to its small ligand field splitting. Although numerous reports on iron catalyzed reactions are known so far, numbers of studies on well-defined iron catalysts are still limited compared to those of precious metal catalysts due to their complicated paramagnetic nature,[6] i.e. difficulty in identification, controlling the reactivity, etc. Thus, detailed reactivity investigation of iron complexes is still a big challenge in organometallic chemistry.

For the design of well-defined iron complexes, employing a strong-field ligand is effective. A strong-field ligand enlarges d-orbital splitting and stabilizes diamagnetic complexes in low-spin states. In this context, a pincer ligand is one of the most useful ligand candidates. Shaw and co-workers have reported the first pincer ligand in 1976 [7a] (Scheme 1) and the term ‘pincer’ was coined by van Koten in 1989.[7b] It was mainly applied on precious metals with exception of Ni (3d transition metal) metal in the early stage of its chemistry.[8]

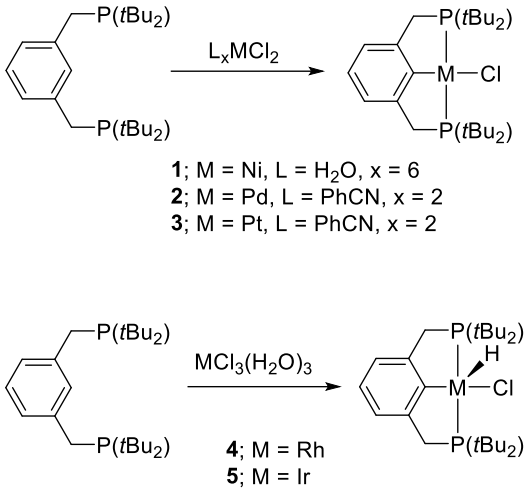

Scheme 1. Synthesis of pincer transition metal complex reported by Shaw[7a].

The remarkable feature of these pincer ligands is that their structure can be optimized by tuning side-arm-linker such as CH_2, NH, and O (Scheme 2). Due to this character, the pincer ligands were successfully applied in recent years in the precise design of iron complex.[9] The first iron pincer complex PNP complexes were synthesized by Dahlhoff and Nelson in 1971 by the reaction of 2,6-bis(diphenylphosphinomethyl)pyridine with FeX_2 (X = Cl, Br, I, NCS) (Scheme 3).[8a] Since then, iron pincer chemistry become a prime interest in the development of iron catalysts.

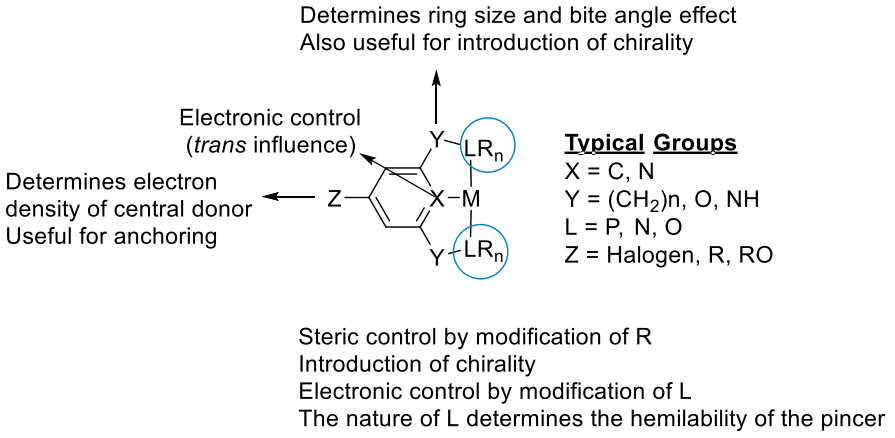

Scheme 2. Generalized structure of pincer metal complex.[9]

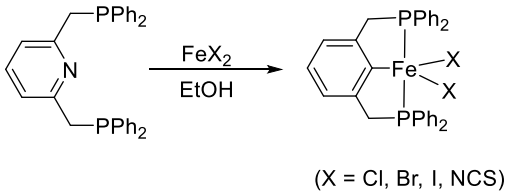

Scheme 3. Typical structure of pincer ligands with benzene or pyridine backbone.

Metal ligand cooperation (MLC)

Recently, one significant breakthrough has been made in the chemistry of pincer ligands, a metal ligand cooperation (MLC), wherein a redox active ligand cooperatively facilitates multi-electron reaction.[10] As a result, MLC now becomes a powerful tool for bond activation process and facilitates various chemical and biological catalytic reactions.[12] Therefore, iron pincer complexes have gained attention in seek of rational design of catalyst, which can utilize MLC behavior.

MLC has different kinds of modes, hemilability,[10c-d] redox activity[10e] and bifunctional behavior[10a,b], where the ligand and the metal work in a synergetic way by interacting with a substrate during a bond activation step. Hemilability involves reversible dissociation of ligand to create vacant coordination sites for activation of substrate during the reaction (Scheme 4a). Redox active ligand serves as an electron reservoir in the bond activation of substrate without changing the oxidation state of the metal center (Scheme 4b). Bifunctional behavior, where both a metal and a ligand work in a cooperative fashion, resulting in the simultaneous bond-formation and bond-breaking (Scheme 4c).

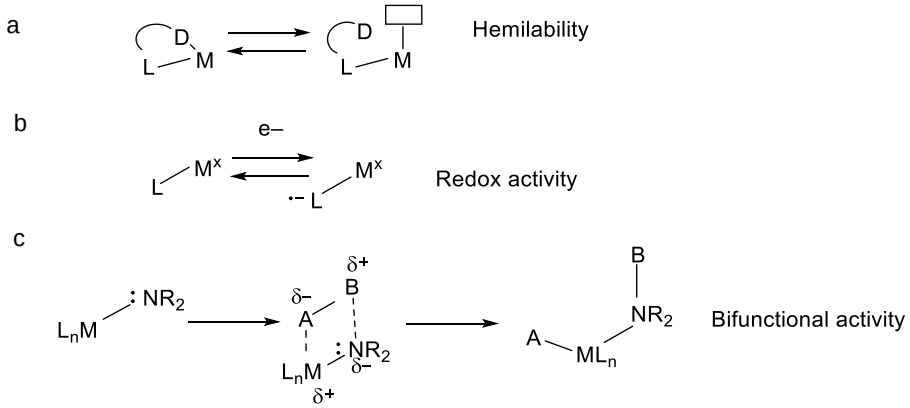

Scheme 4. Different modes of metal ligand cooperation (a) Hemilability, (b) Redox activity, (c) Bifunctional activity.

One of the prominent works with the use of bifunctional activity of MLC were demonstrated by Noyori, Ikariya and co-workers.[11] Ru complexes bounded with an amido ligand (R_2N–M) undergo heterolytic cleavage of H–H bond and achieve hydrogenation of carbonyl compounds. Recently, Milstein explained the bifunctional activity in the pyridine-based PNP or PNN pincer ligand systems, i.e.a dearomatization-rearomatization sequence in MLC enables bond activation (Scheme 5).[13] In pyridine-based pincer ligand systems, a linker such as CH_2, NH has an acidic proton, which undergo deprotonation in the presence of a base, resulting in the dearomatization of pyridine-based pincer backbone, leaving exocyclic double bond. Rearomatization mediated by cooperation of metal plays a driving force. As a result, dearomatized ligands activate various bonds such as O–H, N–H, H–H etc. without change in formal oxidation state of metal center.[13]

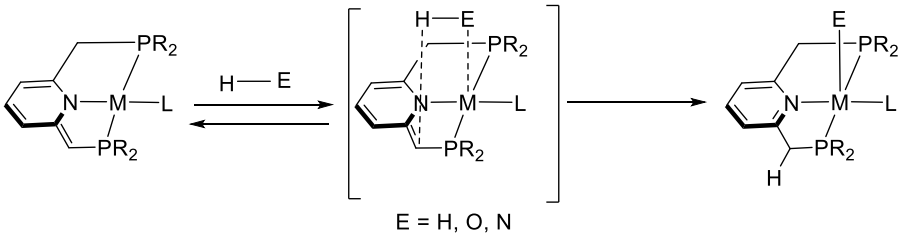

Scheme 5. Metal ligand cooperation based on dearomatization/rearomatization.

MLC in 3d transition metal complexes has been extended in catalysis with application of bifunctional property, aromatization/dearomatization, and redox activity of ligands. For example, inspired by Noyori's amine/amido ligand system, Morris's group synthesized iron complex with unsymmetrical chiral [PN^HP] ligand (Scheme 6a) for asymmetric hydrogenation of ketones and imines.[14a] Furthermore, application of aromatization/dearomatization was extended to the iron pincer PNP complex (Scheme 6b), and hydrogenation of ketones was reported by Milstein et al.[14b] In these systems, heterolytic cleavage of E–H (E= H, O, N etc) bond proceeds, where bifunctional activity of a metal and a ligand involved during the reaction. Different from this, it is also known that redox active ligands have assisted MLC in the application of 3d transition metal catalyst, wherein redox active ligand serves as an electron reservoir during the reactions. Chirik and co-workers featured the redox active ligand based on the bis(imino)pyridine (PDI) (Scheme 6c) framework in iron chemistry and achieved hydrogenation of simple olefins.[14c] As shown above, there is no doubt that ligand design has led to give various modes of MLC.

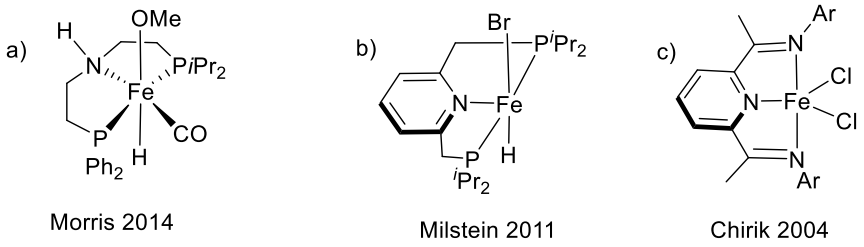

Scheme 6. Different iron pincer system demonstrated by: (a) Morris group[14a], (b) Milstein group[14b], and (c) Chirik group.[14c]

Tetradentate PNNP ligand

Tetradentate PNNP-Ph (2,9 bis((diphenylphosphino)methyl)-1,10-phenanthroline)) ligand was first developed by Ziessel in 1980. PNNP-R ligand (R = Ph, Cy, *t*Bu etc) (Scheme 7) exhibits unique features, which could be useful in the application of 3d transition metals. It has 4 σ-donor atoms and π-acidic phenanthroline backbone, which behaves as a redox active ligand.[15] By acquiring all these features, PNNP-R binds to a metal center via tetradentate coordination in a rigid meridional coordination mode and thus promotes ligand-field splitting to afford a diamagnetic complex. The properties of PNNP-R can be further tuned by introducing different substituents (R = Ph, Cy, *t*Bu etc) on phosphine which compliments to it for application in catalysis. It is well known that steric properties of monodentate phosphine is studied by using Tolman's cone angle. Along with steric properties of R substituent, electron-donating ability of phosphines is also governed by R substituents. Thus, R substituents influences the electron donating property and steric property around the metal center.

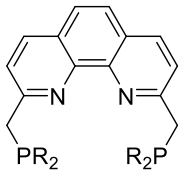

(R = Ph, Cy, *t*Bu)

Scheme 7. Structure of PNNP-R ligand.

As explained above, tridentate pincer ligands with a pyridine backbone have set up a definition of MLC based on dearomatization/rearomatization sequence. Such the MLC concept has been extended by using PNNP-*t*Bu-Ru as it shows an unprecedented long-range MLC. Thus, they revealed a unique

long-range metal ligand cooperation, in which hydride migrates to the endocyclic phenanthroline backbone (Scheme 8).[15]

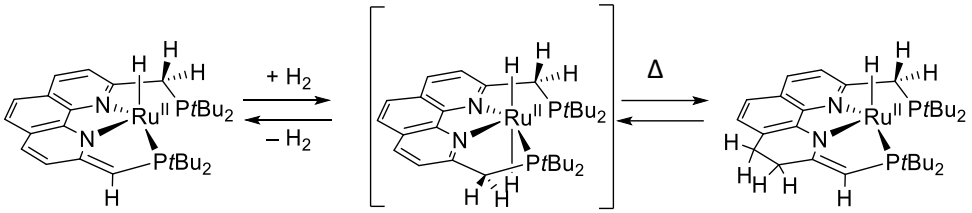

Scheme 8. Long-range metal ligand cooperation in PNNP-*t*Bu-Ru complex.[15]

Considering that the PNNP ligand exhibits strong σ-donating ability via tetradentate coordination and acts as strong field ligand, we focus on the PNNP ligand as a next generation rigid meridional ligand and set out for the development of PNNP-Fe complexes.[16a-b] Recently, we reported a synthesis of a series of Fe complex bearing PNNP-R (R=Ph, Cy) ligand, it efficiently activates hydrosilanes and behaves as a good catalyst for dehydrogenative coupling of silanols with hydrosilanes (Scheme 9a).[16a] With the use of well-defined PNNP-Fe complexes, MLC was also demonstrated (Scheme 9b).[16b-c] It was also revealed that Co complexes bearing a PNNP-Ph ligand exhibits a unique long-range metal ligand cooperation, wherein reversible H–H bond was cleaved and phenanthroline backbone acts as a hydrogen reservoir (Scheme 9c).[16c-d] These results suggested a capability of PNNP-3d metal system towards bond cleavages via metal ligand cooperation based on dearomatization/rearomatization.

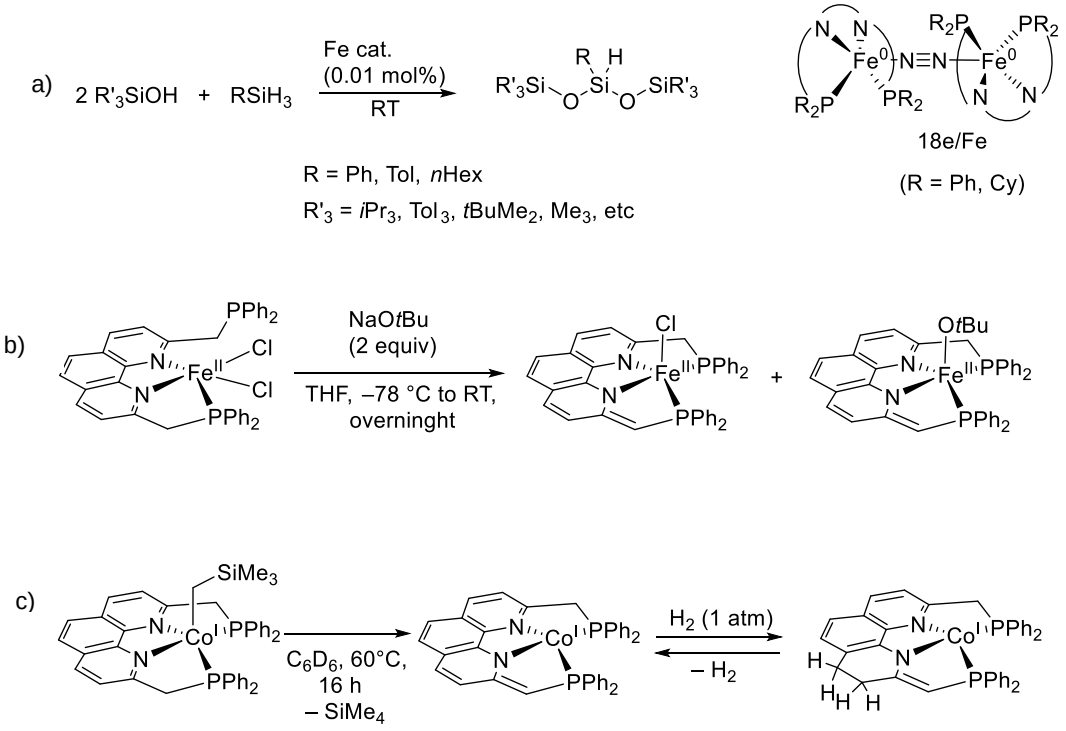

Scheme 9. (a) Selective preparation of hydrosiloxane catalyzed by PNNP-Fe catalyst,[16a] (b) MLC in PNNP-Fe complex,[16b] (c) Unique long range metal ligand cooperation in PNNP-Co complex.[16c]

Thesis outline

In this context, I focus on the fundamental reactivity and metal ligand cooperation of Fe complexes bearing a PNNP ligand. Dr. Takeshita reported pre-liminary results of Si–X oxidative addition with use of PNNP-Fe complexes in his doctorate thesis. The result inspired me to investigate reactivity of [{Fe(PNNP-R)}$_2$(μ-N$_2$)] (R = Ph, Cy) towards C–X. Thus, I started my research in keen interest to cleave C–X bond via oxidative addition with PNNP-Fe (0) complex**.** Thus, Chapter 2 includes the oxidative addition of C–X bond and its mechanism was closely investigated. Furthermore, heterolytic cleavage of H–H bond was demonstrated via MLC.

In Chapter 3, I describe the reactivity PNNP-Cy Fe(II) hydride towards various type of substrates. Resulting complexes were characterized by elemental analysis and NMR. A single-crystal X ray diffraction study revealed structures of some of the complexes. The unique long-range MLC was observed through the reactions.

In chapter 4, I present the isolable rare square planar 14e Fe(II) complex bearing PNNP-Cy or PNNP-*t*Bu ligand and their reactivity.

References

1. (a) Ackermann, L. *Acc. Chem. Res*. **2014**, *47*, 281-285. (b) Baudoin, O. *Acc. Chem. Res*. **2017**, *50*, 1114-1123. (c) Della, N. M.; Fontana, E.; Motti, M.; Catellani, *Acc. Chem. Res*. **2016**, *49*, 1389-1400. (d) Kim, J.; Chang, S. *Angew. Chem. Int. Ed*. **2014,** *53*, 2203-2207. (e) Ye, B.; Cramer, N. *Acc. Chem. Res.* **2015**, *48*, 1308-1318. (f) Nagamoto, M.; Nishimura, T. *ACS Catal*. **2017**, *7*, 833-847. (g) Piou, T.; Rovis, T. *Acc. Chem. Res*. **2018**, *51*, 170-180.
2. (a) Egorov, K. S.; Ananikov, V. P. *Angew. Chem., Int. Ed.* **2016**, *55*, 12150-12162. (b) Chirik, P. J.; Morris, R. *Acc. Chem. Res.* **2015,** *48*, 2495-2495.
3. (a) B. Plietkier, *Iron Catalysis in Organic Chemistry*, Wiley-VCH: Weinheim, Germany, **2008**. (b) Bauer, I.; Knolker, H. J. *Chem. Rev*. **2015**, *115*, 3170. (c) Bolmes, C.; Paih, J. L.; Zani, L. *Chem. Rev*. **2004**, *104*, 6217. (d) Furnstner, A. *ACS Cent Sci*. **2016**, *2*, 778. (e) Enthaler, S.; Junge, K.; Beller, M. *Angew. Chem. Int. Ed***. 2008**, *47*, 3317-3321. (f) Loup, J.; Dhawa, U.; Pesciaioli, F.; Wencel-Delord, J.; Ackermann, L. *Angew. Chem. Int. Ed*. **2019**, *58*, 12803-12818.
4. K. H. Wedepohl, The Composition of the Continental Crust. *Geochim. Cosmochim. Acta*, **1995**, *59*, 1217-232.
5. (a) Poli, R. *Chem. Rev*. **1996**, *96*, 2135-2204. (b) Harvey, J. N.; Poli, R.; Smith, K. M. *Coord. Chem. Rev*. **2003**, 347-361. (c) Alvarez, S.; Cirera, J. *Angew. Chem. Int. Ed*. **2006**, *45*, 3012-3020.
6. (a) Bart, S. C.; Lobkovsky, E.; Chirik, P. J. *J. Am. Chem. Soc*. **2004**, *126*, 13794-13807. (b) Bart, S. C.; Hawrelak, E. J.; Lobkovsky, E.; Chirik, P. J. *Organometallics*, **2005**, *24*, 23. (c) Yu, R. P.; Darmon, J. M.; Hoyt, J. M.; Margulieux, G. W.; Turner, Z.; Chirik, P. J. *ACS Catal*. **2012**, *2*, 1760-1764. (d) Langer, R.; Leitus, G.; David, Y. B.; Milstein, D. *Angew. Chem. Int. Ed.* **2011**, *50*, 2120-2124. (e) Werkmeister, S.; Junge, K.; Wendt, B.; Alberico, E.; Jiao, H.; Baumann, W.; Junge, H.; Gallou, F.; Beller, M. *Angew. Chem. Int. Ed.* **2014,** *53*, 8722-8726. (f) Li, H.; Luis, C.; Castro, M.; Zheng, J.; Roisnel, T.; Dorcet, V.; Sortais, J. B.; Darcel, C. *Angew. Chem. Int. Ed.* **2013**, *52*, 8045-8049.

7. (a) Moulton, C. J.; Shaw, B. L. *Jr. Chem. Soc. Dalton.* **1976**, *11*, 1020-1024. (b) van Koten, G.; Gossage, R. A. *The Privileged Pincer-Metal Platform: Coordination Chemistry & Applications,* Springer*, 2015, vol 54.* (c) G. V. Koten, D. Milstein, *Organometallic Pincer Chemistry*, Springer, Berlin Heidelberg**, 2013**, *vol. 40*.
8. (a) Dahlhoff, W. V.; Nelson, S. M. *J. Chem. Soc.*, **1969**, *433*, 2036. (b) Ohff, M.; Ohff, A.; van der Boom, M. E.; Milstein, D. *J. Am. Chem. Soc.* **1997**, 119, 48, 11687-11688. (c) Morales, D. M.; Redón, R.; Yung, C.; Jensen, C. M. *Chem. Comm*., **2000**, 1619-1620. (d) Peris, E.; Loch, J. A.; Mata, J.; Crabtree, R. H. *Chem. Commun*., **2001**, 201-202. (e) Grundemann, S.; Albrecht, M.; Loch, J. A.; Faller, J. W.; Crabtree, R. H. *Organometallics*, **2001**, *20*, 5485-5488. (f) Bergbreiter, D. E.; Osburn, P. L.; Liu, Y.S. *J. Am. Chem. Soc.*, **1999**, *121*, 9531-9538. (g) Boom, V.; Misltein, D. *Chem. Rev.* **2003**, *103*, 1759-1792.
9. (a) Crabtree, R. *Chem. Soc. Rev.* **2018**, *47*, 1959. (b) Grutzmacher, H. *Angew. Chem. Int. Ed*. **2008**, *47*, 1814-1818. (c) Vlugtand, J. I.; Reek, J. N. H. *Angew. Chem. Int. Ed.* **2009**, *48*, 8832-8846. (e) Lorraine, S.C. *Polyhedron*, **2018**, *143*, 11-27. (f) Schneider, S.; Meiners, J.; Askevold, B. *Eur. J. Inorg. Chem*. **2012**, 412-429.
10. (a) Khusnutdinova, J. R.; Milstein, D. *Angew. Chem., Int. Ed.* **2015**, *54* ,12236 -12273. (b) Vlugt, J. I. *Eur. J. Inorg. Chem.* **2011**, *3*, 363-375. (c) Jeffrey, J. C.; Rauchfuss, T. B. *Inorg. Chem.*, **1979**, *18*, 10. (d) Braunstein, P.; Naud, F. *Angew. Chem. Int. Ed.* **2001**, *40*, 680 -699. (e) Chirik, P. J.; Wieghardt, K. *Science*, **2010**, *327*, 794-795.
11. (a) Noyori, R.; Hashiguchi, S. *Acc. Chem. Res.* **1997**, *30*, 97-102. (b) Noyori, R. *Angew. Chem. Int. Ed.* **2002**, *41*, 2008- 2022.
12. (a) Bullock, R. M.; Chen, J. G.; Gagliardi, L.; Chirik, P. J.; Farha, O. K.; Hendon, C. H.; Jones, C. W.; Keith, J. A.; Klosin, J.; Minteer, S. D. *Science*, **2020**, 369. (b) Fontecilla-Camps, J. C.; Volbeda, A.; Cavazza, C.; Nicolet, Y. *Chem. Rev.* **2007**, *107*, 4273-4303. (c) Kubas, G. J. *Chem. Rev.*, **2007**, *107*, 4152-4205.
13. (a) Gunanathan, C.; D. Milstein, *Chem. Rev.*, **2014**, *114*, 12024. (b) Gunanathan, C; Milstein, D. *Acc. Chem. Res.* **2011**, *44*, 588-602.
14. (a) Lagaditis, P. O.; Sues, P. E.; Sonnenberg, J. F.; Wan, K. Y.; Lough, A. J.; Morris, R. H. *J. Am. Chem. Soc.* **2014**, *136*, 1367-1380. (b) Langer, R.; Leitus, G.; Ben-David, Y.; Milstein, D. *Angew. Chem. Int. Ed.* **2011**, *50*, 2120-2124. (c) Bart, S. C.; Lobkovsky, E.; Chirik, P. J. *J. Am. Chem. Soc.* **2004**, *126*, 13794-13807.

15. Langer, R.; Fuchs, I.; Vogt, M.; Balaraman, E.; Diskin-Posner, Y.; Shimon, L. J. W.; Ben-David, Y.; Milstein, D. *Chem. Eur. J.* **2013**, *19*, 3407-3414.
16. (a) Takeshita, T.; Sato, K.; Y. Nakajima, *Dalton Trans.* **2018**, *47*, 17004. (b) Takeshita, T.; Nakajima, Y. *Chem. Lett.* **2019,** *48*, 364. (c) Jheng, N. Y.; Ishizaka, Y.; Naganawa, Y.; Sekiguchi, A.; Nakajima, Y. *Dalton Trans.*, **2020**, *49* ,14592. d) Y. Nakajima, T. Takeshita, N. Y. Jheng, *Dalton Trans.* **2021,** *3***,** 31.

Chapter 2

Oxidative Addition of C−X Bond and H−H Cleavage via MLC

Abstract

Iron(0) complex bearing a phenanthroline-based meridional PNNP ligand [{Fe(PNNP)}$_2$(μ-N$_2$)] (**1**) (PNNP = 2,9-bis((diphenylphosphino)methyl)-1,10-phenanthroline) smoothly reacted with CH_3I at ambient temperature to cleave C–I bond, resulting in the formation of the corresponding oxidative addition product, [Fe(CH_3)(I)(PNNP)] (**2**). Complex **2** was fully identified by NMR and its structure was determined by a single crystal X-ray diffraction study. Mechanistic study using cyclopropylmethyl bromide as a radical clock supported a radical pathway for the C–I bond cleavage of CH_3I. Complex **2** underwent deprotonation on treatment with NaO*t*Bu to form **4**, which possessed a dearomatized phenanthroline backbone. Complex **4** further reacted with H_2 to cleave H–H bond. The reaction was mediated by metal-ligand cooperation process that involves re-aromatization of the phenanthroline backbone of the PNNP ligand.

Introduction

Oxidative addition plays a key role in catalysis.[1] Among them, oxidative addition of C−X bonds plays pivotal roles in various organic synthetic processes such as cross coupling reactions[2a-c], and industrial synthesis of acetic acid from methanol.[2d-e] The following three mechanisms are known for oxidative addition reactions, 1) concerted mechanism 2) S_N2-type mechanism, and 3) radical mechanism (Scheme 1).

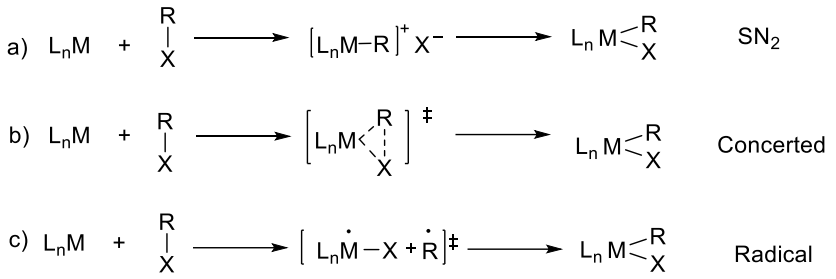

Scheme 1. Mechanism of Oxidative Addition.

Generally, net two-electron oxidative addition of C−X bonds dominated in precious 4d and 5d metal catalysts.[3] The reaction mechanism of these steps was thus far closely studied using various well-defined 4d and 5d metal catalyst systems.[1b] Different from these systems, oxidative addition reaction of C–X bond by radical mechanism often proceeds in iron catalyst systems.[4] As explained in Chapter 1, iron complexes suffer from complicated electronic states and difficulty in their characterization. As a result, examples of detailed mechanistic study on oxidative addition step using well-defined iron complexes are still relatively limited.[5] In spite of the incredible progress of iron-catalyzed cross-coupling reactions in organic synthesis, their reaction mechanisms remain not well-defined. In this context, to study fundamental mechanistic study of oxidative addition reaction using iron complexes is of great importance.[5] The pioneering work by Kochi and co-worker in the 1970s displayed efficient iron catalysts for C−C cross-coupling reactions (Scheme 2).[6] They demonstrated that simple ferric salts catalyze the stereoselective generation of C−C bonds starting from alkenyl halides and Grignard reagents and it involves Fe(I) species, which is converted to Fe(III) species via oxidative addition of C–X bond. In this study, it was also revealed that C−X bond cleavage can either follow the radical pathway.

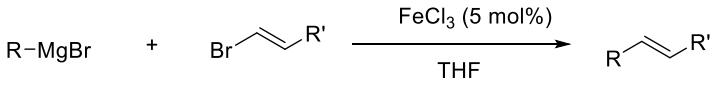

Scheme 2. Iron catalyzed cross coupling reaction reported by Kochi.[6]

One of the remarkable contributions were given by Nakamura and co-workers in iron catalyzed cross coupling reactions and its mechanistic investigation.[7] They have developed novel iron(II) complex bearing a bidentate diphosphine ligand, which was proven to be an efficient catalyst to form $C(sp^3)$ −$C(sp^3)$ bond through cross-coupling of alkyl halide and aryl boronates (Scheme 3).[7b] The mechanistic investigation of oxidative addition of C–X bond using a radical clock revealed that the reaction to proceeds via radical pathway. Finally, they demonstrated one mechanism, which includes a Fe(II)/Fe(III) cycle (Scheme 4).

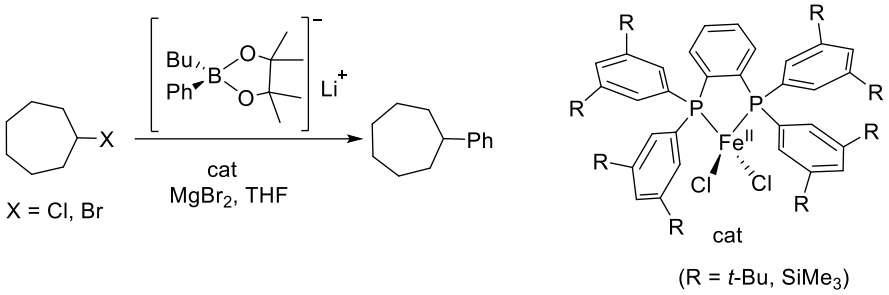

Scheme 3. Cross-coupling reaction catalyzed by iron (II) chloride diphosphine catalyst.[7b]

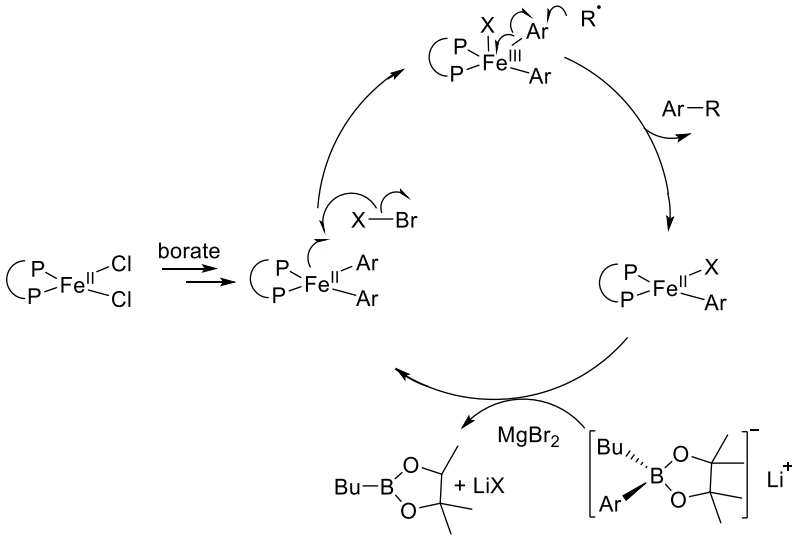

Scheme 4. Mechanism of the iron-catalyzed cross-coupling reaction reported by Nakamura and co-workers.

In 2009, Nakamura's group also performed iron-catalyzed Kumada cross-coupling reaction of alkyl halide with RMgX (Grignard reagent) by using $FeCl_3$ (5 mol%) in the presence of TMEDA as an additive.[7a] They successfully isolated the organoiron intermediate species, and reactivity study of the isolated intermediate towards alkyl halide endorsed the mechanism involved in the reaction. For instance, intermediary species [$FeAr_2$(TMEDA)] (Ar = Mesityl) with 1-bromooctane to give [FeBr(Mes)(TMEDA)] along with octyl-mesitylene (Scheme 5),[7a] where iron was found to be +II oxidation state. Moreover, radical clock experiment showed strong evidence in favor of a radical mechanism. Thus, overall mechanistic study clearly supported a mechanism that conveys C–X bond via radical mechanism.

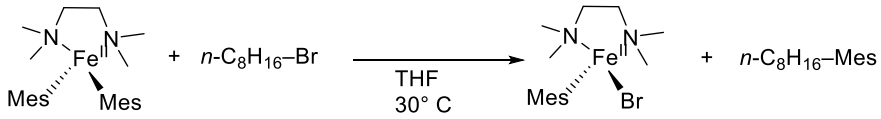

Scheme 5. Reaction of [$FeAr_2$(TMEDA)] (Ar = Mes) with bromooctane.[7a]

Conversely, Fürstner and co-workers demonstrated Cp-supported iron-catalyzed Grignard cross coupling reactions (Cp = Cyclopentadienyl).[8a] In this system, strong C–Cl bond cleavage is achieved via ionic mechanism by a negatively-charged iron ate intermediate (Scheme 6). They further continued detailed mechanistic study and identified some intermediates, such as [$Fe(C_2H_4)_4$][Li(tmeda)]$_2$, [$Fe(cod)_2$][Li(dme)]$_2$, [$CpFe(C_2H_4)_2$][Li(tmeda)], [CpFe(cod)][Li(dme)], or [$Cp^*Fe(C_2H_4)_2$][Li(tmeda)]. Finally, they concluded that the reaction proceeds via a complicated mechanism involving three different catalytic cycles, which are interconnected with different redox cycles of Fe(+1)/Fe(+3), Fe(0)/Fe(+2), and Fe(–2)/Fe(0) (Scheme 7).[8]

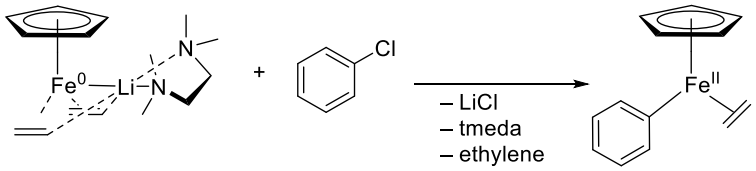

Scheme 6. Reaction of Lithium ferrate complex with chlorobenzene.

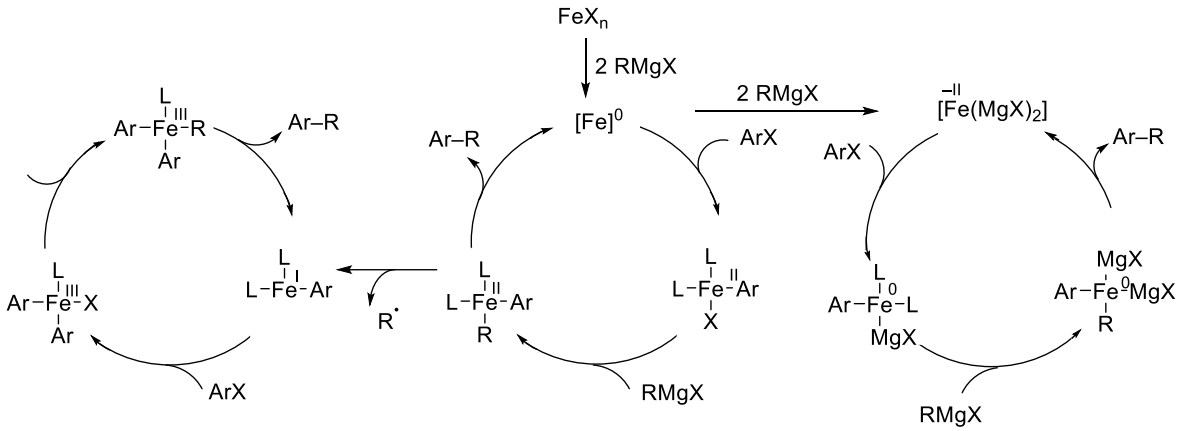

Scheme 7. Plausible reaction mechanism of cross-coupling reaction with interconnected catalytic redox cycles reported by Fürstner.

As shown above, iron complexes offer diverse oxidative addition mechanism of C–X bond by involving either radical mechanism or S_N2 or concerted mechanism. Furthermore, it is apparent that the reactivity of iron complexes is dependent on the ligand properties as well as substrates involved in the reaction.

In this chapter, I focus on the reactivity of the well-defined PNNP-Fe complex towards alkyl halide. Detailed mechanistic study was performed. Furthermore, MLC was applied in this system, and H–H bond cleavage was successfully achieved.

Results & Discussions

Firstly, the reactivity of **1** towards various organic halides, such as PhI, benzyl bromide, and allyl chloride, were investigated. The reaction smoothly proceeded at room temperature, resulting in the formation of complicated mixtures that exhibit several signals in the $^{31}P\{^1H\}$ NMR spectrum.

Different from above reactions, the reaction of **1** with CH_3I afforded the corresponding oxidative addition product as a sole product; i.e. **1** smoothly reacted with CH_3I (4 equiv/Fe) at ambient temperature to cleave a C–I bond, resulting in the formation of [Fe(CH_3)(I)(PNNP)] (**2**) in 85% yield (Scheme 8). In the ^1H NMR spectrum of **2**, the CH_3 signal was observed at δ –2.21 ppm as a triplet ($^3J_{PH}$ = 6.9 Hz). Two PCH_2 moieties were identically observed at δ 4.92 ppm with the integral intensity of 4H as a broad signal. Therefore, a symmetrical structure of **2** with a mirror plane vertical to the

PNNP plane was supported. Consistent with these observations, **2** exhibits one sharp singlet at δ 78.2 ppm in the $^{31}P\{^{1}H\}$ NMR spectrum.

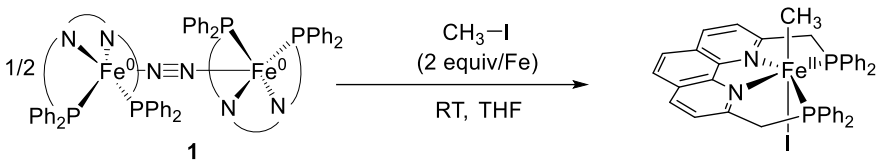

Scheme 8. Reaction of **1** with CH_3I.

Single crystal X-ray diffraction study revealed the octahedral structure of **2**, in which the CH_3 group and the I group occupy apical positions (Figure 1). The Fe–N and Fe–C bonds exhibit typical values as low spin Fe(II) complexes, Fe–N for 1.85-2.08 Å and Fe–C for 2.08-2.18 Å, respectively.[9,10] Complex **2** exhibits bond distances Fe–CH_3 and Fe–I 2.102(7) and 2.7505(12) Å, respectively. Sabatino and co-workers reported $[Fe(CO)_2(PMe_3)_2(CH_3)I]$, where I occupies trans position to methyl, and the bond distance of Fe–CH_3 and Fe–I were found to be 2.083(7) and 2.681(1) respectively.[10e]

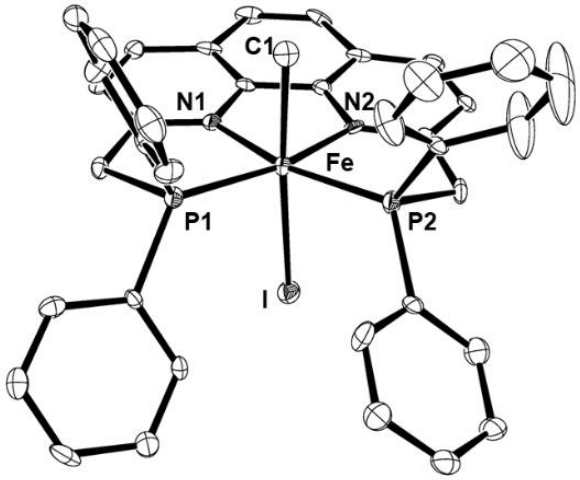

Figure 1. ORTEP diagram of complex **2** with 50% probability thermal ellipsoids. All hydrogen atoms are omitted for clarity. Selected bond lengths[Å] and angles [˚]: Fe–P1 2.227(2), Fe–P2 2.212(2), Fe–N1 1.941(5), Fe–N2 1.944(5), Fe–C1 2.102(7), Fe–I 2.7505(12); P1–Fe–N1 83.84(17), P1–Fe–N2 165.90(18), N1–Fe–N2 82.1(2), P1–Fe–P2 110.85(8), I1–Fe–C1 171.5(2).

To shed light on the reaction mechanism of the C–I bond cleavage, the reaction of **1** with cyclopropylmethyl bromide as a radical clock was examined.[11] Complex **1** immediately reacted with

2.5 equivalent of cyclopropylmethyl bromide at room temperature to give a complex mixture of unidentified products. Next, the reaction was performed in toluende-d_8 and followed carefully by NMR spectroscopy (Scheme 9). The reaction gradually proceeded at –10 °C, and **1** was completely consumed after 15 min. Formation of an unidentified product, which exhibits a broad signal at δ 77.2 ppm in the $^{31}P\{^1H\}$ NMR spectrum, was detected. While the ^1H NMR spectrum was somewhat complicated, concomitant formation of 1-butene, which exhibit signals at δ 5.70(m), 4.91(d), and 4.87(d) ppm as a characteristic ABX pattern, was confirmed (11% yield). The results strongly support the radical pathway for the C–Br bond cleavage, in which ring opening of the *in-situ*-formed cyclopropylmethyl radical proceeded during the reaction. The reaction mixture was further kept at ambient temperature overnight, then brown block crystals of PNNP-Fe dibromide [$Fe(Br)_2$(PNNP-Ph)] (**3**) formed in 44%/Fe isolated yield.

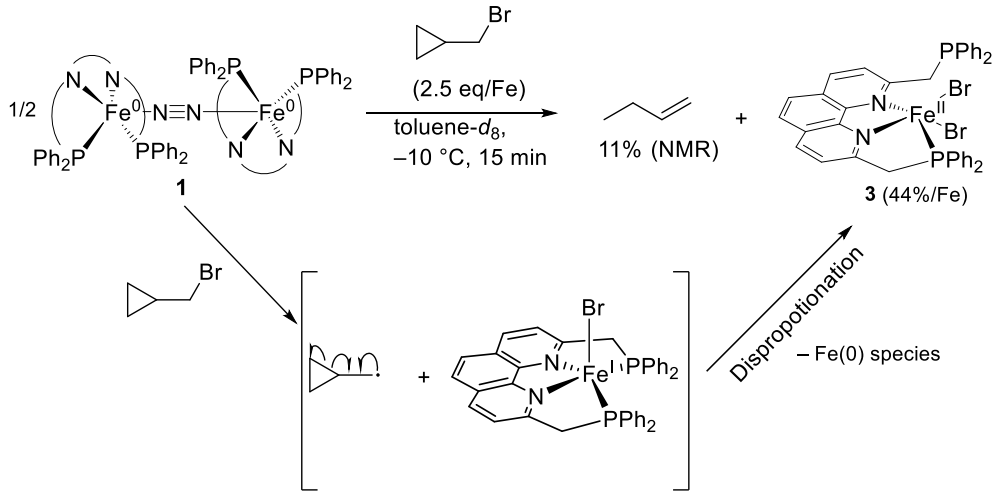

Scheme 9. Reaction of **1** with cyclopropylmethyl bromide.

It is likely that **3** was formed via disproportionation of the resulting Fe(I) monobromide [FeBr(PNNP-Ph)] as is also observed in the previously reported iron alkyl halide complexes.[12] Concomitant formation of the complicated mixture was detected in the reaction, which could be originated from the decomposition of the resulting Fe(0) species as a byproduct.

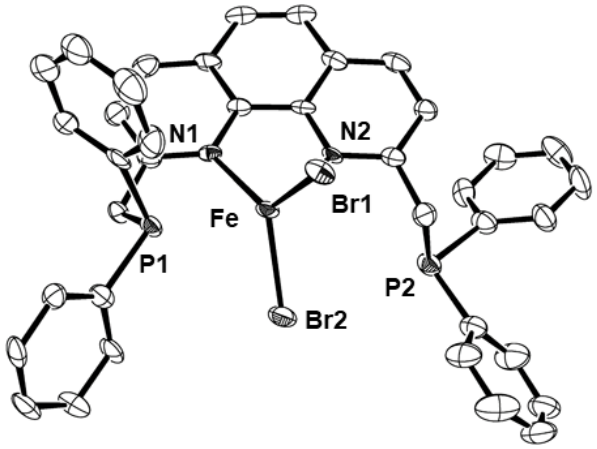

Figure 2. ORTEP diagram of complex **3** with 50% probability ellipsoids. All hydrogen atoms are omitted for clarity. Selected bond lengths[Å] and angles [˚]: Fe–N1 2.131(6), Fe–N2 2.235(6), Fe–Br1 2.445(15), Fe–Br2 2.404(14), Fe–P1 2.673(2); N1–Fe–N2 75.8(2).

For instance, Ozawa and co-workers illustrated disproportionation reaction of bis(phosphaethenyl)pyridine Fe(I) bromide induced by *t*BuNC.[12b] They have proposed one mechanism as follows: initial coordination of *t*BuNC to **A** form 19e complex **C**, and then **A** transfer one-electron to **C**, forming **B** and **D**. At the final step, complex **B** reacts with *t*BuNC to form $[Fe(Br)_2(L)_4]$ and free BPEP-Ph (Scheme 10).

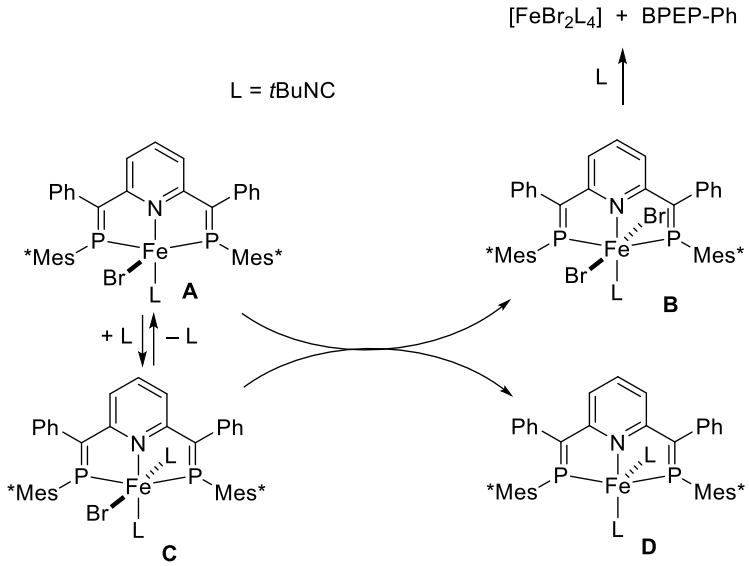

Scheme 10. Disproportionation mechanism in bis(phosphaethenyl)pyridine Fe(I) bromide.

Complex **3** is a paramagnetic and exhibits broad signals in the ^{1}H NMR spectrum. Therefore, complex **3** was identified by a single crystal X-ray diffraction study (Figure 2). The Fe–P bond distances are longer than those in previously reported [Fe(Br)$_2$(PNNP-Cy)] (PNNP-Cy = 2,9-bis((dicyclohexylphosphino)methyl)-1,10-phenanthroline)[9b] and the sum of the covalent radii of Fe (1.23 Å) and P (1.10 Å).[13] As a result, two phosphorus atoms are apart from the iron center, and thus **3** exhibits a distorted tetrahedral structure. Reflective of the paramagnetism of **3**, the Fe–N bonds are longer than those in **2** by ca. 0.2 Å.

Interestingly, **2** reacted with NaO^{t}Bu (2 equiv) at room temperature and underwent deprotonation of one benzylic-H atom, resulting in the formation of [Fe(CH$_3$)(PNNP'-Ph)] (**4)** in 84% yield (NMR) (Scheme 11). Complex **4** gradually decomposed at room temperature. Thus, identification of **4** was performed based on a series of NMR spectroscopy. Complex **4** exhibits an asymmetrical structure, which contains a dearomatized phenanthroline moiety. Thus, **4** exhibits non-equivalent two doublets at δ 78.1 ($^{2}J_{PP}$ = 28.4 Hz) ppm and δ 65.5 ppm in the ^{31}P NMR spectrum. In the ^{1}H NMR spectrum, the benzylic protons are observed at δ 4.38 and 4.52 ppm as a diastereotopic doublets. The methine proton appears at δ 4.32 as a singlet signal. The PNNP-backbone exhibits six doublets, supporting the asymmetric anionic PNNP' ligand system in **4**.

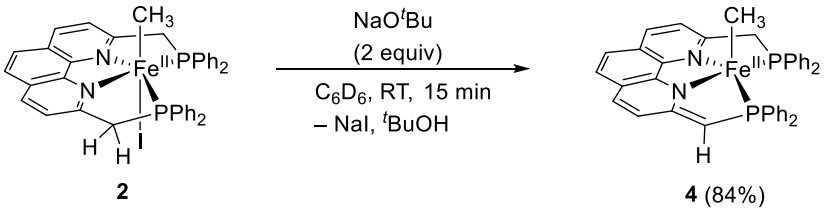

Scheme 11. Reaction of **2** with NaO*t*Bu.

Motivated by the formation of **4** with the dearomatized PNNP' ligand, we next set out to examine the bond cleavage ability of **4** since aromatization and dearomatization sequence of the pyridine ring in the ligand scaffold are known as a powerful tool to cleave various bonds via metal-ligand cooperation (MLC).[14] It was revealed that **4** smoothly reacted with H_2 at room temperature. Thus, treatment of C_6D_6 solution of **4** with H_2 (1 atm) immediately resulted in the color change of the reaction mixture to dark green, and formation of methyl hydrido complex [Fe(CH$_3$)(H)(PNNP)] (**5**) was confirmed after 20 min in 39% NMR yield (Scheme 12), which is accompanied by the formation of several unidentified products.

Isolation of **5** from the reaction mixture was not successful at this moment, and **5** was identified by ^{1}H, $^{13}C\{^{1}H\}$ and $^{31}P\{^{1}H\}$ NMR as well as two-dimensional NMR studies. Complex **5** exhibits one sharp singlet at δ 91.0 ppm in $^{31}P\{^{1}H\}$ NMR. Thus, occurrence of the re-aromatization of the PNNP' ligand to form a symmetric PNNP structure was supported. The hydrido ligand was observed in a typical high field region at δ –8.43 ppm as a triplet due to the coupling with two phosphorus atoms. The benzylic protons were observed at δ 4.49 and δ 4.14 ppm as diastereotopic doublets with the integral intensity of 2H, respectively. The result supports the occurrence of H–H bond cleavage, which is associated with the re-aromatization of the phenanthroline backbone in **5**.

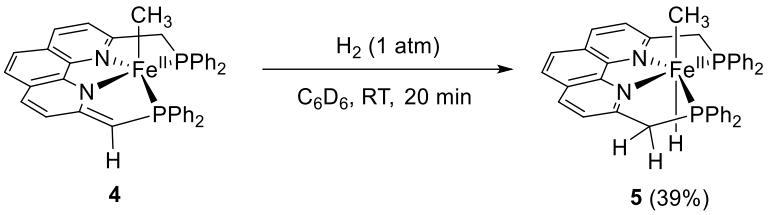

Scheme 12. Reaction of **4** with H_2.

Conclusion

In summary, a well-defined bond cleavage reaction was demonstrated using the PNNP-Fe system. PNNP-Fe(0) complex **1** achieved facile C–I bond cleavage of CH_3I. The resulting oxidative addition product **2** was isolated, and the structure was fully determined. Radical clock reaction supported the occurrence of the oxidative addition reaction via radical pathway for the C–I bond cleavage. Complex **2** underwent deprotonation to form **4** bearing a dearomatized PNNP ligand. Complex **4** reacted with H_2 to cleave H–H bond, which is facilitated by re-aromatization of the phenanthroline backbone. This is, to the best of our knowledge, the first example of a well-defined example of bond cleavage via metal-ligand cooperation of the PNNP-Fe system.

Experimental section

General Consideration

All experiments were carried out under nitrogen atmosphere using Schlenk techniques or a glovebox. *n*-Hexane, tetrahydrofuran, C_6H_6, toluene, and dichloromethane were purified by a solvent purification system (MBraun SPS -800 or a Glass Contour Ultimate Solvent System). Toluene-d_8, benzene-d_6, and THF-d_8 were dried over sodium benzophenone ketyl and distilled before use. CD_2Cl_2 was dried over CaH_2 and dilled. [$FeCl_2$(PNNP)] and [{Fe(PNNP)}$_2$(μ-N_2)] (**1**) were synthesized by following the reported procedure.[9b] CH_3I and cyclopropylmethyl bromide were dried over CaH_2 and distilled before use, All other reagents were purchased from commercial suppliers and used without purification. ^{1}H, ^{13}C{^{1}H}, and ^{31}P{^{1}H} NMR spectra (^{1}H, 600 MHz; ^{13}C, 150 MHz; ^{29}Si, 119 MHz; ^{31}P, 243 MHz) were recorded on a Bruker AVANCE III HD 600 spectrometer. Chemical shifts are reported in δ (ppm) and referenced to the residual solvent signals for ^{1}H and ^{13}C and 85% H_3PO_4 as an external standard for ^{31}P. The high-resolution ESI mass spectra were obtained on a Bruker microTOF II. Gas Chromatographic (GC) analyses were performed on a Shimadzu GC-2014 using an InertCap-1 column (0.25 mm × 30 m, GL Sciences Inc.).

Synthesis of 2

Complex **1** was prepared by the reaction of [$FeCl_2$(PNNP)] (50.0 mg, 0.072 mmol) with $LiBEt_3H$ (1.7 M/THF, 0.084 mL, 0.14 mmol) in C_6H_6 (5 mL). After the filtration of the reaction mixture, CH_3I (40.3 mg, 0.28 mmol) was added to the solution at room temperature. The solution was stirred for 2 h, and all the volatiles were removed *in vacuo*. The resulting solid was washed with hexane (3 mL) and dried under vacuum to give **2** (46.5 mg, 0.060 mmol, 85%). A green crystal of **3** was obtained from saturated C_6H_6 solution of **2** at ambient temperature.

Spectrum of **2**: ^{1}H NMR (600 MHz, THF-d_8, 25 °C) δ 8.12 (d, 2H, $^3J_{HH}$ = 8.1 Hz, phen), 7.96 (d, 2H, $^3J_{HH}$ = 8.1 Hz, phen) 7.89 (s, 2H, phen), 7.71 (br, 4H, Ph), 7.30-7.26 (m, 6H, Ph), 7.18-7.14 (m, 10H, Ph), 4.93 (br, 4H, PCH_2), –2.22 (t, 3H, $^3J_{HP}$ = 6.9 Hz) ppm. ^{31}P{^{1}H} NMR (243 MHz, THF-d_8, 25 °C) δ 78.2 (s) ppm. ^{13}C{^{1}H} NMR (150 MHz, THF-d_8, 25°C): δ (ppm) 164.0 (s, phen), 149.9 (s, phen), 139.4 (t, $^1J_{CP}$ = 12.6 Hz, Ph), 138.4 (t, $^1J_{CP}$ = 15.7 Hz, Ph), 135.7 (t, $^2J_{CP}$ = 4.6 Hz, Ph), 133.3 (t, $^2J_{CP}$ = 3.91 Hz , Ph), 129.4 (s, phen), 129.2 (s, Ph), 129.1 (s, Ph), 128.8 (s, phen), 127.9 (s, Ph×2), 127.5

(s, Ph), 126.1 (s, phen) 119.7 (s, phen), 48.4 (dd, $^{1}J_{CP}$ = 12.6 Hz, CH_2P), 6.9 (t, $^{2}J_{CP}$ = 19.2 Hz, $FeCH_3$). ^{1}H-^{1}H COSY (THF-d_8, 25°C): δ_H-δ_H 8.12 to 7.96, 7.71 to 7.30-7.26, 7.71 to 7.18-7.14, 7.30-7.26 to 7.18-7.14. ^{1}H-^{13}C HSQC (THF-d_8, 25°C): δ_H-δ_C 8.12-128.8, 7.96-119.7, 7.89-126.1, 7.71-135.7, 7.26-133.3, 7.28-129.2, 7.15-127.9, 7.14-127.5.

Elemental analysis data of **2**: Calc. for $C_{39}H_{33}FeIN_2P_2$: C, 60.49; H, 4.30; N, 3.62; Found: C, 60.10; H, 4.32; N, 3.70.

Reaction of 1 with cyclopropylmethyl bromide

Complex **1** was *in-situ* prepared by the reaction of [$FeCl_2$(PNNP)] (5.0 mg, 0.0071 mmol) with $LiBEt_3H$ (1.7 M/ THF, 0.0082 mL, 0.014 mmol) in toluene-d_8 (0.6 mL) and filtered. To the solution, were added cyclopropylmethyl bromide (4.0 mg, 0.029 mmol) and mesitylene (2.0 mg, 0.016 mmol) as an internal standard. The reaction was followed by ^{1}H NMR. Complex **1** was completely consumed at 263 K for 15 min. In the ^{31}P NMR spectrum, a new singlet signal appeared at δ 77.3 ppm. Formation of 1-butene (0.0032 mmol, 11%) was confirmed by ^{1}H NMR. 1-butene was also identified by GC by comparing the retention time with the authentic sample. The reaction mixture was kept at room temperature overnight, and **3** was formed as red crystals (2.5 mg, 0.0030 mmol, 44%).

Spectrum of 1-butene: ^{1}H NMR (600 MHz, toluene-d_8, –10 °C) 5.74-5.70 (m, 1H), 4.91 (d, 1H, $^{3}J_{HH}$ = 17.6 Hz), 4.88 (d, 1H, $^{3}J_{HH}$ = 10.1 Hz), 1.8* (m, 2H), 0.88 (t, 3H, $^{3}J_{HH}$ = 7.5 Hz). ^{1}H-^{1}H COSY (toluene-d_8, –10 °C): δ_H-δ_H 5.74-4.91, 5.74-4.88, 5.74-1.8, 1.8-0.88. *the signal position was determined by ^{1}H-^{1}H COSY NMR

Spectrum of **3**: ^{1}H NMR (600 MHz, CD_2Cl_2): δ 49.54 (br), 37.02 (br), 24.38 (br), 19.60 (br), 17.03 (s), 12.26 (br), 11.12 (br), 10.14 (s), 7.32(s), 6.97 (br), 4.03 (br), 2.52 (br), –6.83 (br).

Elemental analysis data of **3**: Calc. for $C_{38}H_{30}Br_2FeN_2P_2$: C, 57.61; H, 3.82; N, 3.54; Found: C, 58.25; H, 3.56; N, 3.49.

Synthesis of 4

2 (5.0 mg, 0.0064 mmol) was dissolved in C_6D_6 (0.6 mL). To the solution, NaO^tBu (1.2 mg, 0.013 mmol) were added at room temperature, and the solution was filtered. To a reaction mixture, mesitylene (0.001ml, 0.0072 mmol) as an internal standard was added. Formation of **4** (84%) was confirmed by ^{1}H NMR spectra. The reaction of **2** (4.0 mg, 0.0052 mmol) with NaO^tBu (1.0 mg, 0.010 mmol) was also performed in THF-d_8 (0.6 mL), and **4** was identified ^{1}H, $^{31}P\{^{1}H\}$, $^{13}C\{^{1}H\}$ NMR, ^{1}H-^{1}H COSY and ^{1}H-^{13}C HSQC spectra. Complex **4** started to be decomposed within a few hours at

ambient temperature. Complex **4** also decomposed immediately decomposed under vacuum to form complicated mixture.

Spectrum of **4**: ^{1}H NMR (600 MHz, THF-d_8 25 °C) δ 7.85 (d, 1H, phen, $^{3}J_{HH}$ = 7.9 Hz), 7.55 (d, 1H, phen, $^{3}J_{HH}$=8.5 Hz), 7.48 (br, 4H, Ph), 7.39 (br, 4H, Ph), 7.33-7.31 (m, 6H, Ph), 7.20-7.18 (m, 6H, Ph), 7.2* (1H, phen), 7.04 (d, 1H, phen, $^{3}J_{HH}$ = 9.0 Hz), 6.83 (d, 1H, phen, $^{3}J_{HH}$ = 7.9 Hz), 6.75 (d, 1H, phen, $^{3}J_{HH}$ = 8.7 Hz), 4.52 (d, 1H, PCH_2, $^{2}J_{HP}$ = 17.2 Hz),), 4.38 (d, 1H, $^{2}J_{HP}$ = 17.2 Hz), 4.32 (s, 1H, PCH), –0.52 (br, 3H, $FeCH_3$) ppm. ^{31}P {^{1}H} NMR (243 MHz, THF-d_8 25 °C) δ 78.1 (br), 65.6 (br) ppm. ^{13}C{^{1}H} NMR (150 MHz, THF-d_8 , –10 °C) : δ 167.3 (d, $^{2}J_{CP}$ = 22.1 Hz), 159.1 (d, J_{CP} = 7.9 Hz), 152.0 (d, J_{CP} = 5.8 Hz), 147.1 (d, J_{CP} = 5.6 Hz), 139.9 (d, J_{CP} = 39.4 Hz), 138.6 (d, J_{CP} = 40.3 Hz), 138.2 (d, J_{CP} = 30.3 Hz), 135.4 (d, J_{CP} = 39.5 Hz), 134.3 (d, J_{CP} = 10.9 Hz), 133.8 (m, ×2), 133.1 (m, ×3), 132.6, 130.0, 129.9, 129.6, 129.4, 128.9 (m, ×2), 128.5 (m, ×2), 127.9 (d, J_{CP} = 8.4 Hz), 127.7 (d, J_{CP} = 8.4 Hz), 127.2, 126.8, 126.3, 120.5, 119.2, 118.6 (d, J_{CP} = 16.7 Hz), 112.1 (s, Phen), 73.8 (PCH), 48.6 (PCH_2), 5.6 (br, $FeCH_3$) *the signal was determined by ^{1}H-^{1}H COSY. ^{1}H-^{1}H COSY (THF-d_8, 25 °C): δ_H-δ_H 7.85 to 7.55, 7.2 to 6.83, 7.04 to 6.75, 7.48 to 7.20-7.18, 7.39 to 7.33-7.31.

Synthesis of 5

Complex **5** was *in-situ* prepared by the reaction of **2** (12.0 mg, 0.015 mmol) with NaO^{t}Bu (3.0 mg, 0.031 mmol) in C_6D_6 (0.5 mL). To this solution, mesitylene (2 μL, 0.014 mmol) as an internal standard. The solution was frozen at –196˚ C, and H_2 (1 atm) was introduced into the solution at room temperature. The solution was kept for 20 min at the temperature. Formation of **5** as well as unidentified complexes was confirmed by ^{1}H NMR spectroscopy. After the filtration, some of the impurities were removed, and the solution exhibited rather clear sharp signals in the ^{1}H NMR spectrum. Formation of **5** in 39 % NMR yield was confirmed.

Spectra of **5**: ^{1}H NMR (600 MHz, C_6D_6 , 25°C) δ 7.74 (br, 4H, Ph), 7.44 (br, 2H, Ph), 7.39 (s, 2H, Phen), 7.36-7.32 (br, 4H, Phen+Ph) 7.16 (2H, Phen)*, 7.05-7.00 (m, 12H, Ph), 4.49 (d, 2H, PCH_2, $^{2}J_{HP}$ =18.6 Hz), 4.14 (d, 2H, PCH_2 $^{2}J_{HP}$ =18.6 Hz), –0.97 (t, 3H, Fe-CH_3, $^{2}J_{HP}$ = 6.3 Hz), –8.43 (t, Fe-H, $^{2}J_{HP}$ = 68.6 Hz). ^{13}C{^{1}H} NMR (150 MHz, C_6D_6, 25 °C) δ 160.0 (phen), 145.4 (phen), 138.7 (Ph), 133.7 (Ph ×2), 133.0 (Ph), 125.7 (phen), 120.8 (phen), 114.9 (phen), 48.7 (dd, $^{1}J_{CP}$ =10.9 Hz), 3.8 (t, $^{2}J_{CP}$=19.5, Fe-CH_3). *the signal position was determined by COSY. Two phen signals and three Ph signals are obscured in the residual benzene signal. ^{31}P{^{1}H} NMR (243 MHz, C_6D_6, 25°C) δ 91.0 (s). COSY (C_6D_6, 25 °C): 7.74 to7.00-7.05, 7.44 to 7.00-7.05, 7.36 to 7.16. HSQC (C_6D_6, 25°C): 7.74-

133.3, 7.44-133.3, 7.39-114.5, 7.36-132.7,125.2.

ESI: m/z calcd for $[C_{39}H_{33}FeN_2P_2]^+$ (M–H): 647.1468 ; found 647.1464

Single crystal X-ray diffraction studies.

The single crystal X-ray diffraction measurement of **3** and **4** was performed under a cold nitrogen stream on a Rigaku XtaLAB P200 diffractometer with a Pilatus 200 K detector using multilayer mirror monochromated Mo Kα radiation. The determination of crystal system and unit cell parameters and data processing were performed with the CrystalClear program package [15]. All structures were solved by direct method using the SHELXS97 program[16] and refined by full-matrix least squares calculations on F^2 for reflections (SHELXL-2014/7)[17] using the CrystalStructure 4.2 program.[18] CCDC-1961638 (**2**), 1961639 (**3**) contain the supplementary crystallographic data for this paper. These data can be obtained free of charge from The Cambridge Crystallographic Data Centre via www.ccdc.cam.ac.uk/data_request/cif.

Table S1. Crystallographic parameters for **2** and **3**

	2	**3**
Empirical formula	$C_{45}H_{39}FeIN_2P_2$	$C_{38}H_{30}Br_2FeN_2P_2$
Formula weight	852.52	792.27
Temperature	93(2) K	93(2) K
Crystal system	monoclinic	monoclinic
Space group	$P2_1/n$ (#14)	$P2_1/c$ (#14)
a/Å	14.376(3) Å	11.952(3) Å
b/Å	15.381(4) Å	20.775(6) Å
c/Å	16.904(4) Å	14.131(4) Å
α/deg	90°	90°
β/deg	93.737(5) °	106.443(6) °
γ/deg	90°	90°
Volume	3729.8(15) Å^3	3365.1(17) Å^3
Z	4	4
Density (calculated)	1.518 g/m^3	1.564 g/m^3
F(000)	1728.00	1592.00
Goodness-of-fit on F^2	1.025	1.053
Final R indices [I>2(I)]	$R1$ = 0.0744, $_wR2$ = 0.1712	$R1$ = 0.0805, $_wR2$ = 0.1339
R indices (all data)	$R1$ = 0.1111, $_wR2$ = 0.1405	$R1$ = 0.1855, $_wR2$ = 0.1688

References

1. (a) Vaska, L.; DiLuzio, J. W. *J. Am. Chem. Soc*. **1961**, *83*, 2784-2785. (b) Collman, J. P.; Roper, W. R. *J. Am. Chem. Soc.* **1965**, *87*, 4008-4009. (c) Labinger, J. A. *Organometallics* **2015**, *34*, 4784- 4795.
2. (a) Espinet, P.; Echavarren, A. M. *Angew. Chem., Int. Ed.* **2004**, *43*, 4704. (b) Miyaura, N.; Suzuki, A. *Chem. Rev.* **1995**, *95*, 2457. (c) Satoh, T.; Kawamura, Y.; Miura, M.; Nomura, M. *Angew. Chem., Int. Ed*., 1997, **36**, 1740. (d) Maitlis, P. M.; Haynes, A.; Sunley, G. J.; Howard, M. J., *J. Chem. Soc*. *Dalton Trans*. **1996**, 2187-2196. (e) Haynes, A.; Maitlis, P. M.; Morris, G. E.; Sunley, J. G.; Adams, H.; Badger, W. P.; Bowers, M. C.; Cook, B. D.; Elliott, I. P.; Ghaffar, T.; Green, H.; Griffin, R. T.; Payne, M.; Pearson, M. J.; Vickers, W. P.; Watt, R. *J. Am. Chem. Soc*. **2004**, *126*, 2847-2861.
3. (a) Pearson, R. G.; Muir, R. *J. Am. Chem. Soc*. **1970**, *92*, 5519-5520. (b) Stille, J. K.; Kreisler, *Acc. Chem. Res*. **1977,** *10*, 434-441. (c) Lau, K. S. Y.; Wong, P. K.; Stille, J. K. *J. Am. Chem. Soc*. **1976**, *98*, 5832-5840. (d) Becker, Y.; Stille, J. K. *J. Am. Chem. Soc*. **1978**, *100*, 838-844. (e) Crespo, M.; Puddephatt, R. J. *Organometallics*, **1987**, *6*, 2548-2550. (f) Monaghan, P. K.; Puddephatt, R. J. *J. Chem. Soc., Dalton Trans.* **1988**, 595-599. (g) Rendina, L. M.; Puddephat, R. J. *Chem. Rev.*, **1997**, *97*, 1735-1753. (h) Labinger, J. A.; Osborn, J. A.; Coville, N. J. *Inorg. Chem.*, **1980**, *19*, 3236-3243. (i) Basson, S. S.; Leipoldt, J. G.; Nel, J. T. *Inorganica Chimica Acta*, **1984**, *84*, 161-112.
4. (a) Krusic, P. J. *J. Am. Chem. Soc.*, **1977**, *99*, 250-252. (b) Hill, D. H.; Panez, M. A.; Sen, A. *J. Am. Chem. Soc*. **1994**, *116*, 2889-290. (c) Hill, D. H.; Sen, A. *J. Am. Chem. Soc*, **1988**, *110*, 1650-1652.
5. (a) Kleimark, J.; Hedstrçm, A.; Larsson, P.; Johansson, C.; Norrby, P. *ChemCatChem*, **2009**, *1*, 152-16. (b) Dongol, K. G.; Koh, H.; Sau, M.; Christina, L. L. *Adv. Synth. Catal*. **2007**, *349*, 1015-1018. (c) Martin, R.; Fürstner, A. *Angew. Chem. Int. Ed*. **2004**, *43*, 3955-3957. (d) Gurinot, A.; Reymond, S.; Cossy, J. *Angew. Chem. Int. Ed*. **2007**, *46*, 6521-6524. (e) Hedstrçm, A.; Bollmann, U.; Bravidor, J.; Norrby, P. *Chem. Eur. J.* **2011**, *17*, 11991-11993. (f) Bedford, R. B.; Bruce, D. W.; Frostc, R. M.; Hird, M. *Chem. Commun.*, **2005**, 4161-4163. (j) Qian, X.; Daweb, L. N.; Kozak, C. M. *Dalton Trans*., **2011**, *40*, 933. (k) Xue, F.; Zhao, J.; Andy-Hor, T. S. *Dalton Trans.*, **2011**, *40*, 8935. (l) Weber, K.; Schnçckelborg, E.; Wolf, R. *ChemCatChem.* **2011**, *3*, 1572-1577. (m) Hatakeyama, T.; Yoshimoto, Y.; Gabriel, T.;

Nakamura, M. *Org. Lett.*, **2008**, *10*, 5341-5345. (n) Meyer, S.; Orben, C. M.; Demeshko, S.; Dechert, S.; Meyer, F. *Organometallics*, **2011,** *30***,** 6692-6702. (o) Adams, C. J.; Bedford, R. B.; Carter, E.; Nicholas, J.; Haddow, M. F.; Harvey, J. N.; Huwe, M.; Cartes, M. Á.; Mansell, S. M.; Mendoza, C.; Murphy, D. M.; Neeve, E. C.; Nunn, J. *J. Am. Chem. Soc.* **2012**, *134*, 10333-10336. (p) Valle´e, F.; Mousseau, J.; Charett, A. B. *J. Am. Chem. Soc.* **2010**, *132*, 1514-1516.

6. (a) Smith, R. S.; Kochi, J. K. *J. Org. Chem.*, **1976**, *41*, 502-509. (b) Kochi, J. K. *Journal of Organometallic Chemistry*, **2002**, 11-19. (c) Kwan, C. L.; Kochi, J. K. *J. Am. Chem. Soc*., **1976**, *98*, 4903-4912. (d) Tamura, M.; Kochi, J. K. *J. Am. Chem. Soc*., **1971**, *93*, 1487-1489. (e) Tamura, M.; Kochi, J. K. *J. Organometal. Chem.*, **1971**, *31*, 289-309.
7. (a) Noda, D.; Sunada, Y.; Hatakeyama, T.; Nakamura, M.; Nagashima, H. *J. Am. Chem. Soc.* **2009**, *131*, 6078-6079. (b) Hatakeyama, T.; Hashimoto, T.; Kondo,Y.; Fujiwara, Y.; Seike, H.; Takaya, H.; Tamada, Y.; Ono, T.; Nakamura, M. *J. Am. Chem. Soc.*, **2010**, *132*, 10674-10676. (c) Hatakeyama, T.; Fujiwara, Y.; Okada, Y.; Itoh, T.; Hashimoto, T.; Kawamura, S.; Ogata, K.; Takaya, H.; Nakamura, M. *Chem. Lett.* **2011**, *40*, 103.
8. (a) Fürstner, A.; Martin, R.; Krause, H.; Seidel, G.; Goddard, R.; Lehmann, C. W. *J. Am. Chem. Soc*. **2008**, *130*, 8773-8787. (b) Sherry, B. D.; Fürstner, A. *Acc. Chem. Res.* **2008**, *41*, 1500-1511. (c) Cahiez, G.; Duplais, C.; Moyeux, A. *Org. Lett.*, **2007**, *9*, 3253-3254. (d) Neidig, M. L.; Carpenter, S. H.; Curran, D. J.; DeMuth, J. C.; Fleischauer, V. E.; Iannuzzi, T. E.; Neate, G. N.; Sears, J. D.; Wolford, N. J. *Acc. Chem. Res.* **2019**, *52*, 140-150.
9. (a) Ziessel, R. *Tetrahedron Lett*., **1989**, *30*, 463-466. (b) Takeshita, T.; Sato, K.; Nakajima, Y. *Dalt. Trans*. **2018**, 47, 17004–17010. (c) Takeshita, T.; Nakajima, Y. *Chem. Lett.* **2019**, *48*, 364-366.
10. (a) Bouwkamp, M. W.; Bart, S. C.; Hawrelak, E. J.; Trovitch, R. J.; Lobkovsky, E.; Chirik, P. J. *Chem. Commun.* **2005**, 3406-3408. (b) Trovitch, R. J.; Lobkovsky, E.; Chirik, P. J. *Inorg. Chem*. **2006**, *45*, 7252-7260. (b) Langer, R.; Diskin-Posner, Y.; Leitus, G.; Shimon, L. J. W.; Ben-David, Y.; Milstein, D. *Angewandte, Chem. Int. Ed.* **2011**, *50*, 9948-9952. (c) Kuriyama, S.; Arashiba, K.; Nakajima, K.; Matsuo, Y.; Tanaka, H.; Ishii, K.; Yoshizawa, K.; Nishibayashi, Y. *Nat. Commun.* **2016**, *7*, 12181. (d) Thompson, C. V.; Arman, H. D.; Tonzetich, Z. J. *Organometallics* **2017**, *36*, 1795-1802. (e) Bellachioma, G.; Cardaci, G.; Macchioni, A.; Reichenbach, G.; Foresti, E.; Sabatino, P. *Journal of Organometallic Chemistry*, **1997**, *531*, 227-235.

11. Liu, K. E.; Johnson, C. C.; Newcomb, M.; Lippard, S. J. *J. Am. Chem. Soc.* **1993**, *115*, 939-947.
12. (a) Therien, M. J.; Ni, C. L.; Anson, F. C.; Osteryoung, J. G.; Trogler, W. C. *J. Am. Chem. Soc.* **1986**, *108*, 4037-4042. (b) Lin, Y.-F.; Ichihara, N.; Nakajima, Y.; Ozawa, F. *Organometallics*, **2014**, *33*, 6700-6703. (c) Witzke, R. J.; Haite, D.; Head-Gordon, M.; Tilley, T. D. *Organometallics* **2021**, *40*, 1758.
13. J. A. Dean in *Lange's Handbook of Chemistry 15th Ed, McGraw-Hill, Inc.,* **1999**, pp. 4.35-4.46.
14. (a) Gunanathan, C.; Milstein, D. *Acc. Chem. Res.* **2011**, *44*, 588-602. (b) Gunanathan, C.; Milstein, D. *Science* **2013**, *341*, 1229712. (c) Gunanathan, C.; Milstein, D. *Chem. Rev.* **2014**, *114*, 12024-12087. (d) Khusnutdinova, J. R.; Milstein, D. *Angew. Chem. Int. Ed.* **2015**, *54*, 12236-12273. (e) van der Vlugt, J. I. *Eur. J. Inorg. Chem.* **2012**, 363-375. (f) Ozawa, F.; Nakajima, Y. *Chem. Rev.* **2016**, *16*, 2314-2323. (g) Higashi, T.; Kusumoto, S.; Nozaki, K. *Chem. Rev.* **2019**, *119*, 10393-10402.
15. *Crystal Clear*; Rigaku Corp., The Woodlands, TX, USA, 2011.
16. Sheldrick, G. M. SHELXT-Integrated Space Group and Crystal-Structure Determination. *Acta Crystallogr., Sect. A: Found. Adv*. **2015**, 71, 3-8
17. Sheldrick, G. M. A. Short History of SHELX. *Acta Crystallogr*., Sect.A: *Found. Crystallogr*. **2008**, 64, 112-122
18. Crystal Structure Analysis Package, Rigaku Corporation (2000-2015). Tokyo 196-8666, Japan.

Chapter 3

Reactivity Investigation of PNNP-Fe Hydrides

Abstract

An iron hydride complex bearing a phenanthroline-based PNNP-Cy ligand [Fe(H)$_2$(PNNP-Cy)] (**1**) reacted with benzophenone and azobenzene, resulting in the formation of [Fe(OCHPh$_2$)(PNNP'-Cy)] (**2**) and [Fe(NPhNHPh)(PNNP'-Cy)] (**3**), respectively. Through these reactions, the hydride and the benzylic H atom were transferred to the ligand backbone, leading to partial dearomatization of the phenanthroline moiety. In a similar manner, treatment of *t*-butyl dimethyl silanol leads to protonation with concomitant of long-range metal ligand cooperation to form [Fe(OSi(Me)$_2$(C$_4$H$_9$))(PNNP'-Cy] (**4**). All these complexes were fully identified by a single crystal X-ray diffraction and elemental analysis.

Introduction

In 1931, first transition metal hydride [$Fe(CO)_4(H)_2$] was discovered by Hieber and Leutert.[1a] Since then, synthesis and reactivity studies of irons metal hydrides have remained an active area of chemical research. Iron metal hydride serves as a key intermediate in various catalytic reactions and biological reacions.[1] For instance, Holland group synthesized iron hydride complexes bearing a β-diketiminates ligand for study of their reactivity patterns, which mimic to FeMo-cofactor of nitrogenase.[1k] However, the detailed reactivity investigation, which is essential for the development of high-performance catalysts of iron complex catalysts, is often hampered due to their thermal instability as well as the complicated paramagnetic nature. Thus, study of well-defined iron complex system is essential to get more insights of their catalytic application in the homogeneous catalysis. Recently, iron pincer systems have gained interest in the development of well-defined iron systems for industrial application and biocatalytic activities since pincer ligands can offer a stable reaction sphere through rigid meridional ligand with an iron metal.[2] By modulating the pincer-iron platform, recently the concept of MLC was also introduced in the pincer-iron chemistry.[3] Through these study, a variety of pincer ligands have been thus far synthesized and implemented in iron hydride systems, however, examples of well-defined iron hydride complexes are still limited.[4] Conventional MLC behavior was studied based on amine/amido (Scheme 1a) and aromatization/dearomatization based on pincer PNP ligand (Scheme 1b). For instance, Morris group reported an amine/amido iron pincer system and involvement of an "NH-effect", which accelerates the bond activation of substrates (Scheme 1a).[3i, 5] The "NH-effect" can be explained as it possesses cooperative effect of an N–H functionality and the metal center, which is responsible for the bond activation of substrate as mentioned in Chap 1. Milstein's group revealed a reversible aromatization/dearomatization sequence in pyridine-based PNP/PNN ligand systems, and it was applied to PNP-Fe systems for hydrogenation of ketones (Scheme 1b).[6a-b]

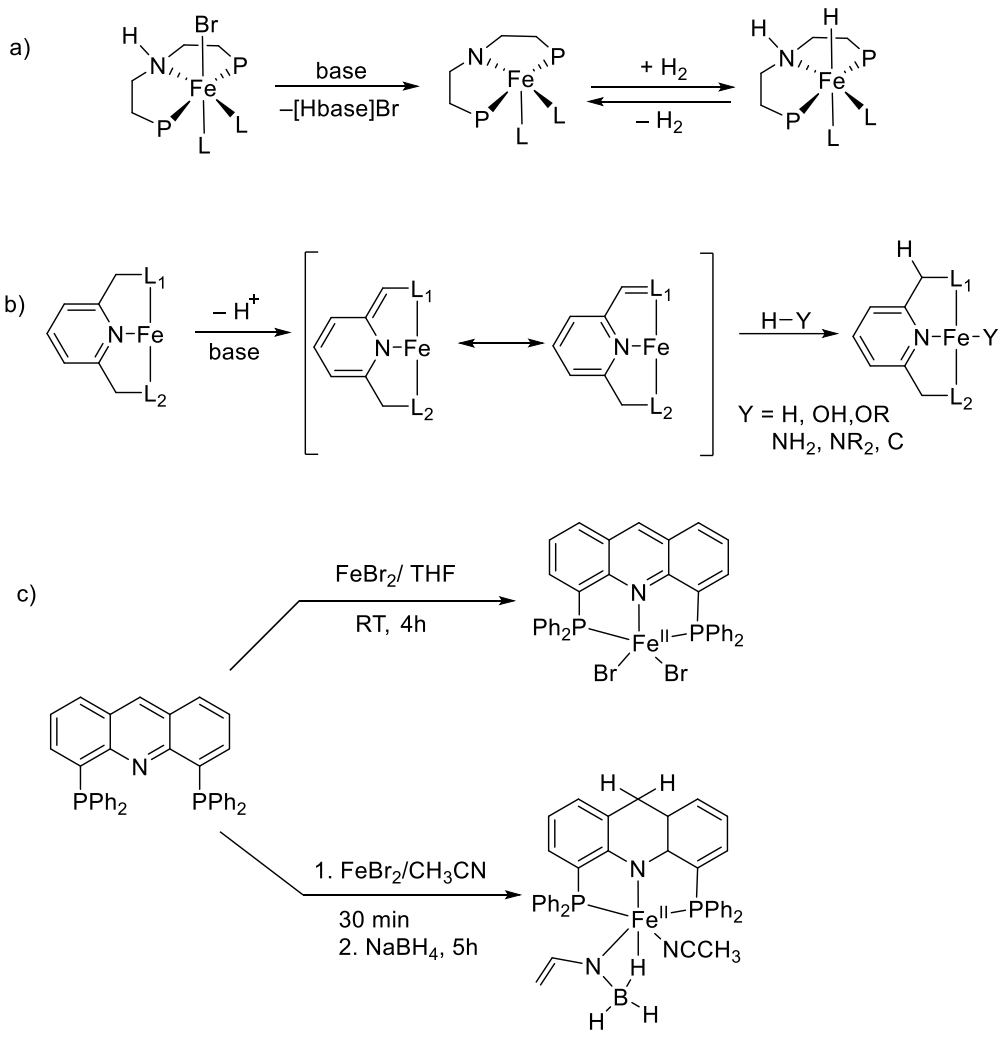

Scheme 1. Iron pincer hydride involved in MLC (a) amine/amido based pincer complex[5], (b) PNP/PNN pincer-based complex[6a-b], (c) acridine based pincer complex.[6c]

In recent years, novel long-range MLC could also be observed in different kinds of pincer ligand systems such as acridine-based PNP[8] and tetradentate PNNP[7a, b] (2,9 bis((diphenylphosphino)methyl)-1,10-phenanthroline). In iron acridine complex, dearomatization occurs at the C9 position of acridine in the presence of $NaBH_4$. The acridine-based iron catalysts were revealed to take part in the catalytic reaction for selective hydrogenation of alkynes to alkenes (Scheme 1c). To get insights into the acridine-based long-range MLC, Milstein and co-workers synthesized a series of transition metal complexes of Fe, Co, Ni, Mn bearing an acridine pincer ligand and found that the complexes undergo dimerization via C–C coupling bond formation at the C9 position of the acridine backbone. The

different reaction conditions were employed based on metal centers to form dimer complex via generation of radical species on acridine. For example, Ni dimer complex can be prepared by using Na/Hg as a reductant while Mn dimer can be prepared in the presence of strong base KO*t*Bu. (Scheme 2).[9]

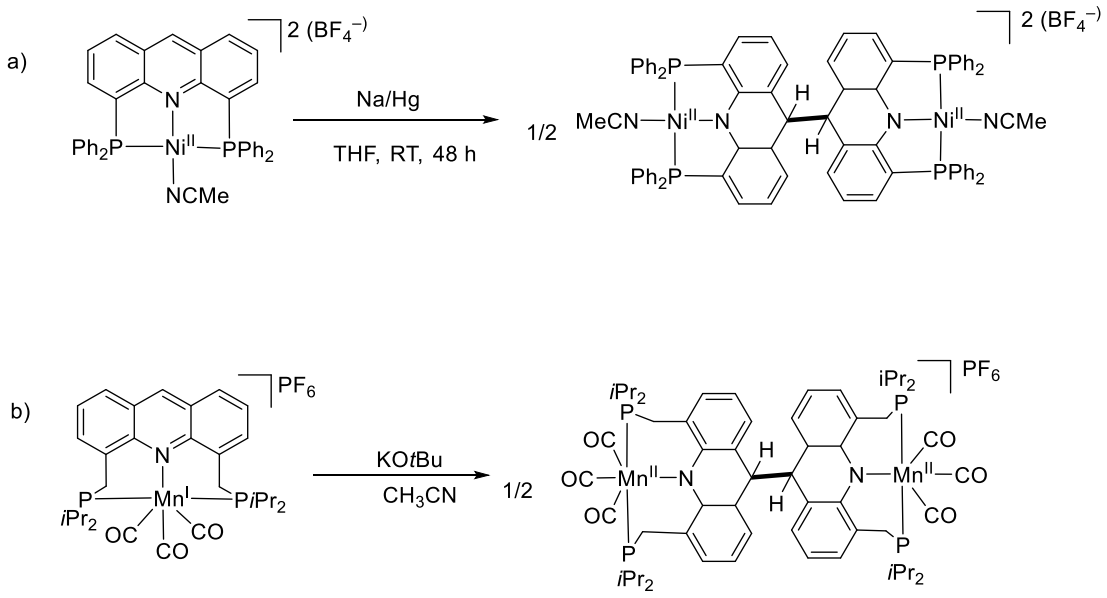

Scheme 2. Synthesis of (a) nickel dimers of acridine-based complexes (b) manganese dimers of acridine-based complexes.[9]

In the case of a Co complex, treatment of complex **A** with $NaBEt_3H$ (1 equiv) lead to the formation of **B**, where two intermediates **I** and **II** were formed (*insitu* condition and confirmed by EPR spectroscopy) (Scheme 3a). They proposed one possible reaction path; formation of hydride intermediate **I** and successive homolysis of C9–H bond of the acridine backbone to form radical species **II** and H_2.[10] Intermediate **II** undergoes dimerization to give complex **B**.

They also reported that iron complex with an acridine-based PNP ligand forms the dimerized product (Scheme 3b). Different from the Co system, the dimer formation proceeded starting from $Fe(CO)_5$ and the acridine ligand under UV irradiation. They proposed one possible mechanism that a Fe(0) species **III** is once formed**,** then undergoes metal to ligand electron transfer to form **IV**, which finally undergoes dimerization to give **C** (Scheme 3b).

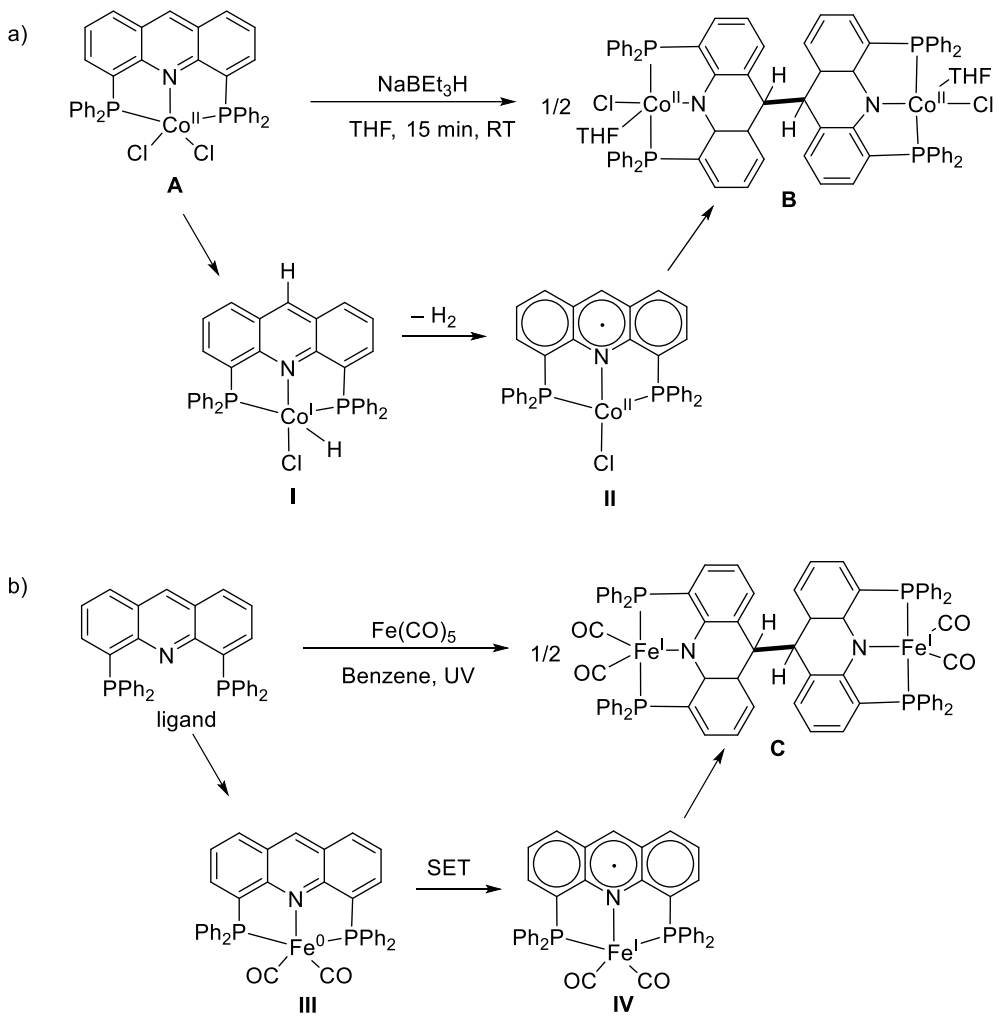

Scheme 3. Synthesis and mechanism of (a) cobalt dimers of acridine-based complexes (b) iron dimers of acridine-based complexes.[9]

PNNP-*t*Bu-Ru also exhibits unique long-range metal–ligand cooperation (MLC), where the hydride migrates to the endocyclic phenanthroline backbone (Scheme 4). In this system, the H atom was supplied by the hydride reagents, such as $NaBEt_3H$, or alcohol.

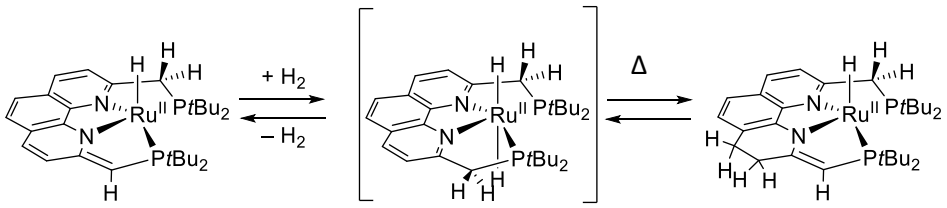

Scheme 4. Long-range MLC in Ru-PNNP complex.[7b]

Recently, our group revealed the similar long-range MLC in PNNP-Co system, where the phenanthroline backbone also behaves as a H atom acceptor. It should be mentioned that the reversible uptake of a molecular hydrogen via facile H–H cleavage was achieved in our PNNP-Co MLC system (Scheme 5). The mechanistic study supported that the observed MLC behavior of the PNNP-Co systems is based on the radical properties of Co complexes. Especially, inclusion of the occurrence of Co–H homolysis and/or benzylic C–H homolysis was demonstrated based on the mechanistic study using PNNP-Co alkyl analogues.[11b]

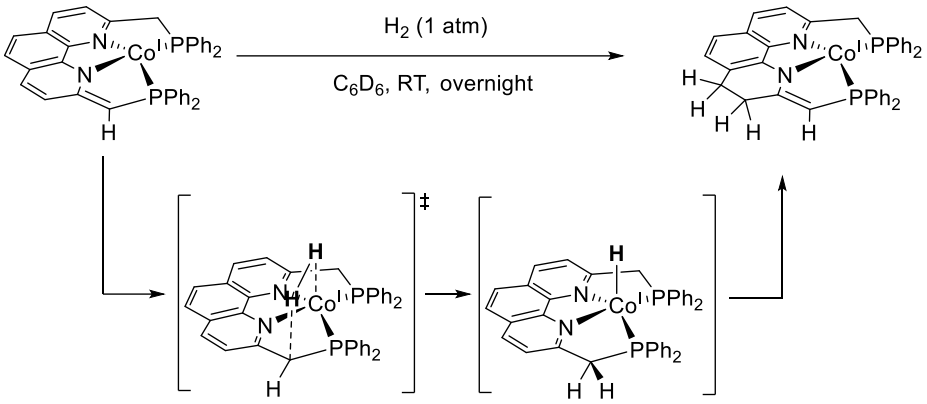

Scheme 5. H–H cleavage in Co-PNNP complex by long MLC.[11b]

In this study, I studied the reactivity of low spin (trans) Fe–H bearing a PNNP-R (R = Cy, *t*Bu) ligand [$Fe(H)_2$(PNNP-Cy)][11a]. It was found that [$Fe(H)_2$(PNNP-Cy)]) exhibits unique long-range MLC through insertion reactions with benzophenone and azobenzene, wherein insertion of unsaturated bonds into Fe–H bond proceeded associated with dearomatization of the phenanthroline backbone.

Results & Discussion

This study started with the preparation of [$Fe(H)_2$(PNNP-Cy)] (**1**) as described in the previously reported procedure by following the reaction of [$Fe(Br)_2$(PNNP-Cy)] and with $NaBEt_3H$ (2 equiv).[11] The reaction of [$Fe(H)_2$(PNNP-Cy)] (**1**) with benzophenone and azobenzene were carried out for reduction of these substrates. Complex **1** smoothly reacted with benzophenone at ambient temperature to afford insertion product [$Fe(OCHPh_2)$(PNNP'-Cy)] (**2)** in 81% isolated yield (Scheme 6). Interestingly, partial dearomatizarion of the phenanthroline backbone proceeded in this reaction. As

a result, **2** was supported by an unsymmetrical PNNP'-Cy, in which two phosphino-groups were connected to the ligand backbone via one methylene carbon and one exomethylene carbon, respectively. Complex **1** was also active towards N=N bond insertion. Reaction of **1** with 1.5 equiv of azobenzene (PhN=NPh) smoothly proceeded at room temperature to form the corresponding inserted product [Fe(NPhNHPh)(PNNP'-Cy)] (**3**) (Scheme 6). The reaction is again accompanied by the dearomatization of the ligand backbone, and thus **3** bears asymmetric PNNP'-Cy ligand. The reactivity nature of **1** resembles with fundamental steps proposed in the nitrogenase catalytic mechanism. For instance, reduction of N=N is recognized as a key step for NH_3 formation from N_2[17] although mechanistic study of N_2 reduction on the Fe catalyzed systems has been challenged so far by the high reactivity of Fe(NxHy) intermediates and their varied spin states. We believe that the isolated **3** provide important insight into the mechanism for N_2 reduction in a nitrogenase system.

Complexes **2** and **3** are a paramagnetic species and identified by elemental analysis. The structures of **2** and **3** were finally determined by a single crystal X-ray diffraction study. Complex **2** exhibits a distorted square pyramidal structure with an alkoxy ligand at the apical position (Figure 1a). The Fe–P bonds (2.5260(7) Å and 2.5013(7) Å) and Fe–N bonds (2.094(2) Å and 2.159(2) Å) are within the range of structurally analogous Fe(II) complexes with a high spin state.[12] The O1–C1 bond exhibits a typical single bond length, 1.393(3) Å. The bond angles around the C1 atom are ca. 109.9(2) °. Thus, the formation of alkoxide complex via hydride insertion was evidenced. The dihedral angle of N1–C15–C16–C17 is 30.1(4), supporting the dearomatization of the phenanthroline backbone. The C14–C15 bond (1.374 (4) Å) exhibits a double bond character and is significantly shorter than C20–C21 bond (1.484 (4) Å).

Similar to **2**, complex **3** also adopts a distorted square pyramidal structure (Figure 1b). Complex **3** exhibits similar Fe–P and Fe–N bond lengths as observed in **3**, supporting the oxidation state of iron (II) with a high spin state. The N–N bond lengths is 1.451(4)Å, which correspond to a single bond character. It is to be noted that the observed dearomatization of the phenanthroline ligand backbone during the above-mentioned reactions strongly supports the long-range metal-ligand cooperation behavior, where the hydride and the benzylic H atom are transferred to the ligand backbone. Such the structural transformation of the PNNP-R ligand was also reported in previously reported PNNP-Ph-Co system[11b] and PNNP-*t*Bu-Ru[7b] system. Although the mechanism of this behavior is not completely elucidated, the preliminary mechanistic study of the PNNP-Ph-Co system suggested the occurrence of homolysis of both Co–H and benzylic C–H bonds (Scheme 5). Thus, the observed long-range MLC

by **1** is also likely to proceed via a similar mechanism. The detailed mechanistic study is still underway to elucidate the process.

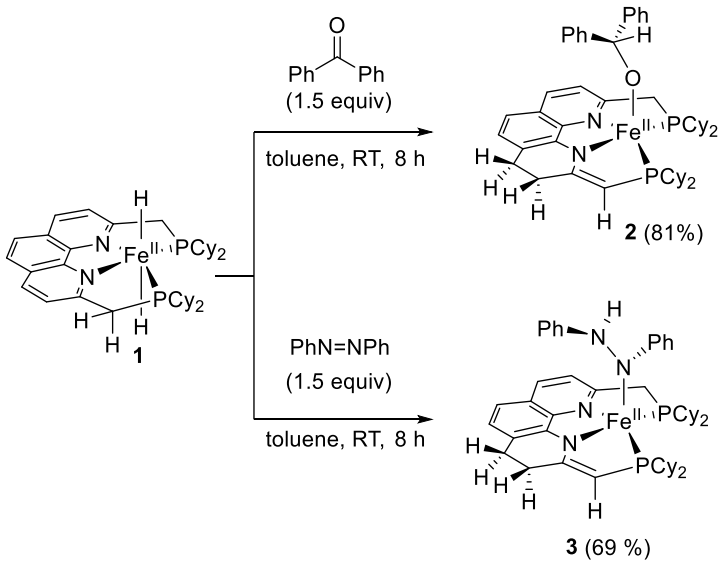

Scheme 6. Reaction of complex **1** with benzophenone and azobenzene.

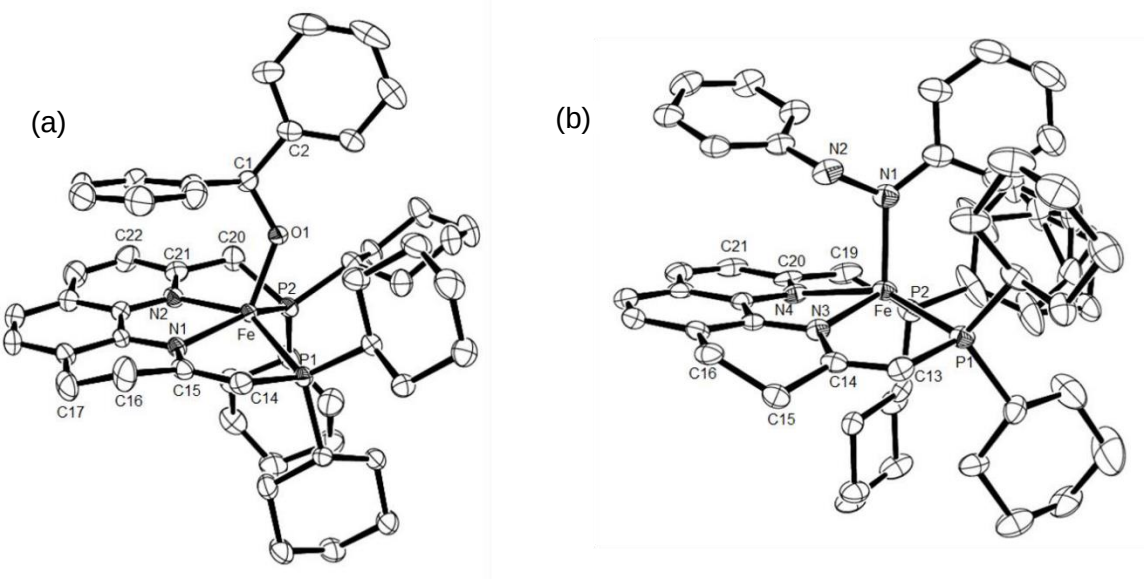

Figure 1. (a) ORTEP diagram of complex **2** with 50% probability thermal ellipsoids. All hydrogen atoms are omitted for clarity. Selected bond lengths[Å] and angles [˚]: Fe–P1 2.526(8), Fe–P2 2.501(8), Fe–N1 2.159(2), Fe–N2 2.104(2), Fe–O1 1.885(17), O1–C1 1.394(3), C14–C15 1.375(4), C15–C16 1.477(3), C16–C17 1.455(3), C20–C21 1.483(4); P1–Fe–N1 76.35(16), P1–Fe–N2 143.23(6), N1–Fe–N2 77.69(16), P1–Fe–P2 119.05(3), O1–C1–C2 109.9(2). (b) ORTEP diagram of

complex **3** with 50% probability thermal ellipsoids. All hydrogen atoms are omitted for clarity. Selected bond lengths[Å] and angles [˚]: Fe–P1 2.539(16), Fe–P2 2.519(14), Fe–N3 2.088(3), Fe–N4 2.211(3), Fe–N1 1.981(3), N1–N2 1.451(4), C13–C14 1.354(5), C14–C15 1.521(5), C15–C16 1.524(5), C19–C20 1.511(6); P1–Fe–N3 78.23(9), P1–Fe–N4 149.90(9), N3–Fe–N4 73.69(8), P1–Fe–P2 117.81(4), Fe1–N1–N2 110.9(2), N2–N1–C1 114.4(3), Fe1–N1–C1 129.0(3), N3– C14–C15–C16 –37.3(5).

Next, reaction of complexes **2** and **3** with H_2 gas (1 atm) were performed to achieve further hydrogenation of the substrates. However, hydrogenation reactions of complexes **2** and **3** weren't successful. In case of complex **2**, no reaction was observed whereas reaction of **3** with H_2 resulted in the formation of unidentified complexes and free ligand. The products were analyzed by using NMR spectroscopy. The ^{31}P NMR spectra of the obtained resultant exhibits one singlet signal at 2.6 ppm which confirmed the presence of PNNP-Cy. The isolated yield of PNNP-Cy was observed 75% from reaction mixture. (Scheme 7).

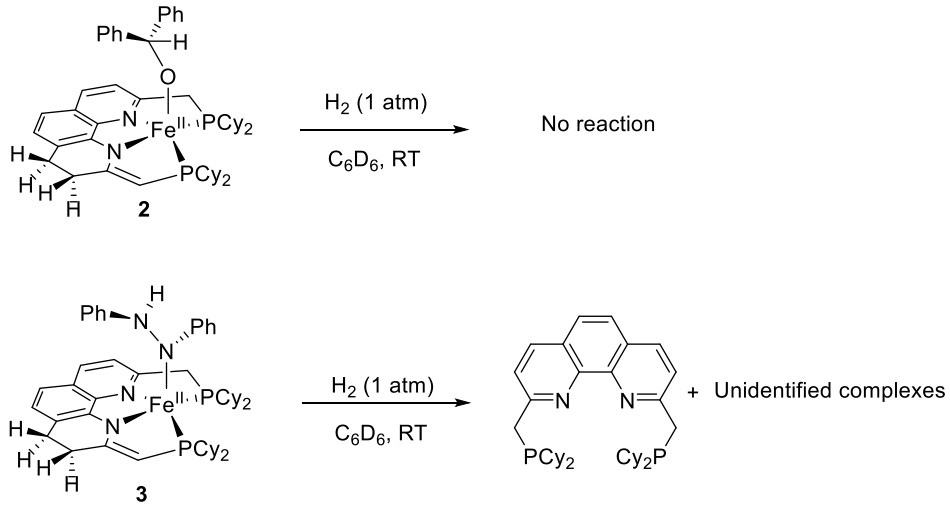

Scheme 7. Hydrogenation reaction of complex **2** and **3.**

Furthermore, reactivity of $[Fe(H)_2(PNNP\text{-}Cy)]$ towards Bronsted acids were examined. It was found that treatment of **1** with silanol (pK_a = 13.6)[14a] gave $[Fe(OSi(Me)_2(C_4H_9))(PNNP`\text{-}Cy)]$ (**4)** in 83% yield (Scheme 8). In this reaction, protonation proceeded with concomitant partial dearomatization of the phenanthroline backbone. The structure of **4** was characterized by X-ray diffraction and ^1H NMR spectroscopy. The geometry of complex around the iron center is best described as distorted square pyramidal (Figure 2a). The bond length of Fe–N1 (2.084(3)A and 2.191(3)A) and Fe–P (2.511(12) and 2.492(12)Å exhibits same pattern as in case of complex **2** and

complex **3** indicating high spin state Fe(II). The O1-Si1 exhibits single bond length is 1.612(3)Å and bond angles around Si1 is 108.7°. Complex **4** shows the dihedral angle N1–C3–C4–C5 44.5° (5) which is comparable to those of **2** and **3**, supporting the hydrogenated phenanthroline backbone. Hence, long-range MLC was also observed during the reaction of **1** with silanol. Conversely, reaction of **1** with more acidic substrate than silanol such as phenol (pK_a = 9.9)[14b] lead to the formation of [Fe(OPh)$_2$(PNNP-Cy)] (**5)**. In this reaction, any structural changes in the ligand backbone did not proceed. complex **5** is also paramagnetic in nature and characterized by a single crystal X-ray diffraction study. Complex **5** adopts distorted tetrahedral geometry (Figure 2b) and it is similar to [Fe(Cl)$_2$(PNNP-Mes)] complex reported by Dr. Takeshita in his doctorate thesis.[15] The bond lengths around iron center of **5** is analogous to high spin iron(II) complex.

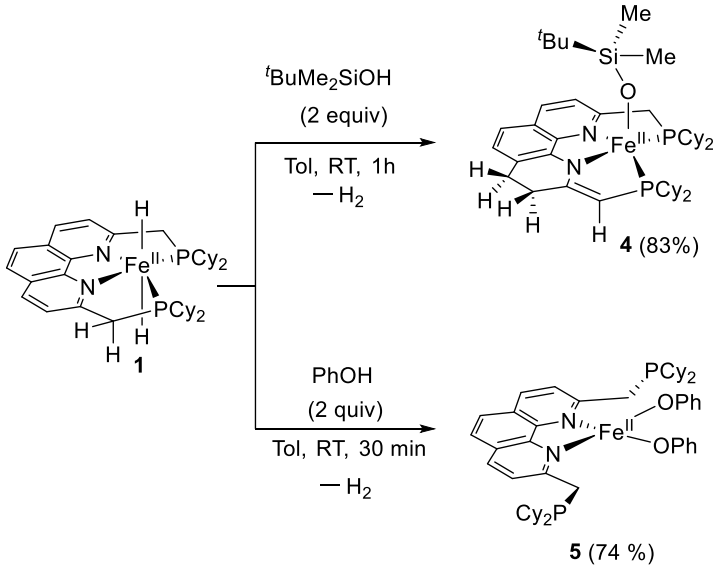

Scheme 8. Reaction of complex **1** with *t*-butyl dimethyl silanol and phenol.

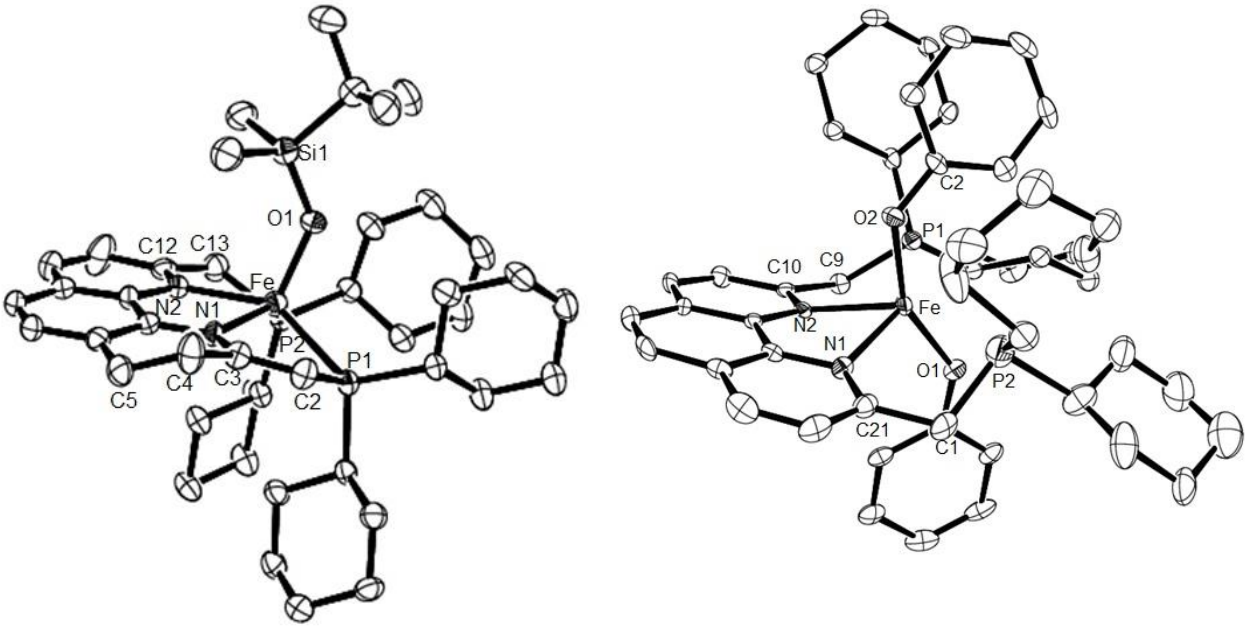

Figure 2. (a) ORTEP diagram of complex **4** with 50% probability thermal ellipsoids. All hydrogen atoms are omitted for clarity. Selected bond lengths[Å] and angles [˚]: Fe–P1 2.491(13), Fe–P2 2.511(12), Fe–N1 2.083(4), Fe–N2 2.192(3), Fe–O1 1.886(3), O1–Si1 1.612(3), C2–C3 1.361(6), C3–C4 1.509(6), C4–C5 1.531(6), C12–C13 1.501(6); P1–Fe–N1 75.90(10), P1–Fe–N2 140.57(10), N1–Fe–N2 75.14(14), P1–Fe–P2 114.88(4), N1–C3–C4–C5 44.5(5). (b) ORTEP diagram of complex **5** with 50% probability thermal ellipsoids. All hydrogen atoms are omitted for clarity. Selected bond lengths[Å] and angles [˚]: Fe–N1 2.086(3), Fe–N1 2.177(4), Fe–N2 2.215(4), Fe–O1 1.933(3), Fe–O2 1.947(3), C9–C10 1.493(7), C21–C22 1.495(6), C18–C19 1.410(5); N1–Fe–N2 75.12(10).

Thus, it is likely that the occurrence of the long-range MLC is dependent on pKa value ofsubstrates. More acidic substrate such as PhOH with pK_a = 9.9 favours only deprotonation, whereas substrates with pK_a 13.6 undergoes protonation along with H-migration via long-range metal ligand cooperation. In this reaction, entails loss of H^- to an acidic proton of the substrate with the release of H_2. In recent studies, it may be noted that protonation of hydride ligand involves in the nitrogen fixation by nitrogenase.[16]

Conclusion

In this chapter, reactivity of **1** was surveyed. Complex **1** achieved insertion of C=O and N=N bonds into the Fe–H bond. The reaction proceeded with concomitant transfer of hydride and benzylic H to ligand backbone, leading to the partial aromatization of the ligand backbone. Thus, the occurrence of unique long-range MLC was demonstrated. In a similar manner, complex **1** underwent protonation by reacting with acidic substrates such as silanol and phenol to release H_2, the long-range MLC also proceeded in the reaction with a silanol. This is, to the best of our knowledge, the first example of a well-defined example of iron hydride to show unique reactivity via long-range MLC of the PNNP-iron system.

Experimental Section

General Consideration

All experiments were carried out under nitrogen or argon atmosphere using Schlenk techniques or a glovebox. *n*-Hexane, tetrahydrofuran, C_6H_6, toluene, and dichloromethane were purified by a solvent purification system (MBraun SPS -800 or a Glass Contour Ultimate Solvent System). Toluene-d_8 and benzene-d_6, were dried over sodium benzophenone ketyl and distilled before use. CD_2Cl_2 was dried over CaH_2 and distilled. $[Fe(Br)_2(PNNP\text{-}Cy)]$[7a] was synthesized by following the reported procedure. All other reagents were purchased from commercial suppliers and used without purification. ^1H, $^{13}C\{^1H\}$, and $^{31}P\{^1H\}$ NMR spectra (^1H, 600 MHz; ^{13}C, 150 MHz; ^{29}Si, 119 MHz; ^{31}P, 243 MHz) were recorded on a Bruker AVANCE III HD 600 spectrometer. Chemical shifts are reported in δ (ppm) and referenced to the residual solvent signals for ^1H and ^{13}C and 85% H_3PO_4 as an external standard for ^{31}P. The high-resolution ESI mass spectra were obtained on a Bruker micro TOF II. Elemental analysis was determined by CHN Coder MT-6 from company Yanaco Technical Science Corporation.

Reaction of 1 with benzophenone

A 14 ml scintillation vial was charged with **1** (39 mg, 0.059 mmol), benzophenone (16 mg, 0.088 mmol), and toluene (5 mL). The solution was stirred at room temperature for 8 h. The volatile materials were removed under vacuum. The residues were extracted with toluene (5 mL) and filtered

through a celite pad. This solution was concentrated to dryness under vacuum. Crystals were grown from saturated of tol/hexane (0.1mL/1 mL) solution at room temperature to give complex **2**. (40 mg, 0.047 mmol, 81%).

^{1}H NMR (600 MHz, C_6D_6, 25^{o}C) δ 40.07 (br), 16.61 (br), 14.58 (br), 12.30 (br), 10.67 (br), 10.19 (br), 9.01 (br), 7.82 (br), 5.82 (br), 4.74 (br), 3.42 (br), 2.64 (br), –16.84 (br), –31.51 (br). EA Calculated for ($C_{51}H_{66}FeN_2OP_2$) C, 72.85; H, 7.91; N, 3.33. Found C, 72.59; H, 8.22; N, 3.77.

Reaction of 1 with azobenzene

A 14 ml scintillation vial was charged with **1** (19.5 mg, 0.029 mmol), azobenzene (8.0 mg, 0.043 mmol), and toluene (3 mL). The solution was stirred at room temperature for 8 h. The volatiles were removed under vacuum. The residue was extracted with toluene (5 mL) and filtered through a Celite pad. After evaporation, the residue was dissolved in hexane (0.6 mL) and left at room temperature, giving **3** as reddish-brown crystals (17.3 mg, 0.020 mmol, 69%).

^{1}H NMR (600 MHz, C_6D_6) δ 71.87 (br), 40.04 (br), 34.01 (br), 12.59 (br), 11.81 (br), 5.97 (br), 5.36 (br), 4.64 (br), 0.50 (br), –2.85 (br), –5.97 (br), –25.58 (br), –62.58 (br). EA Calculated for ($C_{50}H_{66}FeN_4P_2$) C, 71.42; H, 7.91; N, 6.64. Found C, 70.98; H, 7.36; N, 6.67.

Reaction of [Fe(OCHPh$_2$)(PNNP)'-Cy)] (2) with H$_2$

Complex **2** (10 mg, 0.012 mmol) was dissolved in C_6D_6 (0.5 mL). The solution was frozen at –196˚ C, and H_2 (1 atm) was introduced into the solution at room temperature. The solution was kept for 20 min at the temperature. The reaction was monitored by ^{1}H NMR spectroscopy and no new signal appeared in the ^{1}H NMR spectrocopy.

Reaction of [Fe(NPhNHPh)(PNNP-Cy)'] (3) with H$_2$

Complex **3** (18 mg, 0.021 mmol) was dissolved in C_6D_6 (0.5 mL). The solution was frozen at –196˚ C, and H_2 (1 atm) was introduced into the solution at room temperature. The solution was kept for 20 min at the temperature. Formation of free ligand PNNP-Cy as well as unidentified complexes was confirmed by ^{1}H NMR spectroscopy. After the filtration, some of the impurities were removed, and the solution was dried in vacuum followed by washing with ether/hexane to give PNNP-Cy (9.5 mg, 0.016 mmol).

Reaction of 1 with *t*-butyldimethyl silanol

A 14 ml scintillation vial was charged with **1** (25.0 mg, 0.037 mmol), *t*-butyldimethyl silanol (11.0 µl, 0.074 mmol), and toluene (3 mL). The solution was stirred at room temperature for 1 h. The volatiles were removed under vacuum. The residue was extracted with toluene (5 mL) and filtered through a Celite pad. After evaporation, the residue was dissolved in hexane (0.6 mL) and left at room temperature, giving **4** as red purple crystals (26.0 mg, 0.030 mmol, 83%).

^{1}H NMR (600 MHz, C_6D_6) δ 75.00 (br), 56.91 (br), 40.95 (br), 33.41 (br), 20.98 (br), 14.69 (br), 13.19 (br), 11.18 (br), 9.80 (br), 6.45 (br), 4.58 (br), 0.61 (br), –0.03 (br), –18.21(br), –33.29 (br). EA Calculated for ($C_{44}H_{70}FeN_2P_2OSi$) C, 66.99; H, 8.94; N, 3.55. Found C, 66.53; H, 8.26; N, 3.45.

Reaction of 1 with phenol

A 14 ml scintillation vial was charged with **1** (16.5 mg, 0.025 mmol), phenol (10.0 mg, 0.050 mmol), and benzene (1 mL). The solution was stirred at room temperature for 15 min and color was changed from green to red purple immediately. The volatiles were removed under vacuum. The residue was extracted with toluene (5 mL) and filtered through a Celite pad. After evaporation, the residue was dissolved in hexane (0.6 mL) and left at room temperature, giving **5** as red purple crystals (15 mg, 0.018 mmol, 74%).

^{1}H NMR (600 MHz, C_6D_6) δ 45.45 (br), 23.03 (br), 19.73 (br), 13.80 (br), 4.94 (br), 3.95 (br), –12.06 (br), –15.27 (br), –25.38 (br), –41.36 (br).

Single crystal X-ray diffraction studies.

The single crystal X-ray diffraction measurement of **2**, **3**, **4** and **5** was performed under a cold nitrogen stream on a Rigaku XtaLAB P200 diffractometer with a Pilatus 200 K detector using multilayer mirror monochromated Mo Kα radiation. The determination of crystal system and unit cell parameters and data processing were performed with the CrystalClear program package [16]. All structures were solved by direct method using the SHELXS97 program[17] and refined by full-matrix least squares calculations on F^2 for reflections (SHELXL-2014/7)[17] using the CrystalStructure 4.2 program.[18] CCDC-1961638 (**2**), 1961639 (**3**) contain the supplementary crystallographic data for this paper. These data can be obtained free of charge from The Cambridge Crystallographic Data Centre via www.ccdc.cam.ac.uk/data_request/cif.

Table S1. Crystallographic parameters

	2	**3**	**4**	**5**
Empirical formula	$C_{51}H_{66}FeN_2OP_2$	$C_{50}H_{66}FeN_4P_2$	$C_{44}H_{70}FeN_2OP_2Si$	$C50H64FeN_2OP_2$
Formula weight	840.84	840.85	788.93	853.82
Temperature	93(2) K	93(2) K	93(2) K	93(2) K
Crystal system	monoclinic	monoclinic	monoclinic	monoclinic
Space group	$P2_1/n$	$P2_1/c$	$P2_1/c$	$I2/a$
a/Å	14.1301(5)	19.814(10)	10.4478(4)	21.1834(12)
b/Å	19.1928(6)	10.212(5)	22.7664(12)	13.6482(6)
c/Å	16.7798(6)	21.706(12)	36.778(2)	30.4312(13)
α/deg	90 °	90 °	90 °	90 °
β/deg	102.901(4) °	95.548(10) °	96.722(4) °	100.572(5) °
γ/deg	90 °	90 °	90 °	90 °
Volume	4435.7(3) $Å^3$	4371(4) $Å^3$	8687.8(7) $Å^3$	8648.8(7) $Å^3$
Z	4	4	4	4
Density	1.259	1.278	1.560	1.311
Goodness-of-fit on F^2	1.073	1.008	1.023	1.612
Final R indices [I>2sigma(I)]	$R1$ = 0.0587, $wR2$ = 0.1468	$R1$ = 0.0582, $wR2$ = 0.1351	$R1$ =0.0711, $wR2$ = 0.15030	$R1$ = 0.1043, $wR2$ = 0.2677
R indices (all data)	$R1$ = 0.0901, $wR2$ = 0.1652	$R1$ = 0.1469, $wR2$ = 0.1919	$R1$ = 0.1785, $wR2$ = 0.1946	$R1$ = 0.1480, $wR2$ = 0.2810

References

1. (a) Hieber, W.; Leutert, F. *Naturwissenschaften*, **1931**, *19*, 360. (b) Kaesz, H. D.; Saillant, R. B. *Chem. Rev.* **1972**, *72*, 231-281. (c) Hoffman, B. M.; Luko-yanov, D.; Yang, Z.-Y.; Dean, D. R.; Seefeldt, L. C. *Chem. Rev.* **2014**, *114*, 4041-4062. (d) Wei, D.; Darcel, C. *Chem. Rev.* **2019**, *119*, 2550-2610. (e) Takegami, Y.; Ueno, T.; Kawajiri, K. *Bull. Chem. Soc. Jpn.* **1966**, *39*, 1-7. (f) Shackleton, T. A.; Baird, M. C. *Organometallics* **1989**, *8*, 2225-2232. (g) Bianchini, C.; Meli, A.; Peruzzini, M.; Frediani, P.; Bo-hanna, C.; Esteruelas, M. A.; Oro, L. *Organometallics* **1992**, *11*, 138-145. (h) Fiedler, A.; Schröder, D.; Schwarz, H.; Tjelta, B. L.; Armentrout, P. B. *J. Am. Chem. Soc.* **1996**, *118*, 5047-5055. (i) Gao, Y.; Holah, D. G.; Hughes, A. N.; Spivak, G. J.; Havighurst, M. D.; Magnuson, V. R.; Polyakov, V. *Polyhedron* **1997**, *16*, 2797-2807. (j) Field, L. D.; Lawrenz, E. T.; Shaw, W. J.; Turner, P. *Inorg. Chem.* **2000**, *39*, 5632-5638. (k) Smith, J. M.; Lachicotte, R. J.; Holland, P. L. *J. Am. Chem. Soc.* **2003**, *125*, 15752-15753. (l) Casey, C. P.; Guan, H. *J. Am. Chem. Soc.* **2007**, *129*, 5816-5817. (m) Fong, H; Peters, J. C. *Inorg. Chem.* **2015**, *54*, 5124-5135.
2. (a) Dahlhoff, W. V.; Nelson, S. M. *J. Chem. Soc. A* **1971**, 2184-2190. (b) Creaser, C. S.; Kaska, W. C. *Inorg. Chim. Acta.* **1978**, *30*, L325-L326. (c) Giannoccaro, P.; Vasapollo, G.; Nobile, C. F.; Sacco, A. *Inorg. Chim. Acta* **1982**, *61*, 69-75. (d) Zhang, J.; Gandelman, M.; Herrman, D.; Leitus, G.; Shimon, L. J. W.; Ben-David, Y.; Milstein, D. *Acta* **2006**, *359* 1955-1960. (e) Benito-Garagorri, D.; Becker, E.; Wiedermann, J.; Lackner, W.; Pollak, M.; Mereiter, K.; Kisala, J.; Kirchner, K. *Organometallics* **2006**, *25*, 1900-1913. (f) Pelczar, E. M.; Emge, T. J.; Jespersen-Krogh, K.; Goldman, A. S. *Organometallics* **2008**, *27*, 5759-5767. (g) Bhattacharya, P.; Krause, J. A.; Guan, H. O*rganometallics* **2011**, *30*, 4720-4729. (h) Smith, A. D.; Saini, A.; Singer, L. M.; Phadke, N.; Findlater, M. *Polyhedron* **2016,** *114*, 286-29.
3. (a) Zell, T; Milstein, D. *Acc. Chem. Res.* **2015**, *48*, 1979-1994. (b) Gorgas, N.; Kirchner, K. *Acc. Chem. Res.* **2018,** *51*, 1558-1569. (c) Alig, L.; Fritz, M.; Schneider, S. *Chem. Rev.* **2019**, *119*, 2681-2751. (d) Elsby, M. R.; Baker, R. T. *Chem. Soc. Rev.* **2020**, *49*, 8933-8987. (e) Srimani, D.; Diskin-Posner, Y.; Ben-David, Y.; Milstein, D. *Angew. Chem. Int. Ed.* **2013**, *52*, 14131-14134. (f) Alberico, E.; Sponholz, P.; Cordes, C.; Nielsen, M.; Drexler, H.-J.; Baumann, W.; Junge, H.; Beller, M. *Angew. Chem. Int. Ed.* **2013**, *52*, 14162-14166. (g) Chakraborty, S.; Lagaditis, P. O.; Förster, M.; Bielinski, E. A.; Hazari, N.; Holthausen, M.

C.; Jones, W. D.; Schneider, S. *ACS Catal*. **2014**, *4*, 3994-4003. (h) Chakraborty, S.; Brennessel, W. W.; Jones, W. D. *J. Am. Chem. Soc.* **2014,** *136*, 8564-8567. (i) Lagaditis, P. O.; Sues, P. E.; Sonnenberg, J. F.; Wan, K. Y.; Lough, A. J.; Morris, R. H. *J. Am. Chem. Soc.*, **2014,** *136*, 1367-1380. (j) Gorgas, N.; Stöger, B.; Veiros, L. F.; Kirchner, K. *ACS Catal*. **2016**, *6*, 2664-2672. (k) Rezayee, N. M.; Samblanet, D. C.; Sanford, M. S. *ACS Catal*. **2016,** *6*, 6377-6383.

4. (a) Gibson, V. C.; Redshaw, C.; Solan, G. A. *Chem. Rev.* **2007**, *107*, 1745-1776. (b) Chirik, P. J. *Acc. Chem. Res.* **2015**, *48*, 1687-1695. (c) Sluys, L. S. V. D.; Eckert, J.; Eisenstein, O.; Hall, J. H.; Huffman, J. C.; Jackson, S. A.; Koetzle, T. F.; Kubas, G. J.; Vergamini, P. J.; Caulton, K. G. *J. Am. Chem. Soc.* **1990**, *112*, 4831-4841. (d) Field, L. D.; Messerle, B. A.; Smernik, R. J. *Inorg. Chem.* **1997**, *36*, 5984-5990. (e) Britovsek, G. J. P.; Gibson, V. C.; Kimberley, B. S.; Maddox, P. J.; McTavish, S. J.; Solan, G. A.; White, A. J. P.; Williams, D. J. *Chem. Commun.* **1998**, 849-850. (f) Shirasawa, N.; Nguyet, T. T.; Hikichi, S.; Moro-oka, Y.; Akita, M. *Organometallics* **2001**, *20*, 3582-3598. (g) Bart, S. C.; Lobkovsky, E.; Chirik, P. J. *J. Am. Chem. Soc.* **2004**, *126*, 13794-13807. (h) Mankad, N. P.; Whited, M. T.; Peters, J. C. *Angew. Chem. Int. Ed*. **2007**, *46*, 5768–5771.
5. (a) S. A. Smith, P. O. Lagaditis, A. Lüpke, A. J. Lough and R. H. Morris, *Chem. Eur. J.*, **2017**, *23*, 7212–7216. c) A. Zirakzadeh, K. Kirchner, A. Roller, B. Stöger, M. Widhalm and R. H. Morris, *Organometallics*, **2016**, *35*, 3781–3787. d) C. S. Seo, T. Tannoux, S. A. Smith, A. J. Lough and R. H. Morris, *J. Org. Chem.*, **2019**, *84*, 12040–12049.
6. (a) R. Langer, G. Leitus, Y. Ben-David and D. Milstein, *Angew. Chem., Int. Ed.,* **2011**, *50*, 2120–2124. b) R. Langer, M. A. Iron, L. Konstantinovski, Y. Diskin-Posner, G. Leitus, Y. Ben-David and D. Milstein, *Chem. – Eur. J.*, **2012**, *18*, 7196–7209. c) D. Srimani, Y. Diskin-Posner, Y. Ben-David, D. Milstein, *Angew. Chem, Int. Ed.,* **2013,** *52*, 14131-14134.
7. (a) Ziessel, R. *Tetrahedron Lett.* **1989**, *30*, 463-466. (b) Langer, R.; Fuchs, I.; Vogt, M.; Balaraman, E.; Diskin-Posner, Y.; Shimon, L. J. W.; Ben-David, Y.; Milstein, D. *Chem. Eur. J.* **2013**, *19*, 3407-3414. (c) Miura, T.; Naruto, M.; Toda, K.; Shimomura, T.; Saito, S. *Sci. Rep.* **2017**, *7*, 1586. (d) Saito, S.; Ryoji, N.; Miura, T.; Naruto, M.; Iida, K.; Takada, Y.; Toda, K.; Nimura, S.; Agrawal, S.; Lee, S. US Pat., 0107151A1, 2016.
8. (a) C. Gunanathan, B. Gnanaprakasam, M. A. Iron, L. J. W. Shimon, David Milstein, *J. Am. Chem. Soc.* **2010**, *132*, 14763–14765.

9. P. Daw, A. Kumar, D. Oren, N. A. E. Jalapa, D. Srimani, Y. D. Posner, G. Leitus, L. J. W. Shimon, R. Carmieli, Y. B. David, D. Milstein, *Organometallics* **2020,** *39*, 279–285.
10. E. Khaskin, Y. D. Posner, L. Weiner, G. Leitusb, D. Milstein, *Chem. Commun.*, **2013**, *49*, 2771-2773.
11. (a) T. Takeshita, K. Sato, Y. Nakajima, Dalton Trans., 2018, 47, 17004. b) N.-Y. Jheng, Y. Ishizaka, Y. Naganawa, A. Sekiguchi, Y. Nakajima, Dalton Trans., 2020, 49, 14592.
12. (a) Buchard, A.; Heuclin, H.; Auffrant, A.; Le Goff, X. F.; Le Floch, P. *Dalton Trans*. **2009**, *9*, 1659-1667. (b) Holzhacker, C.; Calhorda, M. J.; Gil, A.; Carvalho, M. D.; Ferreira, L. P.; Stöger, B.; Mereiter, K.; Weil, M.; Müller, D.; Weinberger, P.; Pittenauer, E.; Allmaier, G.; Kirchner, K. *Dalton Trans.* **2014**, *43*, 11152-11164. (c) Thompson, C. V.; Arman, H. D.; Tonzetich, Z. J. *Organometallics* **2017**, *36*, 1795-1802.
13. (a) Maseras, F.; Lledós, A.; Clot, E.; Eisenstein, O. Chem. Rev. **2000**, 100, 601. b) Pons, V.; Conway, S. L. J.; Green, M. L. H.; Green, J. C.; Herbert, B. J.; Heinekey, D. M. Inorg. Chem. **2004**, 43, 3475. (c) Dugan, T. R.; Bill, E.; MacLeod, K. C.; Brennessel, W. W.; Holland, P. L. *Inorg. Chem.* **2014**, *53*, 5, 2370-2380.
14. (a) Paul D. Lickiss: The Synthesis and Structure of Organosilanols, Advances in Inorganic Chemistry, 42, **1995**, Pages 147–262. (b) Speight, J. G. *Lange's Handbook of Chemistry*; 16th ed.; McGraw-Hill: New York, 2005.
15. Tomohiro Takeshita: Synthesis and Reactivities of Iron Complexes Bearing a Tetradentate PNNP Ligand, University of Tsukuba, **2019**
16. (a) Henderson, R. A. *Chem. Commun*. **1987**, 1670-1672. (b) Hlatky, G. G.; Crabtree, R. H. *Coord. Chem. Rev.* **1985**, *65*, 1-48. (c) Oglieve, K. E.; Henderson, R. A. *Chem. Commun*. **1992**, 441-443.
17. (a) Hidai, M.; Mizobe, Y. *Chem. Rev.* **1995**, *95*, 1115-1133. (b) Chalkley, M. J.; Drover, M. W.; Peters, J. C. *Chem. Rev.* **2020**, *120*, 5582-5636. (c) Schrauzer, G. N.; Palmer, M. R. *J. Am. Chem. Soc.* **1981**, *103*, 2659-2667. (d) Nakajima, Y.; Suzuki, H. *Organometallics* **2005**, *24*, 1860-1866. (e) Milsmann, C.; Turner, Z. R.; Semproni, S. P.; Chirik, P. J. *Angew. Chem. Int. Ed.* **2012**, *51*, 5386-5390. (f) Anderson, J. S.; Moret, M.-E.; Peters, J. C. *J. Am. Chem. Soc.* **2013**, 135, 534-537.

Chapter 4

Synthesis and Reactivity of Four Coordinate Unsaturated PNNP”-Fe Complexes

Abstract

14 electron iron(II) complexes **3a** and **3b** bearing a PNNP’’-R (R = Cy, *t*Bu) ligand with a square planar geometry were synthesized via long-range metal ligand cooperation and fully characterized. According to a single-crystal X-ray diffraction analysis, complexes **3a** and **3b** were revealed to possess a doubly hydrogenated phenanthroline backbone. These complexes efficiently reacted with π-acceptor ligands such as AdNC and CO to produce the corresponding six-coordinate 18 electron complex at room temperature.

Introduction

Coordinatively unsaturated transition metal complexes play as a key intermediate in various stoichiometric and catalytic reactions.[1] Formally, 14e complex has advantage than 16e complex as it is more coordinatively unsaturated, and thus it has more coordination sites for binding of substrates. Specifically, isolation of 14e complexes of a transition metal is challenging due to their highly reactive nature.[2] The one of the most prominent works in this field is the isolation of 14e $[RuR(CO)(P\textit{t}Bu_2Me)_2]^+$ (R = H, Ph) reported by Caulton and co-workers in 1997.[3a-c] Based on the detailed spectroscopic analysis and a single crystal X-ray diffraction study, these complexes adopt see-saw geometry, which has two C–H agostic interactions to stabilize the vacant site. In 2003, Caulton and co-workers isolated naked 14e square planar complex $[RuCl((\textit{t}Bu_2PCH_2SiMe_2)_2N)]$[3d], which does not have any agostic interactions to support the unsaturated metal center.

Coordinatively unsaturated complexes are more frequently found in the case of Fe complexes compared with Ru complexes.[3e-f] Four coordinate 14e Fe(II) complexes obtained two types of geometry, namely tetrahedral and square planar. Usually, tetrahedral geometry is favored by bulky ligands and thus tetrahedral geometry is governed by steric factors. Due to the small crystal field, tetrahedral complexes normally exhibit high spin state. Conversely, square planar geometry is favored based on electronic stabilization, leaving high energy, unoccupied and antibonding dx2-y2 orbital (Scheme 1).

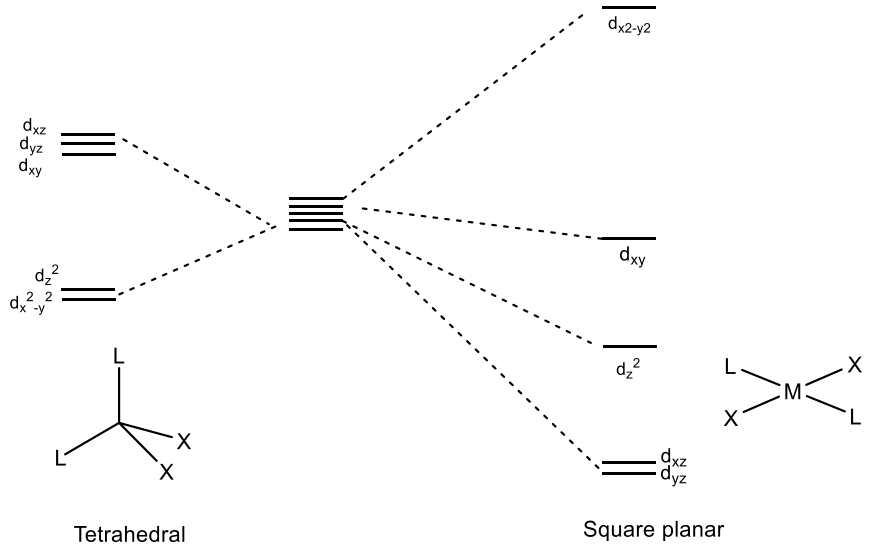

Scheme 1. d-orbital splitting in tetrahedral and square planar.

Chirik and co-workers discussed the flexible structural change between tetrahedral and square planar of 14e Fe(II) complexes, which is dependent on the ligand-field strength of the supporting ligands. For example, iron-(II) bis(mesityl) compounds supported by monodentate or chelating amine ligands exhibits high-spin state (*S* = 2) tetrahedral. On the other hand, for monodentate phosphines and phosphites, the opposite situation is observed, where planar geometry and intermediate-spin (*S* =1) complexes are favored (Scheme 2a, 2b).[4]

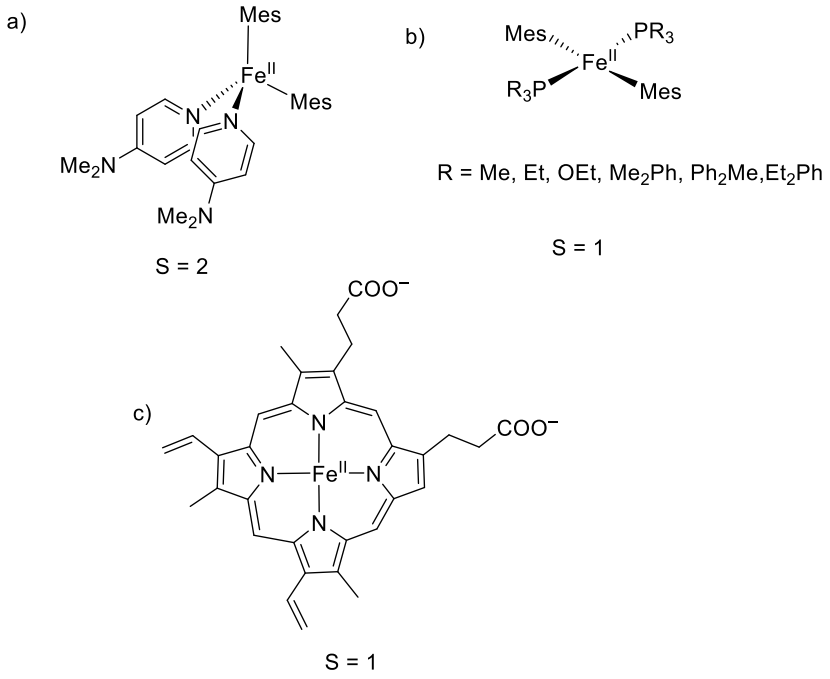

Scheme 2. Four coordinate Fe(II) complexes with: (a) Tetrahedral high-spin[4] (S=2), (b) Square planar[4] (S = 1), (c) Structure of iron-porphyrin subunit of heme B (S =1) in iron porphynito.[5a]

Fe(II) porphyrins without any coordinated ligands at axial positions represent a typical example as 14e square planar Fe complex with intermediate spin state (S =1) (Scheme 2c). It is well known that porphyrins are found as heme cofactors, which plays an important role in biological functions such as O_2 transportation and storage, electron transportation, O_2 activation, and so on.[7a] Thus, to study properties and reactivity of Fe(II) porphyrins is important.[5]

It should be mentioned that the spin states of the square planar Fe(II) complexes, which are closely related to their structural arrangement around the Fe atom, often bring a significant influence on the properties of Fe complexes. Therefore, to shed light on the chemistry of coordinatively 14e square planar Fe complexes, discussion on both structures and spin states are of importance. Coordinatively

unsaturated 14e Fe(II) porphyrin complexes have two vacant axial sites available for binding ligands (Scheme 2c). It is to be noted that Fe(II) porphyrin presents as co-factor of heme which is responsible for O_2-transport and storage in the form of hemoglobin and myoglobin. In the case of deoxy hemoglobin and myoglobin, one of vacant sites is occupied by histidine to give five-coordinate high-spin complex (S =2). However, oxy hemoglobin and myoglobin, where oxygen is coordinated to Fe(II), encountered as low spin (S = 0) octahedral complexes.[7] Iron diphenyl porphyrin [Fe(TPP)] and iron octaethyl porphyrin [Fe(OEP)] systems (Scheme 3) have been well-studied as the model of Fe(II) porphyrin systems to study their properties, such as stereochemistry and spin states.[7a,b] Experiments and theoretical study supported their intermediate spin state in ground state of Fe(II) porphyrin. As seen above, it is widely known that electronic structure of Fe(II) porphyrin changes in accordance with the coordination of axial ligands, which are closely related to their catalytic functions. However, examples of well-defined models of Fe(II) porphyrin system are still limited. Thus, exploring the structural, electronic, and bonding properties of 14e Fe(II) complexes related to iron porphyrin is still a big challenge in this field.[6]

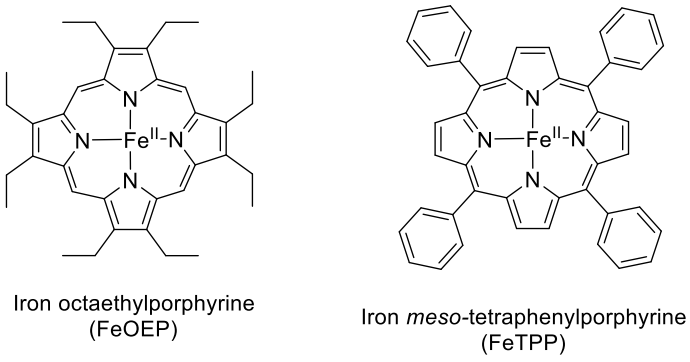

Scheme 3. Structure of (a) iron meso-tetraphenyl porphyrin (FeTPP), (b) iron octaethylporphyrin (FeOEP).

Floriani and co-workers reported the reaction of [Fe(tmtaa)] (tmtaa = dibenzotetramethyltetraazaannulene) with CO in the presence of the coordinating solvents THF and pyridine (Scheme 4).[8a] SQUID measurement revealed that [Fe(tmtaa)] exhibits magnetic moment of S=1 with μ_{eff} = 3.45 μ_B at room.

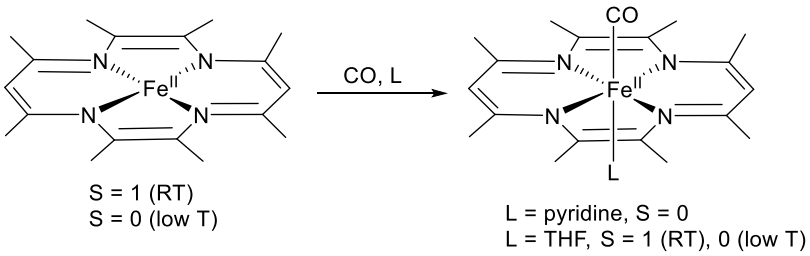

Scheme 4. Reactivity of [Fe(tmtaa)] towards CO.

Similarly, Fitzgerald and co-workers reported Fe systems with tetraaza macrocyclic ligand TATAP (tetraanthracenotetraazaporphyrin), where four anthracene units are connected through β-pyrrolic carbon of porphyrazine macrocycle.[8b] The [Fe(TATAP)] (TATAP =) exhibits an intermediate spin state (S =1). It was observed that interaction of Fe(II) with CO is relatively weaker than Fe(II) porphyrin systems and reversible in nature (Scheme 5). In this system, electron density at the metal center is less than Fe(II) porphyrin due to the presence of TATAP as a strong π-accepting ligand, leading to weak back-bonding to CO.

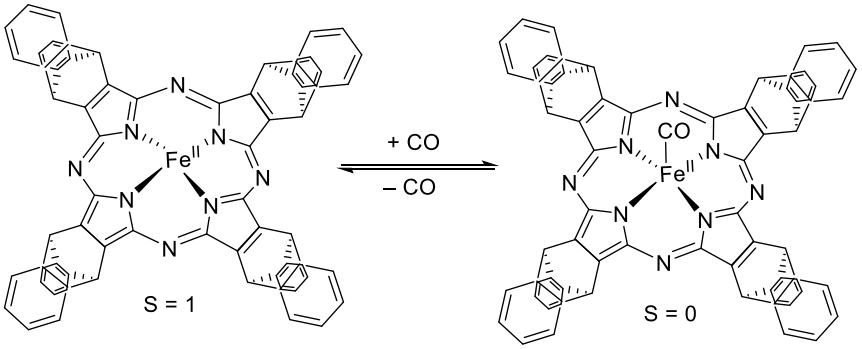

Scheme 5. Reactivity of [Fe(TATAP)] towards CO.

Nazzareno and co-workers reported the reactivity of iron porphodimethene complex [Fe(Et_6N_4)] (Scheme 6) towards various ligands.[8c] It was found that π-accepting ligands such as *t*BuNC and CO rapidly coordinate with [Fe(Et_6N_4)] to form diamagnetic complexes [Fe(Et_6N_4)$(CO)_2$] and [Fe(Et_6N_4)$(t\text{BuNC})_2$].

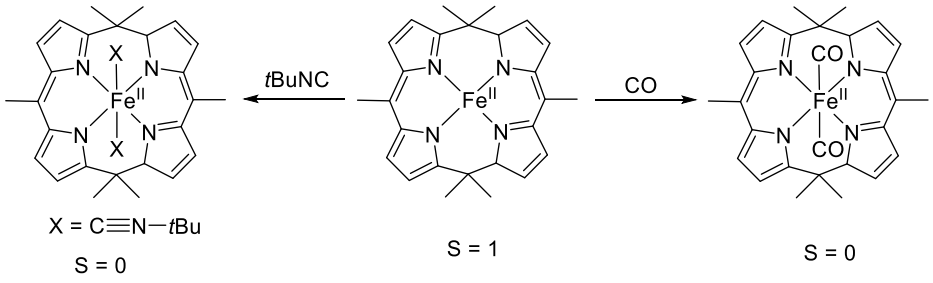

Scheme 6. Axial coordination of CO and *t*BuNC in hexaethylporphodimetheneiron(II).

Recently, Thomas and co-worker reported formally 14e iron complex with an intermediate spin state (S=1) based on P-N-N-P ligand (P-N-N-P = *N*, *N*- bis(2-(diphenylphosphaneyl(phenyl)ethane-1,2 diamine) other than porphyrin or macrocyclic system.[9] They have examined reactivity of the complex towards several ligands such as PMe_3, boranes. It was observed that PMe_3 bound in axial position to give 16e complex, while σ B–H bond activation proceeded on the treatment with HBPin (pinacolborane) and $H_3B{\cdot}SMe_2$ to give coordinatively saturated 18e complexes (Scheme 7).

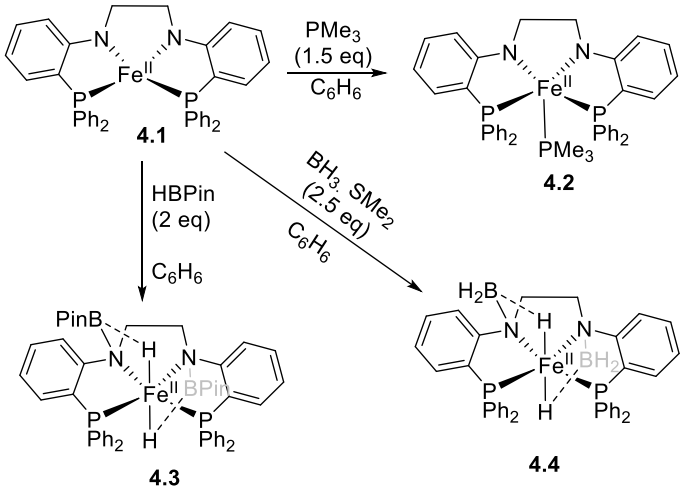

Scheme 7. Reactivity of 14e [Fe(PNNP)] towards PMe_3, HBPin, and $H_3B{\cdot}SMe_2$.

In this chapter, 14e [Fe(PNNP''-R)] (R = Cy, *t*Bu) complexes with square planer geometry have been synthesized from [Fe(H)$_2$PNNP-R] (R = Cy, *t*Bu). Reaction of 14e [Fe(PNNP''-R)](R = Cy, *t*Bu) complexes with π acceptor ligands leads to immediate spin change from S =1 to S = 0 to give 18e [Fe(PNNP'-R)(L$_2$)] (L = CO, RNC) in which CO or RNC occupy axial position.

Results & Discussion

Motivated by the unique long-rang MLC behavior of the PNNP-Cy-Fe system, we next synthesized an iron hydride bearing a bulkier PNNP-*t*Bu ligand (2,9-bis((di-*t*-butylphosphino)methyl)-1,10-phenanthroline), [Fe(H)$_2$(PNNP-*t*Bu)] (**2b**), with the aim of expanding the reaction options. Furthermore, it is expected that **2b** will exhibit a simpler spectrum than [Fe(H)$_2$(PNNP-Cy)] (**2a)** in its NMR spectrum. Synthesis of **2b** was performed by the reaction of [FeBr$_2$(PNNP-*t*Bu)] (**1b**) with NaBEt$_3$H, following the previously reported procedure for the synthesis [Fe(H)$_2$(PNNP-Cy)] (**2a)** (Scheme 8).[10a] Firstly, preparation of [Fe(Br)$_2$(PNNP-*t*Bu)] (**1b**) was achieved from treatment of PNNP-*t*Bu ligand and FeBr$_2$ (1:1) in THF at room temperature and stirred for 12 h. The resulting complex **1b** was isolated in 96% yield and characterized by elemental analysis. In ^{1}H NMR spectrum, broad signals appeared within the range of 55 ppm to –77 ppm. Upon treatment of **1b** with 2 equiv NaBEt$_3$H at room temperature the color of the solution immediately changed to dark green, affording **2b**, quantitatively. In the ^{1}H NMR spectrum, a signal derived from the two hydrido ligands was observed at –7.81 ppm as a triplet, due to the coupling with two phosphorus atoms ($^3J_{PH}$ = 72.1 Hz). Four *t*Bu groups appeared as a singlet with an integral intensity of 36 H, supporting a C_{2v} symmetric structure of **2b**. Consistent with this, one singlet appeared at 130.9 ppm in the ^{31}P{^{1}H} NMR spectrum.

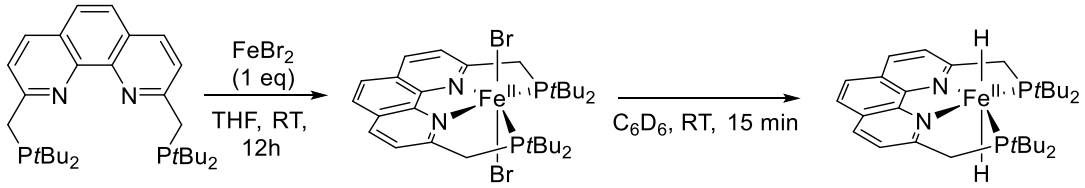

Scheme 8. Preparation of **2b.**

Complex **2b** was somewhat unstable and gradually underwent a structural transformation at ambient temperature. For example, when **2b** was dissolved in C_6D_6 and left at room temperature, **2b** was completely consumed, and new broad paramagnetic signals were observed at 29.74, 17.42, –3.87, and –9.81 ppm in the ^{1}H NMR spectrum after a few days. After crystallization of the resulting mixture, four-coordinate unsaturated complex **3b** was isolated in 83% yield (Scheme 9).

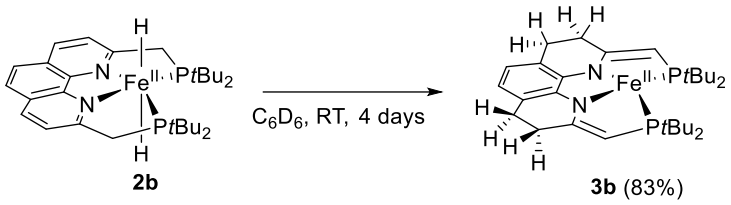

Scheme 9. Preparation of **3b.**

14e complex **3a** was prepared from complex **2a** on heating at ambient temperature in the presence of Ar atmosphere (Scheme 10a). The broad signals were exhibited within range of 29.94 to –19.25 ppm in the ^{1}H NMR spectrum. After keeping the reaction mixture at room temperature for 3 days, red brown color crystals complex **3a** was obtained. This is in sharp contrast to the case of **2a**, which is gradually transformed to [{Fe(PNNP-Cy)}$_2$(μ-N$_2$)] (**1a**) under a N_2 atmosphere via H_2 elimination. Previous studies demonstrated that [Fe(PNNP-R)]$_2$(μ-N$_2$)] (R= Ph, Cy) undergo cleavage of C–X[10c] and Si–X[11] bond via oxidative addition. As expected, cleavage of H–H by [{Fe(PNNP)}$_2$(μ-N$_2$)] (**1a**) was achieved to give a mixture containing **2a** (89 % NMR yield) and **3a** immediately at room temperature (Scheme 10b). Interestingly, red-brown color of crystals was obtained after keeping the reaction mixture at room temperature for 3 days. Thus, a rare 14e complex **3a** and **3b** was prepared from complex **2a** and **2b** at ambient temperature via multiple migration of hydride and benzylic H atom to phenanthroline backbone.

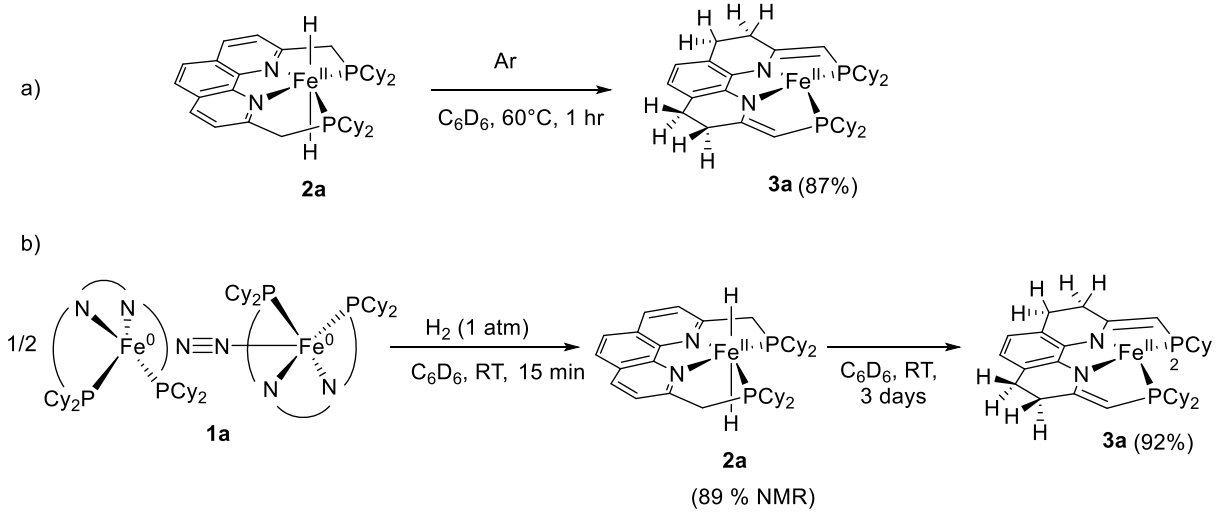

Scheme 10. Preparation of **3a.**

The structure of paramagnetic **3a** and **3b** was determined by a single-crystal X-ray analysis, showing a pseudo-four-coordinate square planar geometry around the Fe atom, supported by a dearomatized PNNP''-*t*Bu ligand and PNNP''-Cy with a doubly hydrogenated phenanthroline backbone respectively (Figure 1). In the structure of **3b**, Fe–N bond lengths are 1.926(18) and 1.932(2) Å, and the Fe–P bond lengths are 2.362(7) and 2.374(7) Å. These values are slightly shorter than those of [Fe($OCHPh_2$)(PNNP'-Cy)] and [Fe($NNHPh_2$)(PNNP'-Cy)] as typical iron(II) complexes with a high-spin state, but within the values of iron(II) complexes with an intermediate-spin state. The C1–C2 bond (1.350(3) Å) and C7–C8 bond (1.353(3) Å) exhibit a typical C–C double-bond length.[12] The distorted dihedral angles of N1–C1–C2–C3–C4 (34.1(3) °) and N2–C8–C9–C10 (39.1(3) °) supported the hydrogenated phenanthroline backbone. The same pattern of bond lengths in Fe–N, Fe–P and backbone of phenanthroline moiety are observed in complex **3a**.

The magnetic moment of **3b** was determined to be μ_{eff} = 2.2 μ_B based on the Evans method, supporting the paramagnetic intermediate state (S = 1).

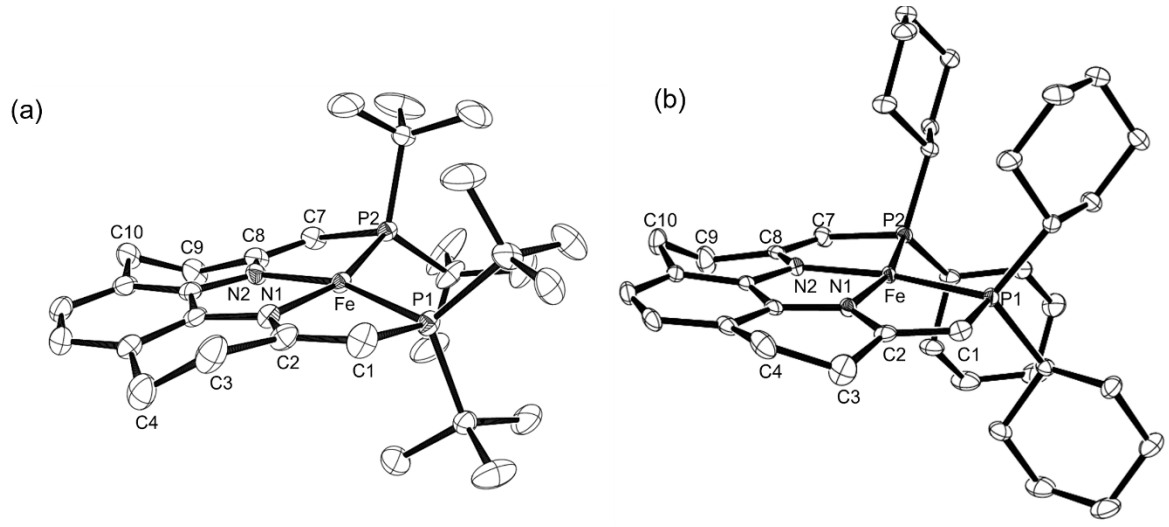

Figure 1. (a) ORTEP diagram of complex **3b** with 50% probability thermal ellipsoids. All hydrogen atoms are omitted for clarity. Selected bond lengths[Å] and angles [˚]: Fe–P1 2.2787(6), Fe–P2 2.2838(6), Fe–N1 1.9150(15), Fe–N2 1.9118(15), C1–C2 1.374(3), C2–C3 1.489(3), C3–C4 1.483(3), C7–C8 1.367(3), C8–C9 1.496(3), C9–C10 1.488(3); P1–Fe–N1 82.21(5), P1–Fe–N2 164.42(5), N1–Fe–N2 82.26(6), N2–Fe1–P2 82.05(5) N1–Fe1–P2 164.24(5), P1–Fe–P2 113.53(2). (b) ORTEP diagram of **3a** with 50% probability thermal ellipsoids. All hydrogen atoms are omitted for clarity. Selected bond lengths[Å] and angles [˚]: Fe–P1 2.362(7), Fe–P2 2.374(7), Fe–N1 1.932(2), Fe–N2 1.927(18), C1–C2 1.350(3), C2–C3 1.505(3), C3–C4 1.497(4), C7–C8 1.353(3), C8–C9 1.510(3),

C9–C10 1.513(4); P1–Fe–N1 80.81(6), P1 Fe–N2 160.62(6), N1–Fe–N2 81.31(8), N2–Fe1–P2 80.86(6), N1–Fe1–P2 161.26(6) P1–Fe–P2 117.59(2), N1–C2–C3–C4 34.1(3), N2–C8–C9–C10 39.1(3).

Thus, long range metal ligand cooperation phenomenon of **2a** and **2b** [$Fe(H)_2$(PNNP-R)] (R = Cy, *t*Bu) was utilized to prepare highly unsaturated complexes **3a** and **3b**. Complexes **3a** and **3b** are coordinatively unsaturated 14e species with a square planar geometry and S = 1 ground state. It is interesting to compare the magnetic behavior of 14e complexes **3a** and **3b** with iron(II) porphyrins in absence of axial ligands.[15] It is widely known that the electronic structure of iron(II) porphyrins changes in accordance with the coordination of axial ligands, and is subsequently closely related to the catalytic functions of porphyrins. Our work reported here demonstrates well-defined iron(II) complexes of a square planar structure with an intermediate spin state , which are analogous to iron(II) porphyrin systems.

With highly coordinatively unsaturated 14e complexes **3a** and **3b** in hands, we next examine the reactivity towards various ligands. Unexpectedly, **3a** and **3b** did not react with donating ligands such as PEt_3 and DMAP (4-dimethylaminopyridine) (Scheme 11).

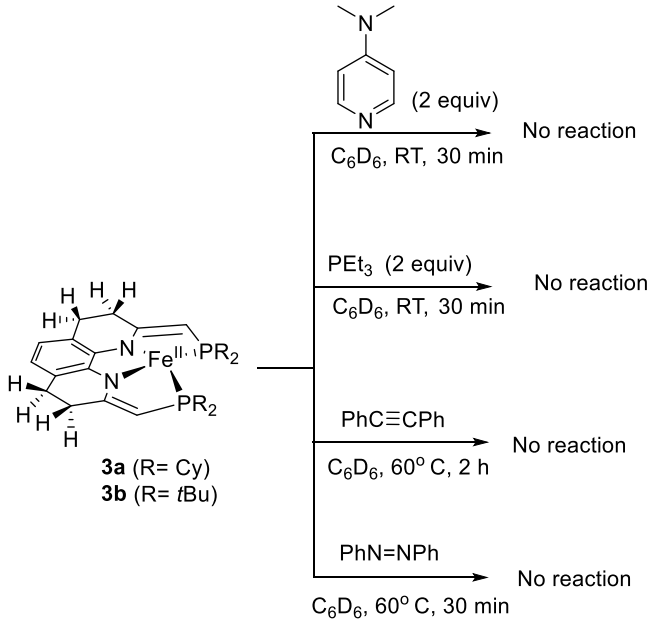

Scheme 11. Reactivity of **3a** and **3b** towards various ligands.

In contrast, complex **3b** smoothly reacted with adamantyl isocyanide (AdNC) as a π-accepting ligand. It was also revealed that the intermediate spin state (S = 1) of **3b** changed to S = 0 upon the

formation of AdNC-coordinated complexes **4** and **5**. On the treatment with AdNC (2.5 eq), **3b** was immediately consumed at room temperature (Scheme 12). Formation of two different complexes are confirmed, Fe(II) complex with hydrogenated PNNP''-*t*Bu ligand, [Fe^{II}(AdNC)$_2$(PNNP''-*t*Bu)] (**4**), and PNNP-*t*Bu-Fe(0) complex, [Fe^0(AdNC)(PNNP-*t*Bu)](**5**) in 45% and 40% NMR yields, respectively (Scheme 12).

Complex **5** could be alternatively synthesized by the reaction of **2b** with AdNC. Thus, **2b** was *in-situ* prepared by mixing [Fe(Br)$_2$(PNNP-*t*Bu)] with $NaBEt_3H$, then added AdNC (1.5 equiv), resulting in the formation of **5** as a sole product (Scheme 13).

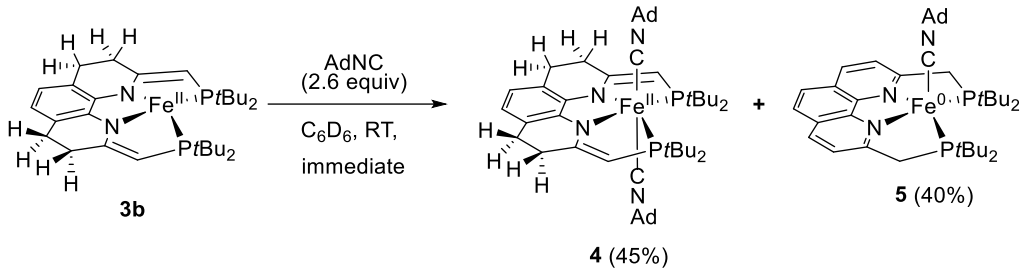

Scheme 12. Reaction of **3b** with AdNC.

Complex **5** exhibits one singlet at 116 ppm in $^{31}P\{^1H\}$ NMR, supporting the symmetrical structure of **5**. In ^1H NMR spectrum, adamantly group appears at 1.29, 1.21 and 1.53 ppm with the integral intensity of 6H, 6H and 3H, respectively. The isocyanide carbon was observed in lower field region at 220.1 ppm.

Scheme 13. Reaction of **2b** with AdNC.

After the full assignment of **5**, complex **4** was identified by ^1H, $^{13}C\{^1H\}$, and $^{31}P\{^1H\}$ NMR spectroscopy, as well as two-dimensional NMR analysis using the reaction mixture containing both **4** and **5**. Complex **4**, which possesses PCH side arms, exhibits its phosphorus signal at a higher field (76.9 ppm) than the signals of **2a**, **2b**, and **5**. A similar trend was also shown previously for [$FeCH_3$(PNNP'-Ph)].[10c] The isocyanide carbon was observed at 174.3 ppm. The signal is slightly shifted to lower field than that of **5**, possibly due to the reduced back-donating ability of **4** with the

Fe(II) center. Reflective of this point, complex **5** exhibited weakened CN stretching at 1913 cm^{-1}, compared with that of **4**, ν_{CN} 2077 and 2035 cm^{-1}. On the other hand, the ν_{CN} values of **4** were observed at lower wavenumber region than in the case of the structurally similar AdNC coordinated Fe(II) complex supported by a N_2P_2 macrocyclic ligand [Fe(AdNC)$_2$(N_2P_2)], which exhibited ν_{CN} at 2124 cm^{-1}.[13] Thus, the more efficient electron-donating ability of PNNP-*t*Bu ligand than N_2P_2 ligand was supported.

The octahedral structure of **4**, which possesses two AdNC at the apical position, was confirmed by a single-crystal X-ray diffraction study (Figure 2a). The shorter Fe–P (2.381(9) and 2.384(9) Å) and Fe–N (1.990(3) and 1.992(3) Å) bond lengths than in [Fe(OCHPh$_2$)(PNNP'-Cy)] and [Fe(NPhNHPh)(PNNP'-Cy)] are consistent with the Fe(II) center with a low-spin state.[14, 10] The C–N bond lengths are 1.153(4) and 1.149(4) Å, which are typical values for a C–N triple bond.[15] The C25–C26 and C31–C32 bonds exhibit typical single-bond lengths, 1.501(6) and 1.509(6) Å, respectively. Thus, a doubly hydrogenated PNNP backbone in **4** was confirmed.

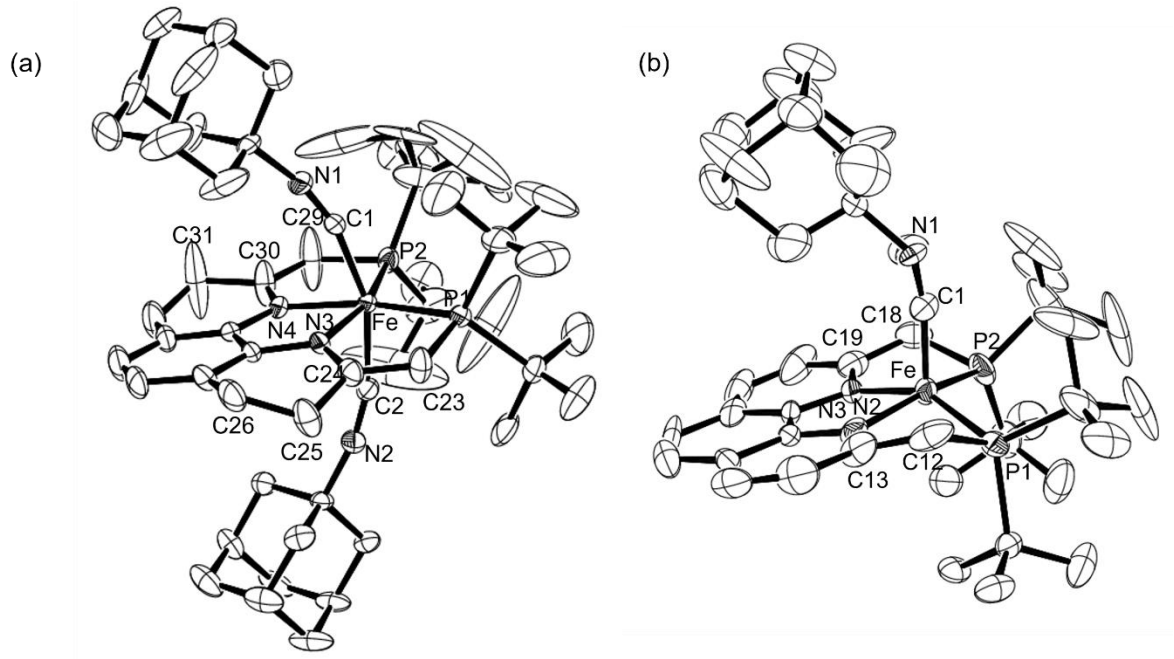

Figure 2. (a) ORTEP diagram of **4** with 50% probability thermal ellipsoids. All hydrogen atoms are omitted for clarity. Selected bond lengths[Å] and angles [˚]: Fe–P1 2.385(9), Fe–P2 2.381(9), Fe–N3 1.990(3), Fe–N4 1.992(3), Fe1–C1 1.863(3), Fe1–C12 1.862(3), C1–N1 1.153(4), C12–N12 1.149(4), C23–C24 1.367(5), C24–C26 1.507(5), C25–C26 1.501(5), C29–C30 1.356(5), C30–31 1.509(6); P1–Fe–N3 80.72(8), P1–Fe–N4 161.59(8), N3–Fe–N4 80.92(11), N4–Fe1–P2 81.11(8),

N3–Fe1–P2 162.03(8) P1–Fe–P2 117.24(3), N3–C24–C25–C26 -31.3(5), N4–C30–C31–C32 -22.9(9). (b) ORTEP diagram of **5** with 50% probability thermal ellipsoids. All hydrogen atoms are omitted for clarity. Selected bond lengths[Å] and angles [˚]: Fe–P1 2.303(17), Fe–P2 2.289(17), Fe–N2 1.934(4), Fe–N3 1.928(5), Fe1–C1 1.774(7), C1–N1 1.192(9), C12–C13 1.468(10), C18–C19 1.470(8); P1–Fe–N2 81.11(15), P1–Fe–N3 152.14(14), N2–Fe–N3 80.10(2), N3–Fe1–P2 81.11(15), N2–Fe1–P2 157.52(18) P1–Fe–P2 113.36(6).

Complex **5** exhibits a square pyramidal structure, where the Fe atom is coordinated with PNNP-*t*Bu and AdNC (Figure 2b). All the metrical parameters around the Fe atom were within the typical range of a coordinatively saturated iron(0) complex.

Reactivity of complex **3b** towards CO as a π-accepting ligand was further examined. Addition of CO (1 atm) to complex **3b** at room temperature leads to formation of [Fe(CO)$_2$(PNNP''-*t*Bu)] (**6**) and [Fe(CO)(PNNP-*t*Bu)] (**7**) in 63% and 28% yields, respectively (Scheme 14). The resulting complexes were fully characterized by ^{1}H, ^{31}P{^{1}H}, ^{13}C{^{1}H} and 2D NMR. The ^{1}H NMR spectrum confirmed the presence of PCH which exhibited at 4.83 ppm with integral intensity of 2H and phenanthroline backbone appeared as a multiplet at 2.89 and 2.76 ppm. In the ^{13}C{^{1}H} NMR spectrum, carbonyl carbon appeared in the lower field at 229.9 ppm as a triplet (J_{CP} = 18.6 Hz).

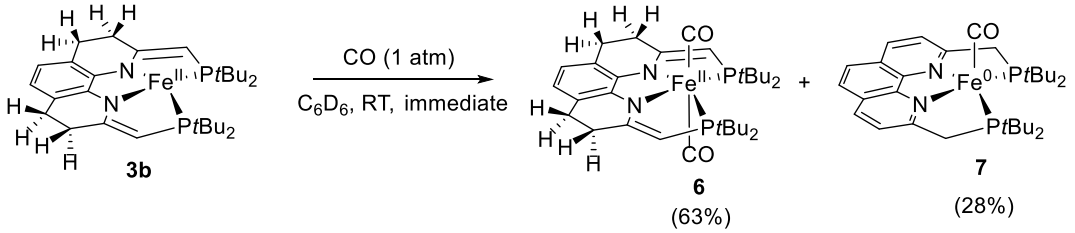

Scheme 14. Reaction of **3b** with CO.

Interestingly, complex **7** could be prepared from reaction of **3b** and CO_2 (1 atm) (Scheme 15). It could be possible that **3b** reacts with CO_2 via MLC, resulting complex **7**. However, unidentified complex with signal 33.32 was appeared along with 123.1 (**7**) in ^{31}P{^{1}H} NMR spectrum. In the ^{1}H NMR spectrum, benzylic protons appeared as doublet with integral intensity of 2H at 3.49 and 3.73 respectively. The carbonyl carbon was observed in the lower field region at 220.3 ppm in ^{13}C{^{1}H} NMR. A single crystal of complex **7** was obtained and determined by single crystal X-ray diffraction. Complex **7** adopts distorted square pyramidal geometry around iron center coordinated with PNNP and CO ligands. The bond length of Fe–N 1.941(4) and Fe–P 2.3055 (12) and 2.3266(12) which endorsed low spin state.

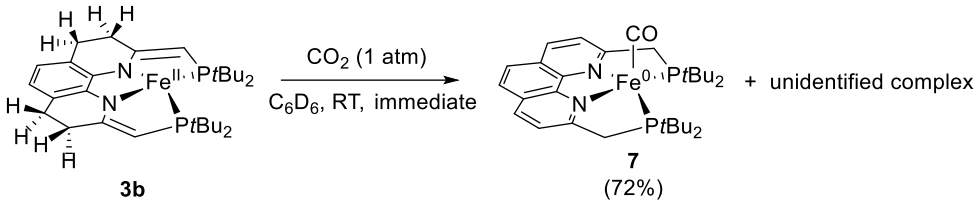

Scheme 15. Reaction of **3b** with CO_2.

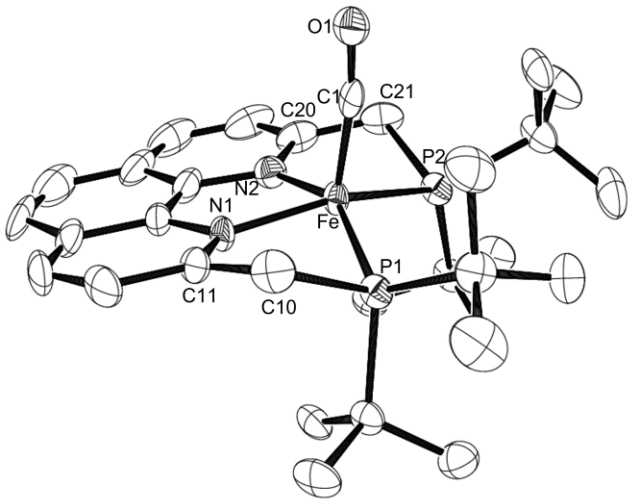

Figure 3. ORTEP diagram of **7** with 50% probability thermal ellipsoids. All hydrogen atoms are omitted for clarity. Selected bond lengths[Å] and angles [˚]: Fe–P1 2.3055(12), Fe–P2 2.3266(12), Fe–N1 1.941(4), Fe–N2 1.941(4), Fe1–C1 1.741(5), C1–O1 1.182(5), C11–C12 1.81(7), C20–C21 1.475(7); P1–Fe–N2 79.02(12), P1–Fe–N3 153.47(12), N2–Fe–N3 80.30(16), N1–Fe1–P2 152.14(12), N2–Fe1–P2 79.02(12) P1–Fe–P2 112.56(5).

Conclusion

Iron(II) hydride complexes bearing PNNP-R (Cy, *t*Bu) ligand underwent a similar structural transformation to form a four-coordinate 14-electron complexes, **3a** and **3b** [Fe(PNNP''-R)] (R = Cy, *t*Bu), which possesses a doubly hydrogenated phenanthroline backbone. This behavior suggested presence of long-range metal ligand cooperation. Furthermore, reactivity of 14e complexes **3a** and **3b** towards π-accepting ligands were examined, and complexes **3a** and **3b** exhibit a similar reactivity pattern as iron(II) porphyrins towards CO and RCN.

Experimental section

General Consideration

All experiments were carried out under nitrogen or argon atmosphere using Schlenk techniques or a glovebox. *n*-Hexane, tetrahydrofuran, C_6H_6, toluene, and dichloromethane were purified by a solvent purification system (MBraun SPS -800 or a Glass Contour Ultimate Solvent System). Toluene-d_8 and benzene-d_6, were dried over sodium benzophenone ketyl and distilled before use. CD_2Cl_2 was dried over CaH_2 and distilled. $[FeCl_2(PNNP)]$[10a] and PNNP-^{t}Bu[10f] were synthesized by following the reported procedure. All other reagents were purchased from commercial suppliers and used without purification. ^1H, $^{13}C\{^1H\}$, and $^{31}P\{^1H\}$ NMR spectra (^1H, 600 MHz; ^{13}C, 150 MHz; ^{29}Si, 119 MHz; ^{31}P, 243 MHz) were recorded on a Bruker AVANCE III HD 600 spectrometer. Chemical shifts are reported in δ (ppm) and referenced to the residual solvent signals for ^1H and ^{13}C and 85% H_3PO_4 as an external standard for ^{31}P. The high-resolution ESI mass spectra were obtained on a Bruker micro TOF II. Elemental analysis was determined by CHN Coder MT-6 from company Yanaco Technical Science Corporation.

Preparation of $[Fe(Br)_2(PNNP\text{-}t\text{Bu})]$ (1b)

A 50 mL Teflon Schlenk was charged with PNNP-*t*Bu (623 mg, 1.25 mmol), $FeBr_2$ (270 mg, 1.25 mmol), and THF (10 ml). The solution was stirred at room temperature for 16 h to give a purple solution. The resulting mixture was filtered at room temperature. The obtained crude solid was washed with toluene (5 ml ×3) and dried under vacuum to give **1b** as a purple solid (860 mg, 1.20 mmol, 96%).

^1H NMR (600 MHz, C_6D_6, 25 °C) δ 55.12 (br), 27.48 (br), 9.16 (br), –0.49 (br), –77.30 (br)

EA Calculated for ($C_{30}H_{48}FeN_2P_2$) C, 50.59; H, 6.51; N, 3.93. Found C, 50.62; H, 6.58; N, 4.32.

Preparation of $[Fe(H)_2(PNNP\text{-}t\text{Bu})]$ (2b)

A Schlenk flask was charged with **1b** (200 mg, 0.28 mmol) and toluene (5 mL). To this purple solution was added $NaBEt_3H$ (1M THF soln, 0.5 ml, 0.5 mmol) at room temperature. The color of the solution turned to dark-green color immediately. The solution was concentrated to dryness under vacuum. The residues were extracted with hexane, filtered through a Celite pad, and dried in vacuo to give **2b** as a dark-green solid (115 mg, 0.21 mmol, 74%).

Spectrum of **2b**: ^{1}H NMR (600 MHz, C_6D_6, 25 °C) δ 7.40 (s, 2H, Phen-H), 7.38 (d, 2H, $^{3}J_{HP}$ = 6.9 Hz, Phen-H), 7.13 (d, 2H, $^{3}J_{H\text{-}P}$ = 6.9 Hz), 3.78 (d, 4H, $^{2}J_{H\text{-}P}$ = 7.7 Hz, CH_2), 1.27 (d, 36H, *t*Bu), –7.81 (t, 1H, $^{3}J_{H\text{-}P}$ = 72.1 Hz, Fe–H) ppm. ^{31}P{^{1}H} NMR (243 MHz, C_6D_6, 25 ^{o}C) δ 130.9 ppm. ^{13}C{^{1}H} NMR (150 MHz, C_6D_6, 25 °C): δ (ppm) 160.8 (Phen), 140.91 (Phen), 125.6 (Phen), 117. 3 (s, Phen), 112. 1 (s, Phen). 110.3 (Phen), 40.3 (m, CH_2), 36.3(*t*Bu), 29.79 (*t*Bu) ^{1}H-^{13}C HSQC 7.40-125.6, 7.38-117.4, 7.13-112.1, 3.78- 40.3, 1.29-29.8

Preparation of 14e [Fe(PNNP"-*t*Bu)] (3b)

Complex **2b** (30 mg, 0.054 mmol) was dissolved in C_6H_6 and left at room temperature for 1 week. The volatile materials were removed under vacuum. The resulting residue was extracted with hexane (9 mL) and filtered through a Celite pad. The filtered solid was slowly evaporated to give **3b** as a red brown crystalline solid (29 mg, 0.045 mmol, 83%). The crystals were grown in concentrated tol/hexane solution *via* vapor diffusion after 3-4 days at room temperature.

^{1}H NMR (600 MHz, C_6D_6, 25^{o}C) δ 29.73 (br), 17.42 (br), –3.87 (br), –9.81 (br). μ_{eff} (Evans, C_6D_6) = 2.2 μ_B. EA Calculated for ($C_{30}H_{48}FeN_2P_2$) C, 64.98; H, 8.73; N, 5.05. Found C, 64.85; H, 8.82; N, 4.85.

Synthesis of 14e complex [Fe(PNNP"-Cy)] (3a)

Complex **2a** (17 mg, 0.026 mmol) was dissolved in C_6D_6 (0.5 mL) and charged in a J-young NMR tube under argon atmosphere. The solution was heated at 60^{o} C for 1 h. The reaction was monitored after 1 h and broad peaks were observed in the region –30 ppm to + 30 ppm. Then reaction mixture was left overnight at room temperature. Gradually, intensity of broad peaks become increase on standing the solution for one week. The solution was concentrated to dryness under vacuum. The residue was extracted with hexane (3 ml) and filtered through a Celite pad. The dark red hexane washings solution reduced to 1 mL, and it could slowly evaporate at room temperature to give a red brown crystalline solid that was characterized by X-ray spectroscopy as complex **3a.** (16.3 mg, 95%)

^{1}H NMR (600 MHz, C_6D_6, 25^{o}C) δ 29.94 (br), 19.94 (br), 8.73 (br), 7.07 (br), 1.76 (br), 0.34 (br), –3.25 (br), –10.59 (br), –14.00 (br), –19.24 (br).

EA Calculated for ($C_{38}H_{56}FeN_2P_2$) C, 69.29; H, 8.57; N, 4.25. Found C, 68.94; H, 8.07; N, 4.71.

Reaction of 3b with AdNC

To a solution of complex **3b** (6 mg, 0.014 mmol) in C_6D_6 (0.5 mL), AdNC (3.0 mg, 0.016 mmol) and HMDSO (6 μL, 0.0006 mmol) were added in J-Young NMR tube. The reaction was monitored by ^1H and ^{31}P NMR spectroscopy. Formation of two different complexes are confirmed, Fe(II) complex with hydrogenated PNNP''-*t*Bu ligand, [Fe^{II}(AdNC)2(PNNP''-*t*Bu)] (**4**), and PNNP-*t*Bu-Fe(0) complex, [Fe^0(AdNC)(PNNP-*t*Bu)](**5**) in 55% and 40% NMR yields, respectively. Complex **5** was crystallized from toluene/hexane via vapor diffusor method at room temperature. After 3 days later, needle kind of crystals were observed and analyzed by X ray diffraction.

4: ^1H NMR (600 MHz, C_6D_6, 25 °C) δ 6.47 (s, 2H, Phen-H), 3.94 (s, 2H, CHPC$(CH_3)_3)_2$, 2.88 (m, 4H, CH_2-Phen), 2.83 (m, 4H, CH_2-Phen), 1.83 (br, 12H, AdNC), 1.65 (br, 6H, AdNC), 1.56 (d, 36 H, P*t*Bu_2), 1.22 (m, 12H, AdNC). $^{31}P\{^1H\}$ NMR (243 MHz, C_6D_6, 25°C) δ 76.9 ppm. ^{13}C $\{^1H\}$ NMR (150 MHz, C_6D_6, 25°C): δ (ppm) 174.3 (t, AdNC), 167.4 (m, Phen), 141.8 (s, Phen), 122.1 (s, Phen), 114.6 (s, Phen), 77.5 (m, CHP$(C(CH_3)_3)_2$, 55.9 (s, AdNC), 43.7 (s, AdNC), 36.2 (s, AdNC), 31.9 (s, P*t*Bu_2), 30.1 (s, CH_2Phen), 29.1 (s, AdNC), 26.6 (s, CH_2Phen). COSY (600 MHz, C_6D_6, 25°C) δ_H-δ_H 1.83-1.64, 1.64-1.22.^1H-^{13}C HSQC (C_6D_6, 25°C): δ_H-δ_C 6.47-114.8, 3.94-77.5, 2.88-31.7, 2.83-26.6, 1.83-43.7, 1.65-36.2, 1.56-31.9, 1.22-29.1. IR (ATR, cm^{-1}): 2077 (υ_{CN}), 2035 (υ_{CN}).

5: ^1H NMR (600 MHz, C_6D_6, 25 °C) δ 7.09 (s, 2H, Phen-H), 7.07 (d, 2H, Phen-H), 7.05 (d, 2H, Phen-H), 4.04-4.01 (m, 2H, CH_2-Phen), 3.67-3.63 (m, 2H, CH_2-Phen), 1.53 (d, 18 H, P*t*Bu_2), 1.29 (br, 6H, AdNC), 1.21-1.13 (m, 6H, AdNC), 1.01 (d, 18H, P*t*Bu_2), 1.53* (3H, AdNC) . $^{31}P\{^1H\}$ NMR (243 MHz, C_6D_6, 25°C) δ 116.9 ppm.$^{13}C\{^1H\}$ NMR (150 MHz, C_6D_6, 25°C): δ (ppm) = 220.1 (t, J_{CP} = 6.1 Hz, AdNC), 159.6 (t, J_{CP} = 2.8 Hz, Phen), 138.6 (s, Phen), 130.9 (s, Phen), 126.0 (s, Phen), 114.7 (s, Phen), 110.3 (s, Phen), 55.9 (s, AdNC), 38.6 (d, $CH_2P(C(CH_3)_3)_2$, 38.5 (d, $CH_2P(C(CH_3)_3)_2$, 45.3 (s, AdNC), 37.6 (d, P*t*Bu_2), 36.5 (d, P*t*Bu_2), 36.1 (s, AdNC), 31.0 (s, P*t*Bu_2), 30.7 (s, AdNC), 29.8 (P*t*Bu_2). *the signal was determined by ^1H-^1H COSY. ^1H-^1H COSY (C_6D_6, 25 °C): δ_H-δ_H 7.07-7.05, 4.04-3.67, 1.53-1.01, 1.53-1.29, 1.59-1.21. ^1H-^{13}C HSQC (C_6D_6, 25°C): δ_H-δ_C 7.09-126.0, 7.07-114.7, 7.05-110.3, 4.04-4.01- 38.6, 3.67-3.63-38.5, 1.53-31.0, 1.01-29.8, 1.29-45.3, 1.53*-31.0, 1.21-36.1.

EA Calculated for ($C_{41}H_{61}FeN_3P_2$) C, 68.99; H, 8.61; N, 5.89. Found C, 69.02; H, 8.79; N, 6.12. IR (ATR, cm^{-1}): 1913 (υ_{CN}).

Alternative synthesis of 5: Reaction of 2b with AdNC

Complex **5** was prepared by the reaction of **2b** (166 mg, 0.23 mmol) with $NaBEt_3H$ (1 M THF soln. 0.46 mL, 0.46 mmol) in C_6H_6 at room temperature. After stirring the reaction mixture for 10 min at room temperature, all the volatile materials were removed under vacuum. The resulting compound was again dissolved in C_6H_6 (20 mL) and added adamantyl isocyanide (56.0 mg, 0.34 mmol). The solution was stirred for 30 min at the temperature. The volatile materials were removed under vacuum. The residues were extracted with toluene and filtered through a Celite pad. After evaporation, the residue was dissolved in hexane and kept at room temperature, giving reddish brown crystals of **5** (128 mg, 0.18 mmol, 75%).

Reaction of 3b with CO

To a solution of complex **3b** (10 mg, 0.018 mmol) in C_6D_6 (0.5 mL) and HMDSO (6 μL, 0.0006 mmol) were added in J-Young NMR tube. After freeze–thaw–pump cycles (×3), CO (1 atm) was introduced into the reaction vessel. The reaction was monitored by ^1H and ^{31}P NMR spectroscopy. Formation of two different complexes are confirmed, Fe(II) complex with hydrogenated PNNP''-*t*Bu ligand, $[Fe^{II}(CO)_2$(PNNP''-tBu)] (**6**), and PNNP-*t*Bu-Fe(0) complex, $[Fe^0$(CO)(PNNP-*t*Bu)](**7**) in 63% and 28% NMR yields, respectively.

6: ^1H NMR (600 MHz, C_6D_6, 25 °C) δ 6.70 (s, 2H, Phen-H), 4.83 (s, 2H, $CHPC(CH_3)_3)_2$, 2.89 (m, 4H, CH_2-Phen), 2.76 (m, 4H, CH_2-Phen), 1.16 (d, 36 H, P*t*Bu_2). $^{31}P\{^1H\}$ NMR (243 MHz, C_6D_6, 25°C) δ 84.6 ppm. ^{13}C $\{^1H\}$ NMR (150 MHz, C_6D_6, 25°C): δ (ppm) 229.9 (t, CO), 168.4 (m, Phen), 145.9 (s, Phen), 123.5 (s, Phen), 115.9 (s, Phen), 96.5 (m, $CHP(C(CH_3)_3)_2$, 31.9 (s, P*t*Bu_2), 29.7 (s, P*t*Bu_2), 27.9 (s, CH_2Phen), 25.7 (s, CH_2Phen). ^1H-^{13}C HSQC (C_6D_6, 25°C): δ_H-δ_C 6.70-115.9, 4.83-96.5, 2.89-27.9, 2.76- 25.7, 1.16-29.7.

7: ^1H NMR (600 MHz, C_6D_6, 25 °C) δ 7.12 (d, 2H, Phen-H), 7.08 (s, 2H, Phen-H), 6.88 (d, 2H, Phen-H), 3.73 (d, 2H, CH_2-Phen), 3.49 (d, 2H, CH_2-Phen), 1.42 (d, 18 H, P*t*Bu_2), 0.93 (d, 18H, P*t*Bu2). $^{31}P\{^1H\}$ NMR (243 MHz, C_6D_6, 25°C) δ 123.1 ppm.$^{13}C\{^1H\}$ NMR (150 MHz, C_6D_6, 25°C): δ (ppm) = 229.5 (br, CO), 158.7 (br, Phen), 146.2 (s, Phen), 138.8 (s, Phen), 125.9 (s, Phen), 116.9 (s, Phen), 111.6 (s, Phen), 38.9 (d, $CH_2P(C(CH_3)_3)_2$, 36.6 (d, $CH_2P(C(CH_3)_3)_2$, 33.6 (d, P*t*Bu_2), 32.2 (d, P*t*Bu_2), 30.9 (s, P*t*Bu_2), 30.0 (s, s, P*t*Bu_2). ^1H-^1H COSY (C_6D_6, 25 °C): δ_H-δ_H 7.12-6.88, 3.73-3.49, 1.42-0.93. ^1H-^{13}C HSQC (C_6D_6, 25°C): δ_H-δ_C 7.12-125.9, 7.08-116.9, 6.88-111.6, 3.73- 38.9, 3.49-36.6, 1.42-

30.9, 0.93-30.0. IR (ATR, cm^{-1}): 1841 (υ_{CO}).

Reaction of 3b with CO_2

To a solution of complex **3b** (24 mg, 0.043 mmol) in C_6D_6 (0.5 mL) and were added in J-Young NMR tube. After freeze–thaw–pump cycles (×3), CO_2 (1 atm) was introduced into the reaction vessel. The reaction was sonicated for 15 min. Formation of [Fe^0(CO)(PNNP-*t*Bu)](**7**) and unidentified complex were observed in ^1H and ^{31}P NMR. The volatile materials were removed under vacuum followed by celite filtration. After evaporation, the residue was dissolved in tol/hexane and kept at room temperature for 3 days, giving reddish brown crystals of green. (18 mg,0.031 mmol, 72 %).

Single crystal X-ray diffraction studies

All single-crystal X-ray diffraction measurements of **3a**, **3b**, **4, 5** and **7** were performed under a cold nitrogen stream on a Rigaku XtaLAB P200 diffractometer with a Pilatus 200K detector using multi-layer mirror monochromated Mo-Kα radiation (λ = 0.71073 Å, 50 kV/24 mA). The determination of crystal systems and unit cell parameters were performed with the CrystalClear program package. Data processing was performed with the CrystalClear program package or CrysAlisPro program package. All structures were solved by direct methods using SIR2014 program[3] and refined by full-matrix least squares calculations on F^2 for all reflections (SHELXL-2014/7)[4], using Yadokari-XG 2009 program[5]. The X-ray crystallographic data for **3a, 3b, 4, 5** and **7** have been deposited at the Cambridge Crystallographic Data Centre (CCDC) under deposition 2107796 for **3a**, 2107795 for **3b**, 2107800 for **4**, and 2107798 for **5**. These data can be obtained free of charge from the CCDC (www.ccdc.cam.ac.uk/data_request/cif).

Table S1. Crystallographic parameters

	3a	**3b**	**4**	**5**	**7**
Empirical formula	$C_{38}H_{56}FeN_2P_2$	$C_{30}H_{48}FeN_2P_2$	$C_{52}H_{76}FeN_4P_2$	$C_{41}H_{61}FeN_3P_2$	$C_{31}H_{46}FeN_2OP_2$
Formula weight	658.63	554.49	874.95	713.71	580.49
Temperature	93(2) K	93(2) K	93(2) K	93(2) K	93(2) K
Crystal system	monoclinic	monoclinic	monoclinic	triclinic	triclinic
Space group	$P2_1/c$	$P2_1/c$	$P2_1/c$	$P\bar{1}$	$P\bar{1}$
a/Å	10.3898(18)	13.4818(7)	10.9291(3)	11.0720(11)	11.3449(8)
b/Å	21.575(4)	12.5182(6)	35.4158(10)	12.9769(13)	11.5319(9)
c/Å	15.702(3)	18.6660(9)	12.8860(4)	13.4214(12)	13.1874(8)
α/deg	90 °	90 °	90 °	101.865(8) °	80.744(6) °
β/deg	103.167(4) °	111.002(6) °	108.074(3) °	91.023(8) °	64.886(7) °
γ/deg	90 °	90 °	90 °	92.713(8) °	70.492(7) °
Volume	3427.2(10) $Å^3$	2940.9(3) $Å^3$	4741.6(2) $Å^3$	1884.3(3) $Å^3$	1472.1(2) $Å^3$
Z	4	4	4	2	2
Density	1.276	1.252	1.226	1.258	1.310
Goodness-of-fit on F^2	1.030	0.869	1.621	1.032	1.037
Final R indices [I>2sigma(I)]	$R1$ = 0.0365, $wR2$ = 0.0813	$R1$ = 0.0435, $wR2$ = 0.1169	$R1$ = 0.0830, $wR2$ = 0.2232	$R1$ = 0.1066, $wR2$ = 0.2139	$R1$ = 0.0749 $wR2$ = 0.1588
R indices (all data)	$R1$ = 0.0558, $wR2$ = 0.0884	$R1$ = 0.0646, $wR2$ = 0.1290	$R1$ = 0.1037, $wR2$ = 0.2339	$R1$ = 0.2242, $wR2$ = 0.2555	$R1$ = 0.1288 $wR2$ = 0.1882

References

1. (a) Hartwig, J. F. Organotransition metal chemistry: from bonding to catalysis; University of Science Books: Sausalito, CA, **2010**. (b) R. F. Jordan, *Adv. Organomet. Chem.* **1991**, *32*, 325. (c) Dyer, P.W.; Gibson, V.C.; Howard, J. A. K.; Whittle, B.; Wilson, C. *J. Chem. Soc., Chem. Commun.*, **1992**, 1666. (d) Huang, D.; Streib, W. E.; Bollinger, J. C.; Caulton, K. G.; Winter, R. F.; Scheiring, T. *J. Am. Chem. Soc.* **1999**, *121*, 8087-8097.

2. (a) Schöffel, J.; Nückel, S.; Sieh, D.; Burger, P. *Eur. J. Inorg. Chem*. **2010**, 4911-4915. (b) Dorta, R.; Stevens, E. D.; Nolan, S. P. *J. Am. Chem. Soc.* **2004**, *126*, 5054-5055. (c) Urtel, H.; Meier, C.; Eisenträger, F.; Rominger, F.; Joschek, J. P.; Hofmann, P. *Angew. Chem. Int. Ed.* **2001**, *40*, 4. (d) Budzelaar, H. M.; Rene de Gelder, A. W. Gal, *Organometallics*, **1998**, 4121-4123 (e) Yared, Y. W.; Miles, S. L.; Bau, R.; Reed, C. A. *J. Am. Chem. Soc*., **1977**, *99*, 21.

3. (a) Huang, D.; Huffman, J. C.; Bollinger, J. C.; Eisenstein, O.; Caulton, K. G. *J. Am. Chem. Soc*. **1997**, *119*, 7398-7399. (b) Huang, D.; Bollinger, J. C.; Streib, W. E.; Folting, K.; Young, V.; Eisenstein, O.; Caulton, K. G. *Organometallics* **2000**, *19*, 2281-2290. (c) Huang, D.; Streib, W. E.; Bollinger, J. C.; Caulton, K. G.; Winter, R. F.; Scheiring, T. *J. Am. Chem. Soc.* **1999**, *121*, 8087-8097. (d) Watson, L. A.; Ozerov, O. V.; Pink, M.; Caulton, K. G. *J. Am. Chem. Soc.* **2003**, *125*, 8426-8427. (e) Askevold, B.; Khusniyarov, M. M.; Herdtweck, E.; Meyer, K.; Schneider, S. *Angew. Chem. Int. Ed.* **2010**, *49*, 7566-7569. (f) Alig, L.; Fritz, M.; Schneider, S. *Chem. Rev.* **2019**, *119*, 2681-2751.

4. Hawrelak, E. J.; Bernskoetter, W. H.; Lobkovsky, E.; Yee, G. T.; Bill, E.; Chirik, P. J. *Inorg. Chem.* **2005,** 44, 3103-3111

5. (a) Scheidt, W. R.; Reed, C. A. *Chem. Rev.* **1981**, *81*, 543-555. (b) Sellers, S. P.; Korte, B. J.; Fitzgerald, J. P.; Reiff, W. M.; Yee, G. T. *J. Am. Chem. Soc.* **1998**, *120*, 4662-4670. (c) Ray, K.; Begum, A.; Weyhermuller, T.; Piligkos, S.; Slageren, J.; Neese, F.; Wieghardt, K. J. *Am. Chem. Soc.* **2005**, 127, 4403-4415. (d) Suzuki, T.; Matsumoto, J.; Kajita, Y.; Inomata, T.; Ozawaa, T.; Masuda, H. *Dalton Trans.*, **2015**, *44*, 1017-1022.

6. (a) Stynes, D. V.; Hui, Y. S.; Chew, V. *Inorg. Chem.* **1982**, *21*, 1222-1225. (b) Rileyf, D. P.; Busch, D. H. *Inorg. Chem.* **1984**, *23*, 3235-3241. (c) Strauss, S. H.; Pawlik, M. J. *Inorg. Chem*. **1986**, *25*, 1923-1925. (d) Alvarez, S.; Cirera, J. *Angew. Chem. Int. Ed.* **2006**, *45*, 3012-3020. (e) Cirera, J.; Ruiz, E.; Alvarez, S. *Inorg. Chem.*, **2008**, *47*, 2871.

7. (a) Liao, M.S.; Scheinera, S. *J. Chem. Phys.*,**2002**, *117*, 1 (b) Liao, M. S.; Scheiner, S. *J. Chem. Phys.*, 2002, *116*, 1. (c) Spiro, T. G.; Soldatova, A. V.; Balakrishnan, G. *Coord. Chem. Rev.* **2013**,

257, 511-527. (d) Stynes, D. V.; Hui, Y. S.; Chew, V. *Inorg. Chem.* **1982**, *21*, 1222-1225. (e) Riley, D. V.; Busch, D. H. *Inorg. Chem.* **1984**, *23*, 3235-3241.

8. (a) Klose, A.; Hesschenbrouck, J.; Solari, E.; Latronico, M.; Floriani, C.; Chiesi-Villa, N. Re, A.; Rizzoli, C. *J. Organomet. Chem.*, **1999**, *591*, 45. (b) Fitzgerald, J. P.; Lebenson, J. R.; Wang, G.; Yee, G. T.; Noll, B. C.; Sommer, R. D. *Inorg. Chem.*, **2008,** *47*, 4520. (c) Silva, C. D.; Bonomo, L.; Solari, E.; Scopelliti, R.; Floriani, C.; Nazzareno, *Chem. Eur. J.*, **2000**, *6*, 4519.

9. Hatzis, G. P.; Thomas, C. M. *Chem. Commun*. **2020**, *56*, 8611-8614.

10. (a) Takeshita, T.; Sato, K.; Nakajima, Y. *Dalton Trans*. **2018**, *47*, 17004-17010. (b) Takeshita, T.; Nakajima, Y. *Chem. Lett*. **2019**, *48*, 364-366. (c) Gautam, M.; Yatabe, T.; Tanaka, S.; Satou, N.; Takeshita, T.; Yamaguchi, K.; Nakajima, Y. *ChemistrySelect* **2020,** *5*, 15-17. (d) Jheng, N.-Y.; Ishizaka, Y.; Naganawa, Y.; Sekiguchi, A.; Nakajima, Y. *Dalton Trans.*, **2020**, *49*, 14592-14597. (e) Nakajima, Y.; Takeshita, T.; Jheng, N.-Y. *Dalton Trans.* **2021**, *50*, 7532-7536. (f) Langer, R.; Fuchs, I.; Vogt, M.; Balaraman, E.; Diskin-Posner, Y.; Shimon, L. J. W.; Ben-David, Y.; Milstein, D. *Chem. Eur. J.* **2013**, *19*, 3407-3414.

11. Synthesis and Reactivities of Iron Complexes Bearing a Tetradentate PNNP Ligand, Tomohiro Takeshita (Doctoral Program in Chemistry 2019).

12. Speight, J. G. *Lange's Handbook of Chemistry*; 16th ed.; McGraw-Hill: New York, 2005

13. Bigler, R.; Mezzetti, A. *Org. Lett.* **2014**, *16*, 6460-6463.

14. (a) Mikhailine, A. A.; Kim, E.; Dingels, C.; Lough, A. J.; Morris, R. H. *Inorg. Chem.* **2008**, *47*, 6587-6589. (b) Sues, P.E.; Lough, A. J.; Morris, R. H. *Organometallics* **2011,** *30*, 4418-4431. (c) Haslinger, S.; Kück, J. W.; Hahn, E. M.; Cokoja, M.; Pöthig, A.; Basset, J.-M.; Kühn, F. E. *Inorg. Chem.* **2014**, *53*, 11573-11583.

15. (a) Keene, T. D.; Komm, T.; Hauser, J.; Krämer, K. W. *Inorg. Chim. Acta* **2011**, *373*, 100-106. (b) Sues, P. E.; Lough, A. J.; Morris, R. H. *Acta Cryst.* **2014**, *E70*, m144. (c) Smith, N. E.; Bernskoetter, W. H.; Hazari, N.; Mercado, B. Q. *Organometallics* **2017**, *36*, 3995-4004.

Chapter 5

Summary

This thesis has demonstrated a comprehensive study of elemental reactions (oxidative addition, insertion, ligand exchange and reductive elimination) using iron complexes bearing a tetradentate PNNP ligand. It includes synthesis and characterization of new iron complexes. The strong electron-donating ability of the PNNP ligand permitted to establish the well-defined reaction platform of iron complexes. Through the study, metal ligand cooperation (MLC) of both the conventional fashion and the new long-range mode were elucidated.

Chapter 1 describes the importance of iron pincer complexes in homogenous catalysis.

Homogeneous catalysis of 3d metal complexes has recently drawn increasing attention, based on their potential to act as cheap and non-toxic surrogates for precious metal catalysts. However, due to the complex paramagnetic nature, the utilization of iron complexes as catalysts are still challenging. To this end, pincer ligands are of great importance. The reasons are explained in this chapter: i.e. pincer ligands allow well-defined coordination sphere around a metal center due to chelating, rigid binding mode. In addition, properties of pincer ligands can be easily optimized by tuning side arm linkers such as CH_2, NH, and O. Related to this topic, the chapter also explains the importance of metal-ligand cooperation (MLC), where both a metal and a ligand participate in substrate bond activation in a synergetic manner. Three different modes of MLC including hemilability, redox activity, and bifunctionality are also explained in this chapter.

Finally, the importance of the PNNP-R (Ph, Cy, *t*Bu) ligand was introduced. As PNNP-R has four strong donor atoms along with π-acidic phenanthroline backbone which behaves as a redox active ligand. Thus, PNNP ligand serves as a strong field ligand and stabilizes iron complexes.

The chapter ends with the short outline of this thesis.

In Chapter 2, ability of binuclear iron (0) complex $[\{Fe(PNNP)\}_2(\mu\text{-}N_2)]$ towards bond cleavage of C–X (X = Br, I) was examined. Treatment of dinuclear iron (0) complex $[\{Fe(PNNP)\}_2(\mu\text{-}N_2)]$ smoothly reacted with CH_3I at room temperature to give $[Fe(CH_3)(I)(PNNP\text{-}Ph)]$ via oxidative addition. The resulting oxidative addition product $[Fe(CH_3)(I)(PNNP\text{-}Ph)]$ was isolated and structurally fully characterized by a single crystal X-ray diffraction study, NMR spectroscopy, and

Elemental analysis. A Single crystal X-ray diffraction study revealed the octahedral structure of [Fe(CH_3)(I)(PNNP-Ph)], in which the CH_3 group and the I group occupy apical positions. To shed light on the reaction mechanism of the C–I bond cleavage, the reaction of iron (0) [{Fe(PNNP)}$_2$(μ-N_2)] with cyclopropylmethyl bromide as a radical clock was examined, where butene as well as [Fe($Br)_2$(PNNP)] were formed (Scheme 1). The results strongly support the radical pathway for the C–Br bond cleavage, in which ring opening of the *in situ* formed cyclopropylmethyl radical proceeded during the reaction.

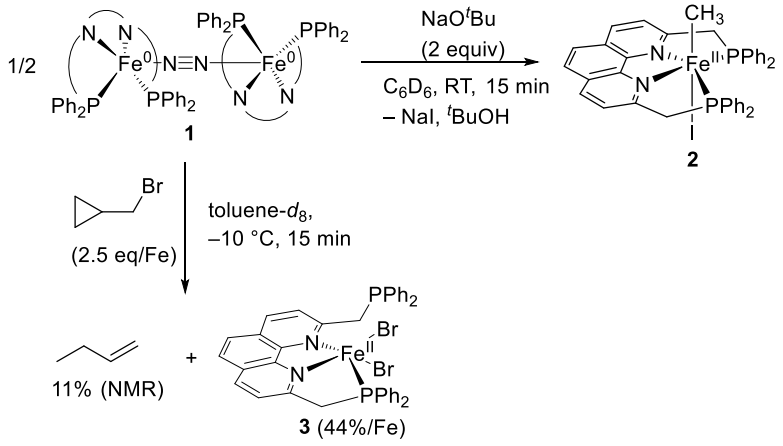

Scheme 1. Oxidative addition of CH_3I and radical clock reaction using cyclopropylmethyl bromide by iron (0) [{Fe(PNNP)}$_2$(μ-N_2)].

In this system, the concept of MLC was applied using [Fe(CH_3)(I)(PNNP-Ph)]. Thus, deprotonation of [Fe(CH_3)(I)(PNNP-Ph)] with NaO*t*Bu resulted in the formation of [Fe(CH_3)(PNNP'-Ph)] bearing a dearomatized PNNP ligand. Complex [Fe(CH_3)(PNNP'-Ph)] reacted with H_2 to cleave H–H bond at ambient temperature. The reaction was facilitated by MLC, where re-aromatization of the phenanthroline backbone concomitantly proceeded (Scheme 2). Hence, the first example of a well-defined example of bond cleavage via involving aromatization-dearomatization metal ligand cooperation of the PNNP-iron system.

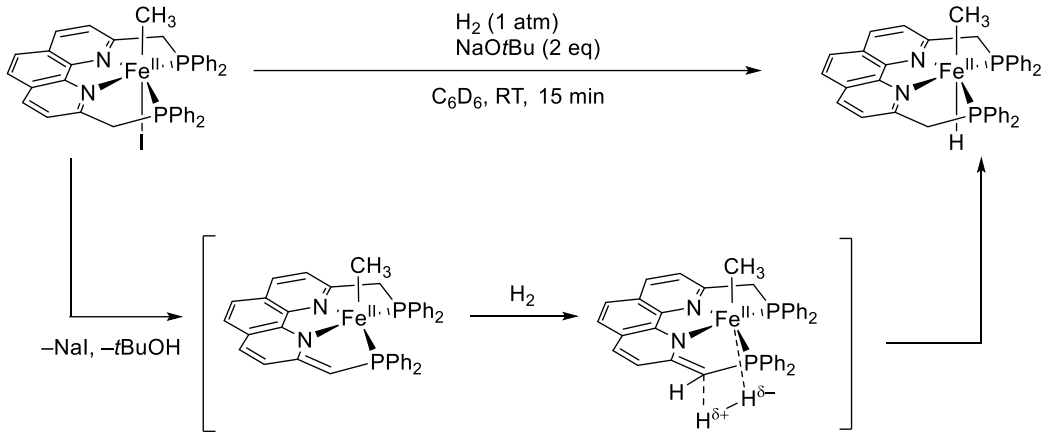

Scheme 2. H–H heterolytic cleavage via conventional metal ligand cooperation (MLC).

Chapter 3 describes the reactivity of iron hydride complex bearing a phenanthroline-based PNNP-Cy ligand [Fe(H)$_2$(PNNP-Cy)] towards various substrates including azobenzene, benzophenone and *tert*-butyldimethylsilanol. [Fe(H)$_2$(PNNP-Cy)] complex reacted with benzophenone and azobenzene, resulting in the formation of [Fe(OCHPh$_2$)(PNNP'-Cy)] and [Fe(NPhNHPh)(PNNP'-Cy)], respectively. Through these reactions, hydride and the benzylic H atom were transferred to the ligand backbone, leading to partial dearomatization of the phenanthroline moiety (Scheme 3). Treatment of [Fe(H)$_2$(PNNP-Cy)] with silanol (pK_a = 13) gave [Fe(OSi(Me)$_2$(C$_4$H$_9$))(PNNP'-Cy)]. In this reaction, deprotonation of silanol proceeded, and partial dearomatization of the ligand backbone concomitantly proceeded via H atom transfer. Thus, a long-range MLC was demonstrated. During this MLC process, phenanthroline lost aromaticity, forming dearomatized PNNP'-Cy. Overall, the phenanthroline backbone acts as a hydrogen acceptor. This phenomenon is categorized as a new mode of MLC, which could set up a new mode long range metal ligand cooperation in the iron pincer chemistry.

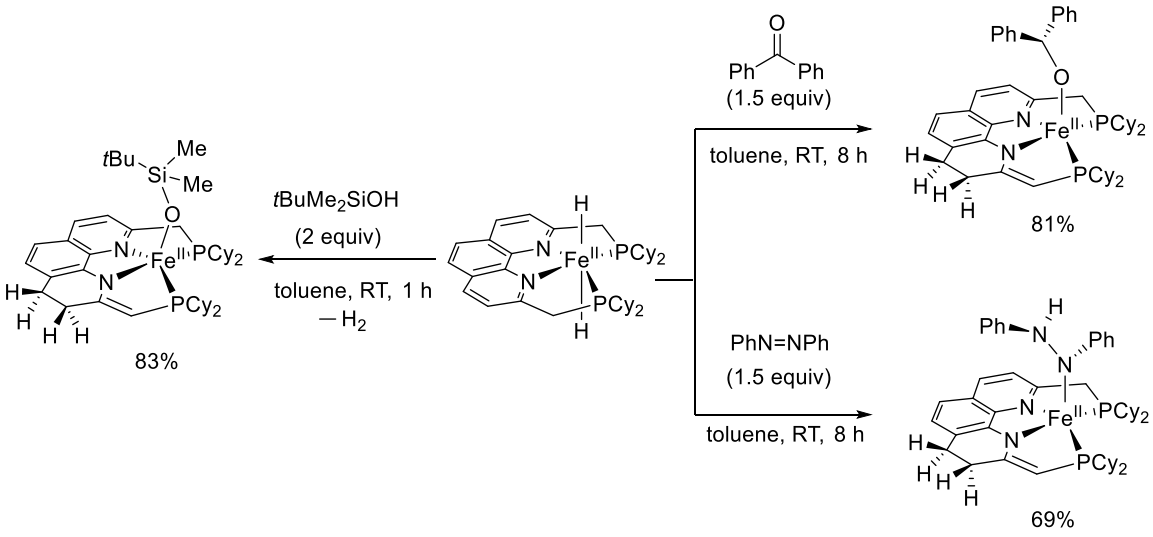

Scheme 3. Reactivity of [Fe(H)$_2$(PNNP-Cy)] triggered by new mode of long-range MLC.

In Chapter 4, long-range MLC behavior of [Fe(H)$_2$(PNNP-Cy)] was investigated. Motivated by the unique long-range MLC, an iron hydride complex bearing a bulkier PNNP-*t*Bu ligand (2,9-bis((di-*t*-butylphosphino)methyl)-1,10-phenanthroline), [Fe(H)$_2$(PNNP-*t*Bu)], was synthesized with the aim of expanding the reaction options. It was revealed that complexes. [Fe(H)$_2$(PNNP-Cy)] and [Fe(H)$_2$(PNNP-*t*Bu)] underwent double dearomatization of the ligand backbone via long-range metal ligand cooperation. As a results, rare 14e complexes [Fe(PNNP"-Cy)] and [Fe(PNNP"-*t*Bu)] were synthesized from [Fe(H)$_2$(PNNP-Cy)] and [Fe(H)$_2$(PNNP-*t*Bu)] respectively via long-range MLC (Scheme 4a). Complexes [Fe(PNNP"-Cy)] and [Fe(PNNP"-*t*Bu)] were isolated and fully characterized by a single crystal X-ray diffraction and elemental analysis. Reaction of [Fe(PNNP"-*t*Bu)] with π-acceptor ligands such as AdNC was performed to give 18e [Fe(AdNC)$_2$(PNNP"-*t*Bu)] and [Fe(AdNC)(PNNP-*t*Bu)] respectively (Scheme 4b). Such the reactivity of unsaturated 14e Fe(II) species towards π-accepting ligands are often found in iron(II) porphyrins as cofactors of heme-containing proteins. Thus, our work reported here demonstrates one of the rare examples of a well-defined model of iron(II) porphyrin systems.

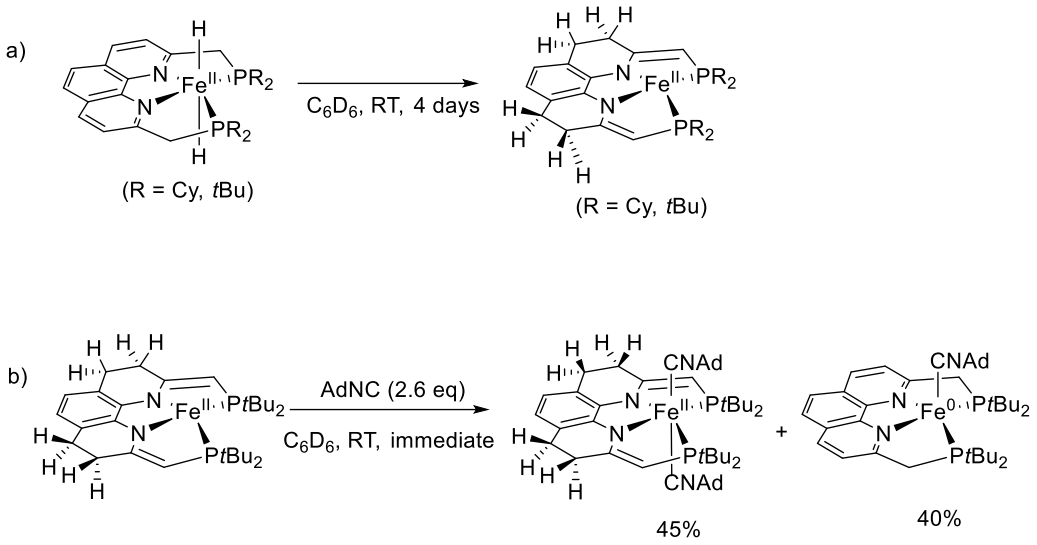

Scheme 4. (a) Formation of rare 14e complex [Fe(PNNP"-Cy)] and [Fe(PNNP"-*t*Bu)] via new mode of long-range metal ligand cooperation (MLC), (b) Reactivity of complex [Fe(PNNP"-*t*Bu)] towards AdNC.

In conclusion, PNNP-Fe chemical reactivity and different mode of MLC was revealed to give scope of development of iron PNNP pincer as catalyst in future. Further studies of PNNP-Fe complex may lead to develop new stoichiometric reaction which has potential to participate in catalytic reaction.

List of Publications

1. M. Gautam, T. Yatabe, S. Tanaka, N. Satou, T. Takeshita, K. Yamaguchi, Y. Nakajima, *Chem. Select*, **2020**, *5*, 15-17.
2. M. Gautam, S. Tanaka, A. Sekiguchi, Y. Nakajima, *Organometallics* **2021**, *40*, 3697-3702.

Acknowledgements

I am deeply indebted to the members of the National Institute of Advanced Industrial Science and Technology (AIST) and the University of Tsukuba for their invaluable support during the Doctoral Program (Ph.D.) in Tsukuba, Japan. It has been a very intellectually rewarding journey for me to work and learn in the intellectually stimulating environment of the institute.

First and foremost, I would like to express gratitude to my supervisor and mentor, Dr. Yumiko Nakajima (Associate Professor), for providing me an opportunity to pursue PhD under her supervision. I am grateful for her kind support, care, encouragement, and patience throughout my research journey. During my tenure, she has mentored me in formulating research methodology, instructing experimental skills and scientific writing skills for manuscripts and thesis. Her expertise in organometallic chemistry and feedbacks pushed me to sharpen my research thinking and articulation in the research domain.

I would like to extend my gratitude and appreciation towards Prof. Akira Sekiguchi and Dr. Shinji Tanaka for their continual inputs and insights during the discussion of the research project. I would like to thank all the laboratory members in “Silicon Chemistry” especially Dr. Yuki Naganawa, Dr. Yasu Minami, Dr. Koya Inomata, Dr. Tomohiro Takeshita, Mr. Yusuke Ishijaka, Mr. Nai-Yuan Jheng for their valuable comments and suggestions during the scientific discussion in seminars. In addition, I would like to thank Mrs.Atsuko Ogawa for her moral support and for making me feel at home in Japan.

I would also like to extend my sincere thanks to Prof. Takahiko Kojima, Dr. Tomoyo Ishizuka, Dr. Hiroaki Kotani and all other faculty members of the Department of Chemistry, University of Tsukuba.

I would like to thank the Director, Deputy Director of Interdisciplinary Research Catalytic Chemistry and Human Resource Department AIST, Japan for allowing me to work as a Research Assistant and providing grants to support my research journey in Japan.

I am fortunate to have a family’s support throughout my journey and always stands as pillar strength.

At last, thanks to all those people who were directly or indirectly involved in making my Ph.D. journey memorable in Japan.

Monika Gautam

October 2021